For Reference

NOT TO BE TAKEN FROM THIS ROOM

Ex libris
universitatis
albertaensis

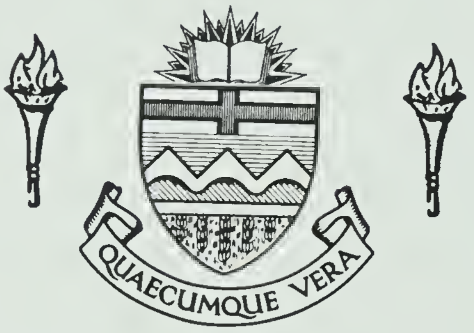

The University of Alberta
Printing Department
Edmonton, Alberta

Digitized by the Internet Archive
in 2019 with funding from
University of Alberta Libraries

https://archive.org/details/Wright1974

THE UNIVERSITY OF ALBERTA

RELEASE FORM

NAME OF AUTHOR .... PETER W. WRIGHT

TITLE OF THESIS .... ELECTRON TUNNELLING INTO SUPERCONDUCTIVE LEAD-INDIUM ALLOYS SUBJECTED TO HYDROSTATIC PRESSURE

DEGREE FOR WHICH THESIS WAS PRESENTED .... DOCTOR OF PHILOSOPHY

YEAR THIS DEGREE GRANTED 1974

Permission is hereby granted to THE UNIVERSITY OF ALBERTA LIBRARY to reproduce single copies of this thesis and to lend or sell such copies for private, scholarly or scientific research purposes only.

The author reserves other publication rights, and neither the thesis nor extensive extracts from it may be printed or otherwise reproduced without the author's written permission.

THE UNIVERSITY OF ALBERTA

ELECTRON TUNNELLING INTO SUPERCONDUCTIVE LEAD-INDIUM ALLOYS SUBJECTED TO HYDROSTATIC PRESSURE

by

© PETER W. WRIGHT

A THESIS

SUBMITTED TO THE FACULTY OF GRADUATE STUDIES AND RESEARCH

IN PARTIAL FULFILMENT OF THE REQUIREMENTS FOR THE DEGREE

OF DOCTOR OF PHILOSOPHY

DEPARTMENT OF PHYSICS

EDMONTON, ALBERTA

FALL, 1974

THE UNIVERSITY OF ALBERTA

FACULTY OF GRADUATE STUDIES AND RESEARCH

The undersigned certify that they have read, and recommend to the Faculty of Graduate Studies and Research, for acceptance, a thesis entitled, ELECTRON TUNNELLING INTO SUPERCONDUCTIVE LEAD-INDIUM ALLOYS SUBJECTED TO HYDROSTATIC PRESSURE, submitted by PETER W. WRIGHT in partial fulfilment of the requirements for the degree of Doctor of Philosophy.

TO VIOLET, WILLIAM, JANET & ANGELA

ABSTRACT

An investigation of the physical properties of the superconductive lead-indium alloy system has been carried out as a function of hydrostatic pressure, the results of which are presented in this thesis.

Samples were prepared in the form of tunnel junctions using standard vacuum deposition techniques from extremely high purity source elements. Pressure was applied to the samples by suspending them in a bath of solid helium and their conductance characteristics, through which most of the information was gained, were recorded using phase sensitive harmonic detection techniques. The chemical composition of the particular alloys investigated ($Pb_{88}In_{12}$ and $Pb_{64}In_{36}$) was determined using residual resistance ratio methods.

The pressure dependence of the energy gap and transition temperature were studied and found to be in excellent agreement with the recent data of Hansen et al (1973) and Galkin et al (1973).

The superconducting energy gap was found to decrease at a greater rate than the transition temperature indicating a trend towards weaker coupling. The magnitude of this trend was determined and found to be in good agreement with the theoretical prediction of Trofimenkoff and Carbotte (1970).

The pressure dependence of the principle phonon peaks of the system was also investigated including the localised mode first observed by Rowell et al (1965), and the corresponding Grüneisen mode gammas for these peaks calculated. Further information

regarding the pressure dependence of the phonon spectrum was obtained using the McMillan inversion programme (1965) for the $Pb_{64}In_{36}$ alloy. Data extracted by this process were used in conjunction with the McMillan equation for T_c (1968) from which fairly good agreement of the predicted pressure dependence of T_c with the directly obtained experimental value was in evidence.

By combining existing experimental data on the density of states at the Fermi surface with experimental results obtained here for the re-normalisation function, the pressure dependence of the band structure density of states has been derived. The values so obtained are in obvious disagreement with that of the free electron gas. Based on existing experimental evidence (Anderson and Gold (1965) and Anderson et al (1966)) and simple assumptions therefore, a value for the pressure dependence of the band structure density of states at the Fermi surface has been derived for the case of pure lead (which is not expected to differ greatly from the case at hand).

The use of tunnel junctions as sensitive pressure monitoring devices is strongly advocated. Their response to pressure has been found to be sensitive and reproducible while being almost independent of temperature.

ACKNOWLEDGEMENTS

I would like to extend my sincerest thanks to Dr. J.P. Franck who in supervising this research has provided inspiration and help while at the same time allowing me the freedom to pursue my own ideas.

A vote of thanks is also extended to Allan O'Shea who provided technical expertise that was second to none.

I am thankful to the Physics Department for their services and financial support. In the latter regard I would also like to gratefully acknowledge the financial support of the National Research Council of Canada.

Janet has done a tremendous job on the typing. Without her by my side I would have been beside myself.

TABLE OF CONTENTS

CHAPTER PAGE

I INTRODUCTION 1

II THEORETICAL CONSIDERATIONS 3

1. Towards the Microscopic Theories of B.C.S. and Bogoliubov 3
2. The B.C.S. Hamiltonian 5
3. The Bogoliubov Valatin Formalism 8
4. The Superconducting Ground State and Energy Gap (T = 0) 16
5. Finite Temperature Considerations and the Transition Temperature 20
6. Theory of Tunnelling and the Density of States 23
7. Strong Coupling Theory 29
8. Observation of Phonon Structure by Tunnelling 36
9. The Localised Mode 37

III EXPERIMENTAL APPARATUS 40

1. The Cryostat 40
2. The Bomb 44
3. Sample Housing and Holder 47
4. High Pressure Production and Measurement . . . 49
5. The High Pressure Electrical Feedthrough . . . 50

CHAPTER PAGE

III 6. Vacuum Deposition 54

7. Temperature Measurement 55

IV ELECTRONIC DETECTION TECHNIQUES 56

1. The Principle of the Measurement 56

2. Detection of the Harmonics 57

3. Circuit Design Considerations 60

4. The Constant Current Bridge 61

5. The Constant Voltage Bridge 65

V EXPERIMENTAL METHOD 68

1. Sample Fabrication 68

2. Mounting Procedure 69

3. Validity Checks 70

4. An Experimental Run 71

5. Determination of Sample Composition 73

VI EXPERIMENTAL RESULTS AND DISCUSSION 78

1. Introduction 78

2. Pressure Dependence of the Transition Temperature 79

3. The Energy Gap and its Dependence on Pressure 83

4. Pressure Dependence of the Phonon Spectrum . . 92

a. Directly Observed Principle Phonon Characteristics 92

b. Inversion of the Eliashberg Gap Equations 105

CHAPTER PAGE

VI 5. The Tunnel Junction as a Pressure Sensing Device 117

6. Pressure Dependence of the Density of States . 130

VII CONCLUSIONS 138

BIBLIOGRAPHY 140

LIST OF TABLES

Table	Description	Page
1	Pressure Dependence of the Transition Temperature	80
2	Comparative Transition Temperatures (at Zero Pressure)	81
3	Pressure Dependence of the Energy Gap	87
4	Comparative Pressure Dependence of the Energy Gap	88
5	Relative Rate of Change of the Energy Gap and Transition Temperature	90
6	Pressure Dependence of the Principle Phonon Peaks	101
7	Comparative Pressure Dependence of the Principle Phonon Peaks	102
8	Grüneisen Gammas of the Predominant Phonon Modes	104
9	Grüneisen Gammas Calculated from the Data of Galkin et al (1973)	104
10	Parameters Obtained from the Inversion Programme	115
11	Temperature and Pressure Values Along Isochores of He^4 at 400 Bar Intervals Starting with the Pressure at 0 K	126
12	Pressure Values (in p.s.i.) Along Isochores of Fluid Helium	128
13	Pressure Dependence of the Density States (Per Unit Volume)	131

LIST OF FIGURES

Figure Page

1 Cryostat 41

2 Energy Gap Region for a Pb Al Junction at ~1.2K 42

3 He^4 Phase Diagram 45

4 High Pressure Bomb 46

5 Sample Housing and Holder 48

6 High Pressure Feedthrough 51

7 Circuit Logic 58

8 Constant Current Bridge (and support systems) 62

9 Constant Voltage Bridge 63

10 Sweep Circuit 64

11 R(293)/R(4) Vs Indium Concentration 75

12 Gap Region for a $Pb_{64}In_{36}$ Sample (T = 2.51) 85

13 Comparison with the B.C.S. Theory (P = 0) 94

14 Comparison with the B.C.S. Theory (P = 0) 95

15 First and Second Derivatives for a $Pb_{64}In_{36}$ Sample (P = 0) 97

16 Conductance Vs Energy for a $Pb_{88}In_{12}$ Sample 98

17 Conductance Vs Energy for a $Pb_{64}In_{36}$ Sample 99

18 First and Second Derivatives (36 at %) in the Vicinity of the Localised Mode 100

19 Input to Inversion Programme for a $Pb_{64}In_{36}$ Sample 108

20 Phonon Spectra of a $Pb_{64}In_{36}$ Sample 109

21 Gap Function for a $Pb_{64}In_{36}$ Sample 110

Figure Page

22 Renormalisation Function for a $Pb_{64}In_{36}$ Sample 111

23 Zero Bias Tunnel Resistance Vs Pressure For a Typical $Pb_{64}In_{36}$ Sample (T~30K) 119

24 Zero Bias Tunnel Resistance Vs Pressure for a Typical $Pb_{88}In_{12}$ Sample (T~30K) 120

25 Tunnel Resistance vs Energy for a Typical $Pb_{64}In_{36}$ Sample - Press = 50,000 p.s.i. 123

26 Tunnel Resistance vs Energy for a Typical $Pb_{64}In_{36}$ Sample - Press = 800 p.s.i. 124

CHAPTER I

INTRODUCTION

The intent of the author in writing this chapter is to bridge the gap between the Table of Contents and the ensuing thesis material.

An attempt has been made in Chapter II to develop the theory which underlies only those aspects relevant to the understanding of the experimental measurements. The chapter begins therefore (after a very brief historical introduction to superconductivity) with an account of the theory leading up to the development of the superconducting transition temperature and energy gap for which a many body approach utilising the Bogoliubov-Valatin transformations has been chosen in favour of the original (and more usually employed) many body theory of Bardeen, Cooper and Schrieffer (1957), henceforth B.C.S. Frequent recourse is however made to the B.C.S. theory. The advantage of this choice is that it can be extended to encompass the theory of electron tunnelling which provided the analytical tool for the study at hand. Extension of the theory to cover the case of the so called strong coupling superconductors follows. The principle difference in the phonon spectrum of the alloys from that of pure lead is the existence of a localised mode of vibration. The final two sections of Chapter II consist firstly of an attempt to account for the observation of phonon processes through electron tunnelling and secondly a simplistic justification for the existence of the localised mode.

Chapters III and IV contain descriptions of the experimental apparatus employed, the latter being devoted entirely to the electronic detection systems (and their operation). Circuit analyses are presented verifying the linear response of the two bridge circuits that were used.

Experimental method is the subject of the fifth chapter.

In Chapter VI, with the exception of section five, ordering of the results (and discussion thereof) has been based on the experimental ease with which they were obtained and more importantly, on the dependence of subsequent sections upon their predecessors.

CHAPTER II

THEORETICAL CONSIDERATIONS

1. Towards the Microscopic Theories of B.C.S. and Bogoliubov

Before developing in detail the theory which underlies the measurements made, it is felt pertinent to very briefly acquaint the reader with some of the historical background leading up to the successful theories of Bardeen, Cooper and Schrieffer (1957) henceforth B.C.S. and of Bogoliubov (1958) the latter being, in the main, the basis of approach used thereafter.

The phenomenon of superconductivity was discovered in 1911 by K. Onnes whilst studying the electrical resistance of mercury at low temperatures when he noticed that at some particular temperature, the resistance of his specimen dropped to a value which he could not differentiate from zero. This temperature came to be known as the transition (or critical) temperature T_c and is probably the best known property characteristic of the superconducting state. Subsequent studies showed this state to exist in numerous metals and alloys and that it was reversible in the sense of other thermodynamic phase changes. Attempts to explain the physical basis for the existence of this new state were first proposed by Gorter and Casimir (1934) and by F. and H. London (1934-1935). Both of these models were of a phenomenological nature treating the electrons in the metal as two fluids, one component being ascribed the properties of normal electrons whilst the other gave rise to the superconducting properties. The

difference in the approaches was that Gorter and Casimir used a thermodynamical treatment whilst the London treatment was electrodynamic in nature.

The first big step towards an understanding of the superconducting state at the microscopic level was achieved by H. Fröhlich (1950) who proposed that the critical temperature of a superconductor was related to its isotopic mass according to $T \propto M^{-\frac{1}{2}}$ and thus indicating that the lattice was instrumental in the onset of superconductivity. In arriving at this result, Fröhlich had considered the interaction of electrons with the lattice (virtual phonon exchange) and concluded that if such interactions, which were attractive, could overcome the normal electrostatic repulsion between these electrons then the superconducting state would be realised. This attempt proved quantitatively inadequate but the lattice involvement had been arrived at which was the key to the eventual successful microscopic theories.

In 1956, Cooper showed that two electrons of opposite momenta and spin interacting via a momentum dependant potential formed a bound state above the Fermi surface if the interaction between them was attractive no matter how weak. At this time, evidence was growing suggesting the existence of an energy gap in the single particle electron density of states near the Fermi surface.

Based mainly on the mechanism proposed by Fröhlich and the refinements of Cooper, invoking the pair concept, an extensive and successful theory of the superconducting state was developed by Bardeen, Cooper and Schrieffer in 1957 and, using a different mathematical approach, by Bogoliubov in 1958 from which such properties as the transition

temperature and the suggested single particle energy gap naturally arose. These theories were later extended to describe the so called strong-coupling superconductors which were found to exhibit structure in the electronic density of states curve which could not be accounted for by either of the above mentioned theories. These and other deviations from the B.C.S. predictions have been attributed to the specific nature of the lattice involvement with superconductivity in which for some classes of superconductors the electron phonon interaction is weak and can be described by the B.C.S. or Bogoliubov theories whilst for others the interaction is strong and necessitates a different approach. That class of superconductors which can be adequately described by the theories of B.C.S. or Bogoliubov have therefore become known as weak coupling (or B.C.S.) superconductors as opposed to those in which the lattice involvement is more prominent which are known as strong-coupling superconductors.

2. The B.C.S. Hamiltonian

In an attempt to arrive at a pervasive theory for superconductivity the search leant towards finding an interaction between electrons which would be attractive since this would lead to a lowering of the total energy of the superconducting state with respect to that of the normal state as was being found experimentally. In view of the growing belief that the lattice was involved with the onset of superconductivity and with the success of the isotope effect, the Hamiltonian of Fröhlich (from which the isotope effect evolved) seemed an obvious starting

point for the development of the theory. This Hamiltonian may be written explicitly in the form

$$H_{Fr} = H_o + \sum_{ksk's'q} W_{kk'q} c^{\dagger}_{k'+q,s} c^{\dagger}_{k-q,s} c_{ks} c_{k's'} \qquad 2\text{-}1$$

where $W_{kk'q}$ is a matrix element of the form $\dfrac{|M_q|^2 \hbar\omega_q}{(\varepsilon_k - \varepsilon_{k-q})^2 - (\hbar\omega_q)^2}$ 2-2

H_o represents the system of noninteracting electrons and phonons whilst the succeeding term represents the interaction of electrons with the lattice. In physical terms we may think of the interactive term as representing a self-energy associated with the electrons in the following way. An electron moving through the lattice distorts the lattice (ion sites), the lattice in turn then reacts on the electron due to its changed electrostatic field. As the electron passes by, the lattice is allowed to relax. Such distortions of the lattice are quantised in terms of phonons and we may therefore think of the electrons moving through the lattice constantly absorbing and re-emitting phonons. This surrounding of the electrons by phonons has given rise to the concept of "dressed" or "clothed" electrons. The ability of such a dressed electron to repel a second electron in its vicinity is therefore reduced by this positive screening effect and it is this reduction of its potential to repel that is referred to as the self-energy of the electron. It should be noted that the exchanged phonons are very short lived and that as a consequence of the uncertainty principle, energy need not be conserved in the process, to this end the phonons involved are virtual.

Fröhlich's proposal therefore was that the desired attractive interaction could be realised if this screening of the conduction

electrons by the positive ion lattice sites was such as to invoke an effective attractive force between electrons which was larger than their ability to repel each other as bare electrons. The lowering in total energy (condensation energy) associated with the superconducting phase change as predicted by this model turned out to be three or four orders of magnitude greater than that observed. It can be seen from 2-1 that the Fröhlich Hamiltonian included interactions between electrons of all momenta and either spin and was in fact the reason for the over estimate of the condensation energy.

A refinement proposed by Cooper in 1956 eventually led to an acceptable form for the Hamiltonian when he showed that if there was a net attraction between a pair or electrons just above the Fermi surface then they could form a bound state. He also showed that such electrons which could form this bound state by phonon mediation must be within an energy range $\simeq\hbar\omega_q$ of the Fermi surface where $\hbar\omega_q$ is of the order of an average phonon energy of the metal, and that for maximum lowering of energy all such pairs must have the same total momentum. This model may be visualised as follows. One electron moving through the lattice distorts the lattice thereby emitting a phonon. The second electron in the vicinity is then affected by this disturbance (phonon absorption) as it propagates through the lattice. If the energy of the phonon which mediates the process is greater than the electronic energy change invoked thereby, then the resulting interaction is attractive. Such pairs of electrons are referred to as Cooper pairs.

This pair concept was extended to the macroscopic occupation level by Bardeen, Cooper and Schrieffer who formulated a reduced

problem in which only pairs whose constituents had equal and opposite momentum were considered. This reduces the Fröhlich Hamiltonian to:-

$$H_{BCS} = \sum_{ks} \varepsilon_k c^\dagger_{ks} c_{ks} - \tfrac{1}{2} \sum_{kk's} V_{kk'} c^\dagger_{k's'} c^\dagger_{-k's} c_{-ks} c_{ks'} \qquad 2\text{-}3$$

where $V_{kk'} = -2W_{-k,k,k'-k} - U_{kk'}$ 2-4

$U_{kk'}$ is a screened Coulomb repulsion term added to the Fröhlich Hamiltonian of 2-1. If $V_{kk'}$ is positive then the electron-electron interaction is attractive.

It can be shown that the ground state energy described by this Hamiltonian is minimised if, in addition to pairing only electrons whose momenta are equal and opposite, we also require that such paired electrons have opposite spin. Thus by imposing this restriction and applying the convention that an operator preceded by a minus sign implies a spin down state whilst one with a positive sign implies a spin up state e.g. $c^\dagger_{k'} \equiv c^\dagger_{k'\uparrow}$; $c^\dagger_{-k'} \equiv c^\dagger_{(-k')\downarrow}$, we can write the Hamiltonian of B.C.S. as

$$H_{BCS} = \sum_{k} \varepsilon_k (c^\dagger_k c_k + c^\dagger_{-k} c_{-k}) - \sum_{kk'} V_{kk'} c^\dagger_{k'} c^\dagger_{-k'} c_{-k} c_k \qquad 2\text{-}5$$

It is at this juncture that we depart from the B.C.S. development and proceed instead to study the eigenvalues and eigenstates of this Hamiltonian according to the Bogoliubov method.

3. The Bogoliubov Valatin Formalism

We next proceed to diagonalise the Hamiltonian given by 2-5 by first introducing a transformation to a new operator system defined by:-

$$\gamma_k = u_k c_k - v_k c_{-k}^\dagger \qquad \gamma_{-k} = u_k c_{-k} + v_k c_k^\dagger$$

and their conjugates

$$\gamma_k^\dagger = u_k c_k^\dagger - v_k c_{-k} \qquad \gamma_{-k}^\dagger = u_k c_{-k}^\dagger + v_k c_k \qquad 2\text{-}6$$

u and v are chosen to be real constants related by the condition

$$u_k^{\,2} + v_k^{\,2} = 1 \qquad 2\text{-}7$$

Such a choice ensures that the newly defined operators satisfy the Fermi anticommutation laws namely:-

$$[A_p^\dagger, A_q^\dagger]_+ = [A_p, A_q]_+ = 0 \qquad [A_p, A_q^\dagger]_+ = \delta_{pq} \qquad 2\text{-}8$$

where the A represents either the newly created operators or the traditional electron (c type) annihilation and creation operators. In order to justify the relationship 2-7 one such commutation relation for the new operator system is shown here.

$$[\gamma_k, \gamma_k^\dagger] = (u_k c_k - v_k c_{-k}^\dagger)(u_k c_k^\dagger - v_k c_{-k}) + (u_k c_k^\dagger - v_k c_{-k})(u_k c_k - v_k c_{-k}^\dagger)$$

multiplying out and regrouping terms yields

$$= u_k^{\,2}[c_k, c_k^\dagger]_+ - u_k v_k [c_k, c_{-k}]_+ - u_k v_k [c_{-k}^\dagger, c_k^\dagger]_+ + v_k^{\,2}[c_{-k}^\dagger, c_{-k}]_+$$

$$= u_k^{\,2} + v_k^{\,2} \equiv 1 \quad \text{using assumption 2-7}$$

The inverses of the B.V. transformations are easily obtained in the following form:-

$$c_k = u_k\gamma_k + v_k\gamma_{-k}^\dagger \qquad c_k^\dagger = u_k\gamma_k^\dagger + v_k\gamma_{-k}$$

$$c_{-k} = u_k\gamma_{-k} - v_k\gamma_k^\dagger \qquad c_{-k}^\dagger = u_k\gamma_{-k}^\dagger - v_k\gamma_k \qquad 2\text{-}9$$

We next proceed to transform the B.C.S. Hamiltonian to our new operator system. Writing 2-5 as the sum of kinetic and interaction terms we have:-

$$H_{BCS} = H_T + H_V = H_{BV} \text{ (in the transformed system)} \qquad 2\text{-}10$$

Considering first the term H_T, we have:-

$$H_T = \sum_k \varepsilon_k (c_k^\dagger c_k + c_{-k}^\dagger c_{-k})$$

$$= \sum_k \varepsilon_k \{(u_k \gamma_k^\dagger + v_k \gamma_{-k})(u_k \gamma_k + v_k \gamma_{-k}^\dagger) + (u_k \gamma_{-k}^\dagger - v_k \gamma_k)$$

$$x(u_k \gamma_{-k} - v_k \gamma_k^\dagger)\}$$

$$= \sum_k \varepsilon_k [u_k{}^2 \gamma_k^\dagger \gamma_k + v_k{}^2 \gamma_{-k} \gamma_{-k}^\dagger + u_k v_k (\gamma_k^\dagger \gamma_{-k}^\dagger + \gamma_{-k} \gamma_k) + v_k{}^2 \gamma_k \gamma_k^\dagger +$$

$$u_k{}^2 \gamma_{-k}^\dagger \gamma_{-k} - u_k v_k (\gamma_{-k}^\dagger \gamma_k^\dagger + \gamma_k \gamma_{-k})] \qquad 2\text{-}11$$

For simplicity we write this expression term by term as

$H_T \equiv \sum_k \varepsilon_k [P + Q + R + S + T + U]$ then using the anticommutation laws

for the γ

$$R + U = 2u_k v_k (\gamma_k^\dagger \gamma_{-k}^\dagger + \gamma_{-k} \gamma_k)$$

$$Q = v_k{}^2 \gamma_{-k} \gamma_{-k}^\dagger = v_k{}^2 (1 - \gamma_{-k}^\dagger \gamma_{-k})$$

$$S = v_k{}^2 \gamma_k \gamma_k^\dagger = v_k{}^2 (1 - \gamma_k^\dagger \gamma_k)$$

$$P + S = v_k{}^2 + (u_k{}^2 - v_k{}^2) \gamma_k^\dagger \gamma_k$$

$$T + Q = v_k{}^2 + (u_k{}^2 - v_k{}^2) \gamma_{-k}^\dagger \gamma_{-k}$$

before re-collecting these terms, new number operators are defined for the gammas in analogy with the electron number operators i.e.

$$\gamma_k^\dagger \gamma_k \equiv m_k \quad \text{and} \quad \gamma_{-k}^\dagger \gamma_{-k} \equiv m_{-k}$$

We can thus write H_T in the following way,

$$H_T = \sum_\kappa \varepsilon_k [(P + S + T + Q) + (R + U)]$$

to get:-

$$H_T = \sum_k \varepsilon_k[2v_k^2 + (u_k^2 - v_k^2)(m_k + m_{-k}) + 2u_k v_k(\gamma_k^\dagger\gamma_{-k}^\dagger + \gamma_{-k}\gamma_k)] \qquad 2\text{-}12$$

The interaction term H_V of equation 2-10 is treated in a similar fashion (more extensive use is made of the commutation relations and the grouping of terms requires greater insight due to the complexity of this term) to yield

$$H_V = -\sum_{kk'} V_{kk'}[u_{k'}v_{k'}u_k v_k(1 - m_{k'} - m_{-k'})(1 - m_k - m_{-k}) +$$

$$u_{k'}v_{k'}(1 - m_{k'} - m_{-k'})(u_k^2 - v_k^2)(\gamma_{-k}\gamma_k + \gamma_k^\dagger\gamma_{-k}^\dagger)] +$$

$$\text{(fourth order off diagonal terms)} \qquad 2\text{-}13$$

The Hamiltonian is now diagonalised for the ground state of the superconductor for which we assume that all the occupation numbers such as m_k vanish. This is achieved by requiring that the sum of off diagonal contributions to H_{BV} from H_T and H_V cancel one another i.e.

$$\sum_k 2\varepsilon_k u_k v_k(\gamma_k^\dagger\gamma_{-k}^\dagger + \gamma_{-k}\gamma_k) - \sum_{kk'} V_{kk'}u_{k'}v_{k'}(u_k^2 - v_k^2)(\gamma_k^\dagger\gamma_{-k}^\dagger + \gamma_{-k}\gamma_k)$$

$$= 0 \qquad 2\text{-}14$$

in which the assumption is made that the expectation value of the fourth order off diagonal elements is negligible in the ground state of the system. Elimination of the off diagonal elements in this manner enables us to consider the system as being composed of independent fermions. Considering equation 2-14 term by term we get:-

$$2\varepsilon_k u_k v_k - (u_k^2 - v_k^2)\sum_{k'} V_{kk'}u_{k'}v_{k'} = 0 \qquad 2\text{-}15$$

which dictates the form that u and v (the B.V. transformation) must have to be consistent with the diagonalisation condition. Since u and v are interrelated they may be defined in terms of a single

parameter as follows:-

$$u_k = (\tfrac{1}{2} - x_k)^{\frac{1}{2}} \quad \text{and} \quad v_k = (\tfrac{1}{2} + x_k)^{\frac{1}{2}} \qquad 2\text{-}16$$

Equation 2-15 then becomes

$$2\varepsilon_k(\tfrac{1}{4} - x_k^{\,2})^{\frac{1}{2}} + 2x_k\,\Delta_k \qquad 2\text{-}17$$

where we have introduced a new quantity defined by:-

$$\Delta_k = \sum_{k'} V_{kk'}(\tfrac{1}{4} - x_{k'}^{\,2})^{\frac{1}{2}} \qquad 2\text{-}18$$

Thus $$x_k = \frac{\pm\varepsilon_k}{2(\varepsilon_k^{\,2} + \Delta_k^{\,2})^{\frac{1}{2}}} \qquad 2\text{-}19$$

substitution for x_k in 2-18 yields a form for Δ_k:-

$$\Delta_k = \tfrac{1}{2}\sum_{k'} V_{kk'} \frac{\Delta_{k'}}{(\varepsilon_{k'}^{\,2} + \Delta_{k'}^{\,2})^{\frac{1}{2}}} \qquad 2\text{-}20$$

This latter equation represents an integral equation which can in principle be solved if we know the form of the interaction potential $V_{kk'}$. In order to conserve the total number of particles in the system we must choose the Fermi surface as the zero level of energy for the system. The proof of this is seen below which also enables us to decide upon the sign in equation 2-19. The number of electrons in the system is given by:-

$$N = \sum_k (c_k^{\dagger} c_k + c_{-k}^{\dagger} c_{-k})$$

The expectation value of N is, using equation 2-12:-

$$\langle o|N|o\rangle = N\langle o|o\rangle = \langle N\rangle = \sum_k \langle o|2v_k^{\,2}|o\rangle + \langle o|(u_k^{\,2} - v_k^{\,2})$$

$$x(m_k + m_{-k})|o\rangle + \langle o|2u_k v_k(\gamma_k^{\dagger}\gamma_{-k}^{\dagger} + \gamma_{-k}\gamma_k)|o\rangle \qquad 2\text{-}21$$

Now for the ground state of the system the $m_k \equiv 0$ in the second term

whilst the third term can be shown to produce only zero eigenvalues by replacing the γ according to equation 2-6. Thus the expectation value of N reduces to:-

$$\langle N\rangle = \sum_k 2v_k^{\,2} = \sum_k (1 + 2x_k) \qquad 2\text{-}22$$

If we had no interactions i.e. all the electrons resided below the Fermi surface then we know that N must have the form

$$\langle N\rangle = \sum_{k<k_f} 2 \quad \text{and} \quad \langle N\rangle = 0 \text{ for } k>k_f \qquad 2\text{-}23$$

where the factor of two arises because of the dual spin nature of fermions. For the non interacting case then we must put $V_{kk'} \equiv 0$ and thus from equation 2-18, $\Delta_k \equiv 0$ also. By substitution then in equation 2-19, we see for the non interacting case that:-

$$x_k = \pm\tfrac{1}{2}$$

Where the positive sign is chosen to represent the system below the Fermi surface and the negative sign for above the Fermi surface thereby making equation 2-22 consistent with the real physical situation of equation 2-23. So for the normal metal the B.V. transformation has the form

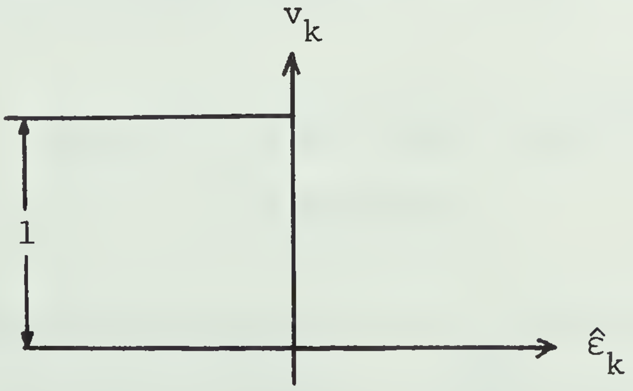

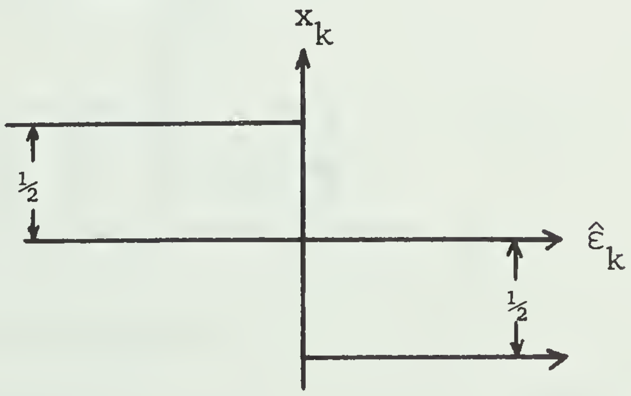

Where $\hat{\varepsilon}_k$ here and henceforth will be used to denote measurements with respect to the Fermi surface. Turning attention now to the

interacting case ($V_{kk'} \neq 0$) of a superconductor we can see from equation 2-22 that for the number of particles to be conserved that x_k must be an odd function of $(\varepsilon_k - \varepsilon_f)$ as was the case above and thus we choose the negative sign for x_k and have therefore:-

$$x_k = -\tfrac{1}{2} \frac{\hat{\varepsilon}_k}{(\hat{\varepsilon}_k^{\,2} + \Delta_k^{\,2})^{\frac{1}{2}}} \qquad 2\text{-}24$$

Notice that $V_{kk'} \to 0$ (and hence $\Delta_k \to 0$) has the highly desirous effect of encompassing the normal metal case. Equation 2-24 describes the form that the B.V. transformations (i.e. the restriction on our original u and v) must have for the Hamiltonian to be of diagonal form and are shown pictorially below.

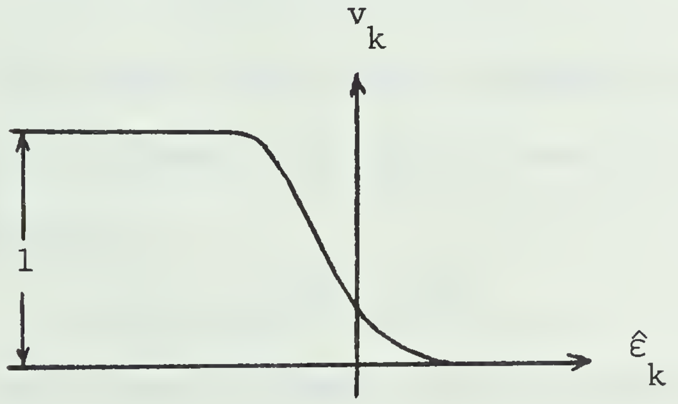

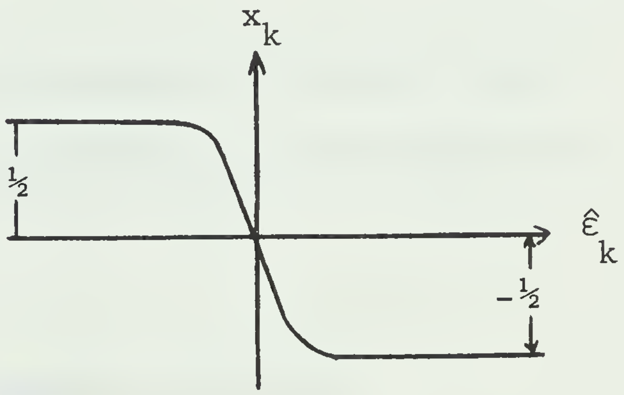

Bardeen, Cooper and Schrieffer solved equation 2-20 for delta using a very simple potential for which they proposed the form

$$V_{kk'} = \begin{cases} V \text{ for } |\hat{\varepsilon}_k| \;\&\; |\hat{\varepsilon}_{k'}| < \hbar\omega_D \\ 0 \text{ otherwise} \end{cases}$$

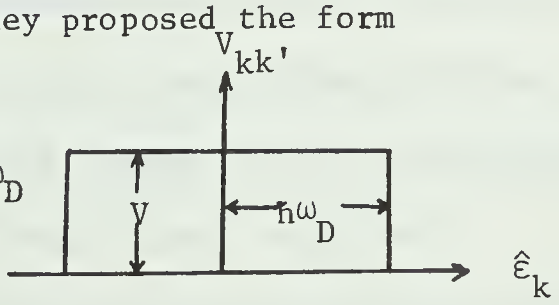

Expressed in integral form, equation 2-20 becomes

$$\Delta_k = \tfrac{1}{2} \int_{-\infty}^{\infty} D(\varepsilon_{k'}) \frac{\Delta_{k'}}{(\hat{\varepsilon}_{k'}^{\,2} + \Delta_{k'}^{\,2})^{\frac{1}{2}}} V_{kk'} \, d\varepsilon_{k'} \qquad 2\text{-}25$$

Since $V_{kk'}$ is constant and so is $\hbar\omega_D$, (the Debeye energy) then it follows that Δ_k is constant and we may therefore omit the subscripts and take V outside the integral. $D(\hat{\varepsilon}_{k'})$ represents the density of electron states (for electrons of one spin) and is assumed constant at the Fermi surface thus equation 2-25 reduces to

$$= \frac{VD}{2} \int_{-\hbar\omega_D}^{\hbar\omega_D} \frac{\Delta}{(\hat{\varepsilon}^2 + \Delta^2)^{\frac{1}{2}}} \, d\hat{\varepsilon}$$

This integral can now be easily solved using the substitution $\hat{\varepsilon} = \Delta \sinh x$ to yield

$$\Delta = \hbar\omega_D / \{\sinh(1/DV)\} \qquad 2\text{-}26$$

For a great many metals, estimates of the quantity (DV) yield values $\lesssim 10^{-1}$ whence it is easy to see from the definition of the hyperbolic function

$$\sinh x = \tfrac{1}{2}(e^x - e^{-x})$$

that we may reasonably make an approximation to 2-26 of

$$\Delta = 2\hbar\omega_D \exp[-1/VD(\varepsilon_f)] \qquad 2\text{-}27$$

Those metals for which the above approximation is valid are said to be weak-coupling superconductors. It can be seen from 2-27 that Δ is an extremely small quantity and that because of this the parameter x_k defined by equation 2-24 differs from $\pm\frac{1}{2}$ only very close (within $\pm\Delta$) of the Fermi surface. Examining this implication from a wider viewpoint we see that as a consequence of x_k having the values $\pm\frac{1}{2}$ in regions remote from the Fermi surface, the values of u and v become either unity or zero and hence from equation 2-6

we see that our newly introduced operators gamma revert back to a single c type operator as in the case of a normal metal.

We have to this point then built up a picture of a superconductor which resembles a normal metal except within a small region bounding the Fermi surface where the electrons interact in a very specific manner. The nature of this interaction is the pair concept alluded to earlier and the gamma operators set forth at the beginning of this section are those which create and destroy such Cooper pairs. The term quasiparticle is used to describe a single electron while in a paired state. The parameter Δ is associated with the energy of formation (or destruction) of such pairs. It is the very small lowering of energy associated with the pairing of electrons combined with the fact that this pairing only occurs in a very restricted region at the Fermi surface that accounts so nicely for the experimentally observed small lowering of the total energy of the metal when in the superconducting state.

4. The Superconducting Ground State and Energy Gap (T = 0)

Having established in the previous section the condition that the off diagonal elements of $H_{BV} = H_T + H_V$ vanish, we are left with the diagonalised Hamiltonian

$$H_{BV} = \sum_k \hat{\varepsilon}_k [2v_k{}^2 + (u_k{}^2 - v_k{}^2)(m_k + m_{-k})] - \sum_{k,k'} V_{kk'} u_{k'} v_{k'} u_k v_k (1 - m_{k'} - m_{-k'})(1 - m_k - m_{-k}) \qquad 2\text{-}28$$

which in the ground state where the $m \equiv 0$ reduces to

$$H_{BVG} = \sum_k 2\hat{\varepsilon}_k v_k^2 - \sum_{kk'} V_{kk'} u_{k'} v_{k'} u_k v_k \qquad 2\text{-}29$$

The ground state wave function Ψ_o for the superconductor must be an eigenfunction of the diagonalised Hamiltonian so that for all possible k:-

$$\gamma_k |\Psi_o> = \gamma_{-k} |\Psi_o> = 0 \qquad 2\text{-}30$$

This in effect is an attempt to create a state lower than the ground state defined by Ψ_o. In order to find the form of Ψ_o the following argument is extended. Since the gammas obey the usual Fermi anticommutation laws, products such as $\gamma_k\gamma_k = \gamma_{-k}\gamma_{-k} = 0$ and so equation 2-30 is satisfied by operating on the vacuum state with all of the possible products of the operators γ_k and γ_{-k} because such products would always contain a product of the type $\gamma_k\gamma_k$ and thereby yield a zero eigenvalue. For all possible k values therefore this may be stated as

$$|\Psi_o> = (\prod_k \gamma_k \gamma_{-k})|o> = [\prod_k (u_k c_k - v_k c_{-k}^{\dagger})(u_k c_{-k} + v_k c_k^{\dagger})]|o> \qquad 2\text{-}31$$

where again use has been made of the original definition of the gammas. This expression simplifies by using the anticommutation relations and normalising throughout by the product of all of the v_k to give for the ground state wave function

$$|\Psi_o> = \prod_k (u_k - v_k c_{-k}^{\dagger} c_k^{\dagger})|o> \qquad 2\text{-}32$$

It is possible to justify the above expression on a purely mathematical basis in which we first propose the form for $|\Psi_o>$ as given in 2-32 and show that it is consistent with the physical proposal of equation 2-30, the derivation for which will not be presented here.

Quasiparticle excitations of the system can be created simply by acting upon the ground state wave function with the creation operators $\gamma_k^\dagger$ and $\gamma_{-k}^\dagger$.

The ground state energy of the superconducting state ε_s can be obtained by calculating the expectation value of the Hamiltonian given by equation 2-29.

$$\varepsilon_s = \langle H_{BVG} \rangle = \langle o | \sum_k 2\hat{\varepsilon}_k v_k{}^2 - \sum_{kk'} V_{kk'} u_{k'} v_{k'} u_k v_k | o \rangle$$

Using the model potential proposed by B.C.S. we see that all of the quantities in the above expression are constants and therefore

$$\varepsilon_s = \sum_k 2\hat{\varepsilon}_k v_k{}^2 - \sum_{kk'} V_{kk'} u_{k'} v_{k'} u_k v_k \qquad 2\text{-}33$$

When excitations are present however ($m \neq 0$) we must revert to the Hamiltonian of equation 2-28 the terms of which may be rearranged to give

$$H_{BV} = \varepsilon_s + \sum_k (m_k + m_{-k})[(u_k{}^2 - v_k{}^2)\hat{\varepsilon}_k + 2u_k v_k \sum_{k'} V_{kk'} u_{k'} v_{k'}]$$

$$+ \text{ higher order terms} \qquad 2\text{-}34$$

and where use has been made of the expression derived for ε_s. By substituting in equation 2-34 (using equations 2-16, 2-20 and 2-22) this expression can be rewritten in the form:-

$$H_{BV} = \varepsilon_s + \sum_k (\hat{\varepsilon}_k{}^2 + \Delta^2)^{\frac{1}{2}} (m_k + m_{-k}) + \ldots\ldots.. \qquad 2\text{-}35$$

It can now be seen that this represents a system whose ground state energy is given by ε_s and whose (quasiparticle) excitations are given by:-

$$E_k = (\hat{\varepsilon}_k{}^2 + \Delta^2)^{\frac{1}{2}} \qquad 2\text{-}36$$

These quasiparticles cannot be created singly since any physical

process is represented by at least two electron operators e.g. scattering, which results in two gamma type operators. The minimum energy required to create (or break up) such a pair of quasiparticles is 2Δ as can be seen from equation 2-36. When a Cooper pair is broken up one electron can be excited across the Fermi surface to a state $(\varepsilon_f + \Delta)$ whilst the other falls back into the Fermi sea $(\varepsilon_f - \Delta)$ until re-pairing with other electrons occurs. In this way the energy gap in the single particle electron density of states that is observed can be visualised.

In analogy with the density of states of a normal metal, the density of quasiparticle states for the superconductor can be deduced from

$$D(E) = \frac{dk}{dE} = \frac{d\hat{\varepsilon}}{dE}\ \frac{dk}{d\hat{\varepsilon}}$$

where $dk/d\hat{\varepsilon}$ is the density of Bloch states of a normal metal.

Using equation 2-36 we find that:-

$$D(E) = \begin{cases} 2D(\varepsilon_f)\dfrac{|E|}{(E^2 - \Delta^2)^{\frac{1}{2}}} & \text{for } |E|>\Delta \\[2ex] 0 & \text{for } |E|\leqslant\Delta \end{cases} \qquad 2\text{-}37$$

Pictorially this compares with the normal metal as below

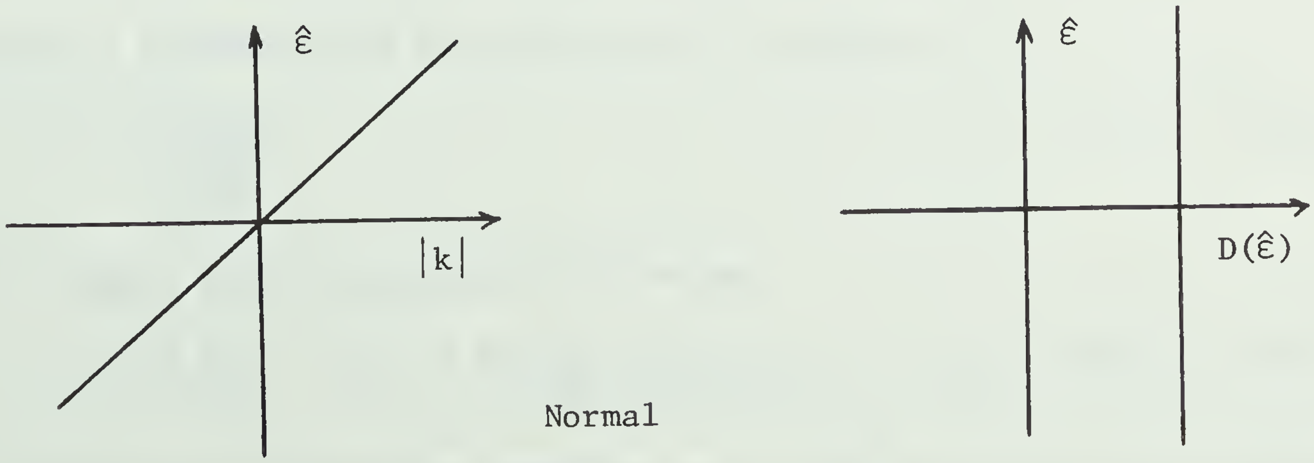

Normal

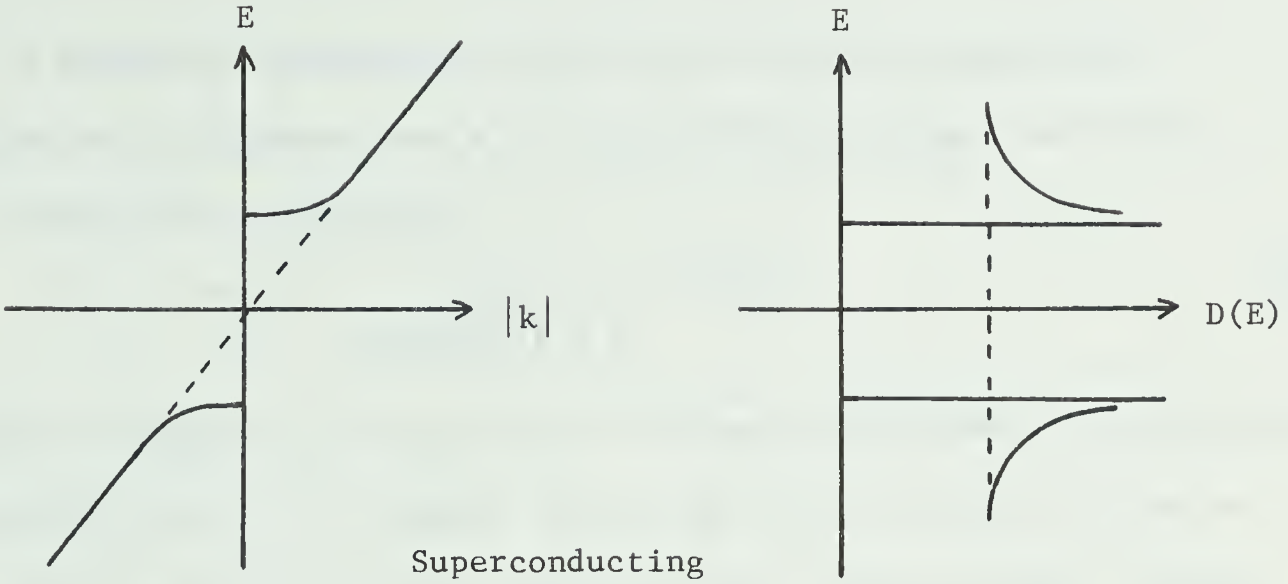

Superconducting

5. Finite Temperature Considerations and the Transition Temperature

In the previous section it had been assumed that the number of quasiparticle excitations was very small, i.e. $\Delta >> kT$, a situation we might envisage as $T \to 0$. We now treat the more physical case of $T \neq 0$ where we no longer assume the number of quasiparticle excitations to be negligible. In so doing we will arrive at a modified form for the quasiparticle excitation energies and energy gap, and derive an expression for the transition temperature. In proceeding, we assume that the Hamiltonian for the system can still be diagonalised (an assumption to be justified). We are left then with the Hamiltonian given by equation 2-28. The energy required to create a quasiparticle excitation will be given by:-

$$E_k = \frac{d\langle H_{BV}\rangle}{d\langle m_k\rangle} \qquad 2\text{-}38$$

If we apply this to equation 2-28 we get

$$E_k = \hat{\varepsilon}_k(u_k^{\ 2} + v_k^{\ 2}) + 2u_kv_k\sum_{k'} V_{kk'}u_{k'}v_{k'}(1 - \langle m_{k'}\rangle - \langle m_{-k'}\rangle) \qquad 2\text{-}39$$

In defining the excitation energies as in 2-38 we may treat the problem

as a system of independent fermions and obtain an approximate solution by replacing the m by their thermal averages according to Fermi-Dirac statistics.

$$\langle m_k \rangle = \langle m_{-k} \rangle = \frac{1}{\exp(E_k/kT) + 1} = f(E_k) \qquad 2\text{-}40$$

The off diagonal terms are treated in exactly the same way as in the previous case (T → 0) except that we do not now assume that the m vanish also, but rather they take the form of their thermal average as in equation 2-40. The resulting expression is:-

$$2\hat{\varepsilon}_k u_k v_k - (u_k^2 - v_k^2)\sum_{k'} V_{kk'} u_{k'} v_{k'} [1 - 2f(E_{k'})] = 0 \qquad 2\text{-}41$$

Comparing this with equation 2-15 we see that they differ only by the factor in the square brackets containing the Fermi function.

We define a modified gap function here which is temperature dependent:-

$$\Delta_k(T) = \sum_{k'} V_{kk'} (\tfrac{1}{4} - x_{k'}^2)^{\frac{1}{2}} [1 - 2f(E_{k'})] \qquad 2\text{-}42$$

The development is now as for the case of T → 0 (with the B.V. transformation x being temperature dependent) and leads to the integral gap equation for non zero T of:-

$$\Delta_k(T) = \tfrac{1}{2}\sum_{k'} V_{kk'} \frac{\Delta_{k'}(T)}{[\hat{\varepsilon}_{k'}^2 + \Delta_{k'}^2(T)]^{\frac{1}{2}}} [1 - 2f(E_{k'})] \qquad 2\text{-}43$$

By substituting into the expression for E_k (equation 2-39) as before and including the explicit form of the Fermi functions given by equation (2-40) we get for the quasiparticle energies

$$E_k = [\hat{\varepsilon}_k^2 + \Delta^2(T)]^{\frac{1}{2}} \qquad 2\text{-}44$$

This expression is exactly that obtained earlier but with the temperature dependent gap function.

Using the model potential of B.C.S. and solving as before the integral equation 2-43 for the gap we find that

$$VD(\varepsilon_f) \int_0^{\hbar\omega_D} \frac{\tanh[(\hat{\varepsilon}^2 + \Delta^2)^{\frac{1}{2}}/2kT]\,d\hat{\varepsilon}}{(\hat{\varepsilon}^2 + \Delta^2)^{\frac{1}{2}}} = 1 \qquad 2\text{-}45$$

This clearly is a very complicated implicit expression for the energy gap at finite temperature. It can be seen however that as T increases, the numerator decreases and therefore for the left hand side of this expression to remain constant equal to unity, the denominator must decrease also. This implies therefore that Δ is a monotonically decreasing function of temperature. Such is the case observed experimentally as shown below; typically

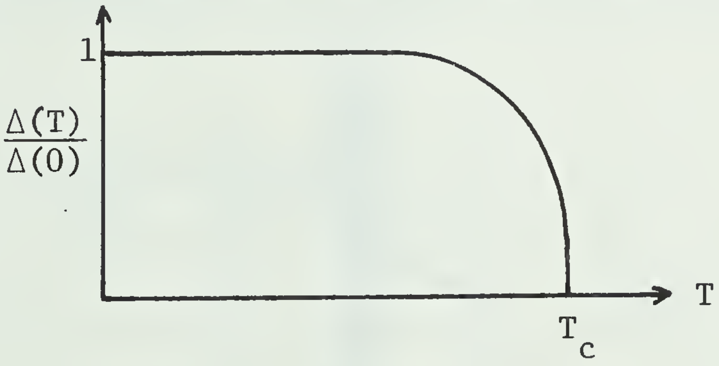

It is very satisfying that if $T \equiv 0$ then this expression yields identically the previous expression derived.

To obtain an expression for the transition temperature we need to impose the condition that $\Delta \to 0$ as $T \to T_c$ in this integral which can then be performed to yield:-

$$kT_c = 1\cdot14\hbar\omega_D \exp[-1/VD(\varepsilon_f)] \qquad 2\text{-}46$$

having made use of the weak coupling approximation $kT_c \ll \hbar\omega_D$.

Recalling the expression for the T = 0 case for $\Delta(0)$ (equation 2-27) and comparing with this we have that, for the simple constant potential model of B.C.S. in the weak coupling assumption:-

$$\frac{2\Delta(0)}{kT_c} = 3.53 \quad \text{UNIVERSALLY} \qquad 2\text{-}47$$

This key result is often used experimentally as an expression of the weak coupling approximation.

6. Theory of Tunnelling and the Density of States

Consideration is now given to the transport of electrons across an insulating barrier. This might be represented by the diagram below for the case when both metals are in the normal state,

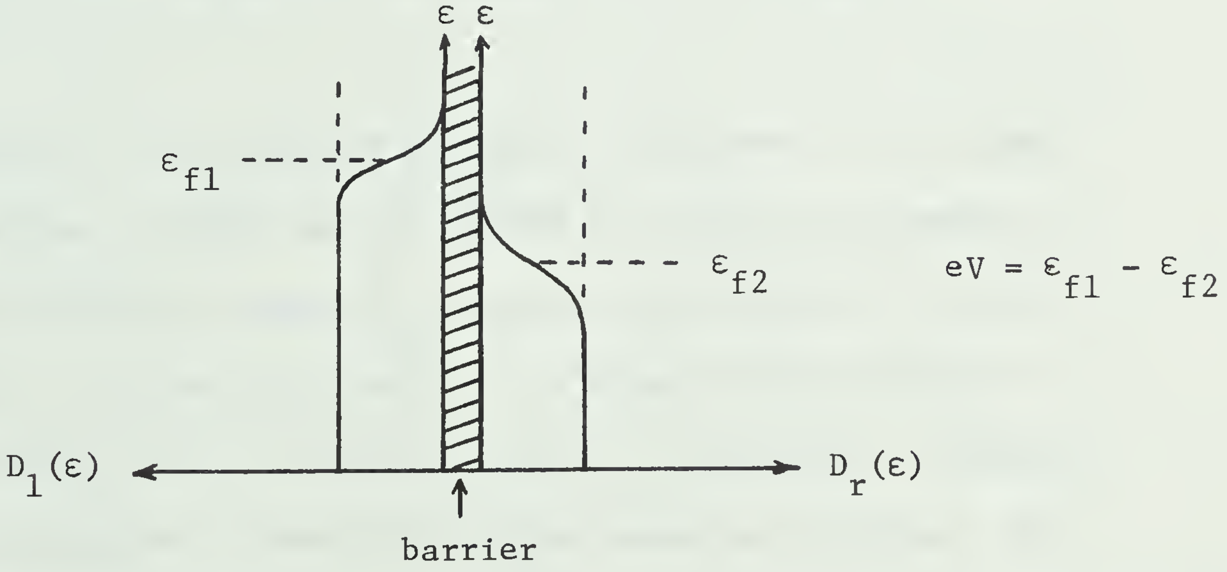

where the Fermi level energy of metal one has been raised by an amount eV with respect to that of metal two. The quantities $D_l(\varepsilon)$ and $D_r(\varepsilon)$ represent the density of electron states in metals one and two respectively. Notice that in accordance with the diagram on page 19 that the dotted line represents the density of available

states in a normal metal whilst the shaded region represents the density of occupied states as obtained by multiplying the $D(\varepsilon)$ by the respective Fermi function.

A Hamiltonian representing this system may be written as the sum of three terms the first of which describes those electrons of metal one on the left hand side and the second for those on the right whilst the third is a term relating to the transfer of electrons from side to side. Thus:-

$$H = \sum_{ks} \varepsilon_k c^{\dagger}_{ks} c_{ks} + \sum_{ks} \varepsilon_k d^{\dagger}_{ks} d_{ks} + \sum_{kk's} T_{kk'} (c^{\dagger}_{ks} d_{k's} + d^{\dagger}_{k's} c_{ks}) \qquad 2\text{-}48$$

Since it is proposed here to calculate the net tunnel current we need only concern ourselves with the third term of this expression. The transition probability in lowest order is given by $|T_{kk'}{}^2| = |T|^2$.

Because of the applied potential difference V, the energy of electrons of metal one are raised in energy by an amount eV. These electrons of energy $\hat{\varepsilon}_k$ can then be elastically scattered (tunnel) to an available state k' in metal two whose energy is given by $(\hat{\varepsilon}_k + eV)$, in this way energy is conserved. A similar argument applies to tunnelling in the opposite direction. The net flow of electrons from left to right is therefore proportional to:-

$$\sum_{kk's} |T^2| [f_k(1 - f_{k'}) - f_{k'}\,(1 - f_k)] \delta(\hat{\varepsilon}_{k'} - \hat{\varepsilon}_k - eV) \qquad 2\text{-}49$$

where the f_k represent the probability of occupancy of a given state k. Expression 2-49 may be interpreted physically if we associate f_k with the probability that the state k from which an

electron originates is occupied and $(1 - f_{k'})$ with the probability that the state k' to which it tunnels is unoccupied, energy conservation being accounted for by the delta function. The tunnel current therefore may be obtained from expression 2-49 by putting it in integral form:-

$$I_{NN} \propto \int T^2 \{f(\hat{\varepsilon}_k) - f(\hat{\varepsilon}_k + eV)\} D(\hat{\varepsilon}_k) D(\hat{\varepsilon}_k + eV) d\hat{\varepsilon}_k \qquad 2\text{-}50$$

In obtaining this we have complied explicitly with the energy conservation aspect. T^2 is taken to be the square of some average tunnelling matrix element. If we were to proceed from this point using the phenomenological approach we would assume that T^2 and D^2 (arising from the density of states product) were constant and extricate them from the integral, here however a brief explanation is given to justify this procedure. Using the particle in a box concept of tunnelling across a narrow potential barrier it can be shown fairly easily that the element T is given by:-

$$T = Ak + B \qquad 2\text{-}51$$

A and B being constants and k being the wave vector in the direction that tunnelling takes place. The kinetic energy $\hat{\varepsilon}_k$ associated with the state k is simply

$$\hat{\varepsilon} = \frac{\hbar^2 k^2}{2m} - \varepsilon_f \Rightarrow \frac{d\hat{\varepsilon}}{dk} = \frac{\hbar^2 k}{m} \qquad 2\text{-}52$$

Thus we see from 2-51 and 2-52

$$T \propto \frac{d\hat{\varepsilon}}{dk} \qquad 2\text{-}53$$

But $$D(\hat{\varepsilon}) = \frac{dN}{d\hat{\varepsilon}} = \frac{dN}{dk}\frac{dk}{d\hat{\varepsilon}} \qquad 2\text{-}54$$

and we can see therefore that the energy dependence of the product

T x D in the integral disappears. If we make the justifiable assumption that dN/dk is constant in the region of the Fermi surface we have for I that

$$I_{NN} \propto D_1(\varepsilon_f) D_r(\varepsilon_f) T^2 \int \{ f(\hat{\varepsilon}_k) - f(\hat{\varepsilon}_k + eV) \} d\hat{\varepsilon}_k \qquad 2\text{-}55$$

This model is consistent with the premise that tunnelling takes place at or near the Fermi surface and that $\varepsilon_f >> eV$.

The factor $f(\hat{\varepsilon}_k + eV)$ in equation 2-55 can now be expanded as a Taylor series about $\hat{\varepsilon}_k$ whereupon after neglecting terms containing powers of (eV) squared and greater we have:-

$$I_{NN} \propto D_1(\varepsilon_f) D_r(\varepsilon_f) T^2 \int eV f'(\hat{\varepsilon}_k) d\hat{\varepsilon}_k$$

At low temperatures, f approximates to a delta function giving:-

$$I_{NN} \propto D_1(\varepsilon_f) D_r(\varepsilon_f) T^2 eV \qquad 2\text{-}56$$

For N - N (normal metal - normal metal) tunnelling thus, an ohmic dependence is predicted.

Attention is now turned to the case where one of the metals is in the superconducting state as depicted below.

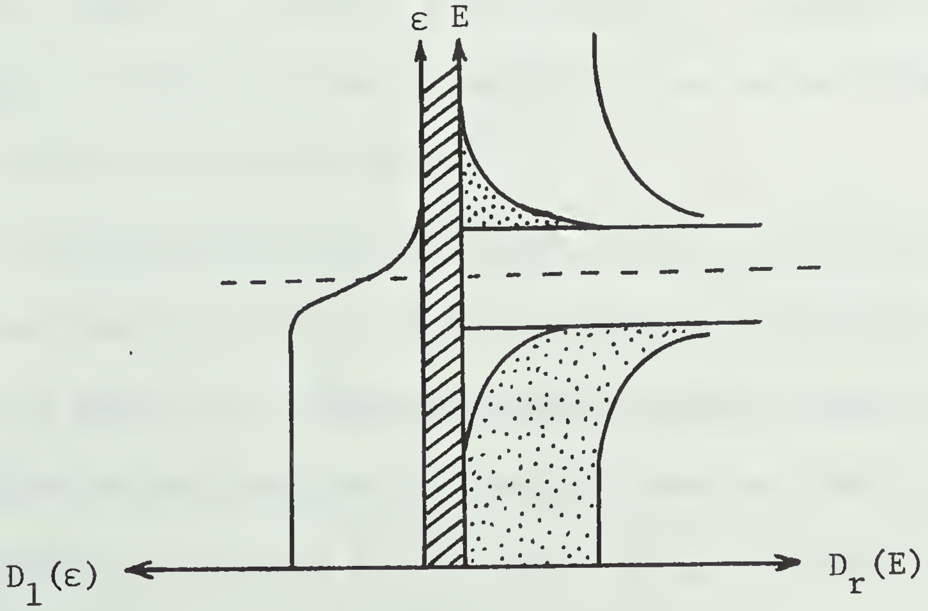

Once again, in an effort to derive an expression for the tunnel current, we need consider only the tunnelling term of the Hamiltonian of equation 2-48 except that those operators previously assigned as d for states on the right hand side (metal two) must now be replaced by their quasiparticle counterparts in keeping with the B.V. formalism adopted earlier. Explicitly we have then:-

$$H_T = \sum_{kk'} T[c_k^\dagger(u_{k'}\gamma_{k'} + v_{k'}\gamma_{-k'}^\dagger) + c_{-k}^\dagger(u_{k'}\gamma_{-k'} - v_{k'}\gamma_{k'}^\dagger) + (u_{k'}\gamma_{k'}^\dagger + v_{k'}\gamma_{-k'})c_k + (u_{k'}\gamma_{-k'}^\dagger - v_{k'}\gamma_{k'})c_{-k}] \qquad 2\text{-}57$$

Notice that the spin has been included explicitly here in keeping with the pair concept and has therefore been omitted from the summation sign, it is also very relevant to recall that if the interaction potential $V_{kk'}$ responsible for the pairing tends to zero then the γ's revert to single electron operators and we have identically the preceeding case for N - N tunnelling.

The physical interpretation of equation 2-57 is as follows. The first term creates an electron on the left hand side of the barrier and either creates or destroys a quasiparticle excitation on the right (above or below the Fermi surface). The other terms may be interpreted in an analogous manner.

For a term such as $c_k^\dagger\gamma_{k'}$ to cause a real scattering (tunnelling) we must have that $E_{k'} = \hat{\varepsilon}_k + eV$ for an applied potential V. Note that in this case we are measuring energies with respect to the Fermi surface as was the case in our previous application of the B.V. formalism. Similarly for the term $c_k^\dagger\gamma_{-k'}^\dagger$ to cause a real scattering process we must have $-\hat{\varepsilon}_k - eV = E_{k'}$.

Extending this type of argument to the remaining terms in 2-57 and proceeding as with the N - N case we get:-

$$I_{NS} \propto \sum_{kk'} |T|^2 (u_{k'}^2 \{f(\hat{\varepsilon}_k)[1 - f(E_{k'})] - f(E_{k'})[1 - f(\hat{\varepsilon}_k)]\} \delta(E_{k'} - \hat{\varepsilon}_k - eV)$$
$$+ v_{k'}^2 \{f(\hat{\varepsilon}_k) f(E_{k'}) - [1 - f(\hat{\varepsilon}_k)][1 - f(E_{k'})]\} \delta(\hat{\varepsilon}_k + E_{k'} + eV)) \quad 2\text{-}58$$

having grouped together terms in u^2 and v^2. By multiplying out, collecting terms and expressing in integral form we have

$$I_{NS} \propto \int T^2 D(\hat{\varepsilon}_k) D(E = \hat{\varepsilon}_k + eV) \{u_{k'}^2 [f(\hat{\varepsilon}_k) - f(\hat{\varepsilon}_k + eV)] +$$
$$+ v_{k'}^2 [f(\hat{\varepsilon}_k) - 1 + f(-\hat{\varepsilon}_k - eV)\} d\hat{\varepsilon}_k \quad 2\text{-}59$$

where the f functions have been included explicitly. Since the metal on the right hand side of the barrier is a superconductor, the density of states function D(E) has the form given by equation 2-37. This expression can be further reduced by noticing that $f(-E) = 1 - f(E)$ to give:-

$$I_{NS} \propto \int T^2 D(\hat{\varepsilon}_k) D(\hat{\varepsilon} + eV) \{f(\hat{\varepsilon}_k)[u_{k'}^2 + v_{k'}^2] - f(\hat{\varepsilon}_k + eV)$$
$$\times [u_{k'}^2 + v_{k'}^2]\} d\hat{\varepsilon}_k \quad 2\text{-}60$$

According to the original B.V. assumption $u^2 + v^2 = 1$ hence we have (replacing $D(\hat{\varepsilon} + eV)$ using 2-37) that:-

$$I_{NS} \propto T^2 D_1(\varepsilon_f) D_r(\varepsilon_f) \int \frac{|E|}{(E^2 - \Delta^2)^{\frac{1}{2}}} [f(\hat{\varepsilon}_k) - f(\hat{\varepsilon}_k + eV)] d\hat{\varepsilon}_k \quad 2\text{-}61$$

where the T^2D^2 term again can be taken outside the integral. This is the first point at which the rigorous physically based theory coincides with the phenomenological approach most often used.

By noting that:-

$$f(\hat{\varepsilon}_k) - f(\hat{\varepsilon}_k + eV) = \begin{cases} 1 \text{ for } 0 < E < eV \\ 0 \ E > eV \text{ or } E < 0 \end{cases}$$

equation 2-61 becomes

$$I_{NS} \propto T^2 D_l(\varepsilon_f) D_r(\varepsilon_f) \int_0^{eV} \frac{|E|}{(E^2 - \Delta^2)^{\frac{1}{2}}} dE$$

where $dE = d\hat{\varepsilon}$ since at $T = 0$, Δ is constant. Finally therefore

$$I_{NS} \propto T^2 D_l(\varepsilon_f) D_r(\varepsilon_f)[(eV)^2 - \Delta^2]^{\frac{1}{2}} \qquad 2\text{-}62$$

For the case $T \neq 0$ the integral is complicated but has been solved. If we now differentiate this expression for I_{NS} with respect to V and divide the result by the derivative of I_{NN} with respect to V, we find that the ratio of these dynamic conductances is:-

$$\frac{\sigma_{NS}}{\sigma_{NN}} = \frac{eV}{[(eV)^2 - \Delta^2]^{\frac{1}{2}}} \qquad 2\text{-}63$$

This expression is precisely the normalised density of states for a superconductor as can be seen from the expression 2-37 derived earlier. We have thus proved that by measuring the normalised dynamic conductance of an N - S tunnel junction we are in fact measuring the electronic quasiparticle density of states of the superconductor. Because of this, fundamental properties such as T_c and $\Delta(0)$ are directly obtainable.

7. Strong Coupling Theory

Whilst the weak coupling theory describes most superconductors extremely well and all superconductors to first order there are some which deviate considerably from its predictions. Mercury and lead are two such examples. Experimental evidence shows the

condensation energy for lead to be less than that predicted using the B.C.S. model and outside the limits of experimental error. The "universal" constant of equation 2-47 relating the gap to transition temperature for lead was found to be 4.47 instead of 3.53.

Yet another striking difference is exhibited by these superconductors in the density of states as observed by tunnelling in that there is considerable departure from the smooth function expected on the basis of equation 2-37. This was first observed in the tunnelling experiments of Giaver et. al. (1962) and Rowell et. al. (1963) and is illustrated below for the case of lead which shows the B.C.S. prediction and the experimentally observed tunnelling density of states of Rowell et. al. (curve ②) taken from R.D. Parks.

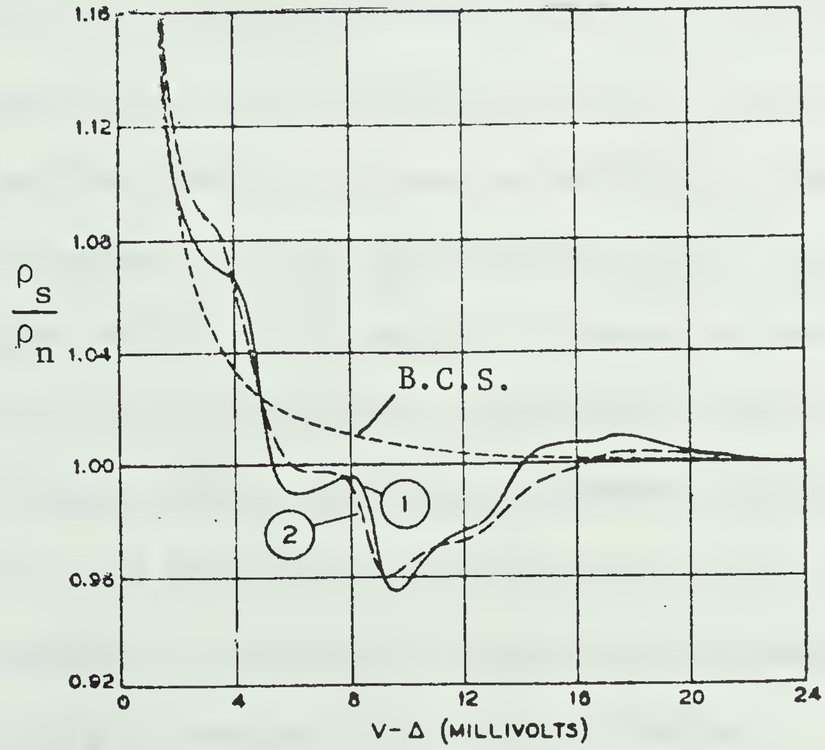

It became clear in the light of such experimental evidence that the existing theory of superconductivity must be modified to explain these differences in behaviour in a class of metals which

have become known as strong-coupling superconductors. The first attempt was to try and extend the weak coupling theory by removing the assumption on the product DV. This was done by D.J. Thouless (1960) who found that even in the unphysical limit of $DV \rightarrow \infty$ the ratio $2\Delta(0)/k_BT_c \rightarrow 4.00$ and although this was a step in the right direction it could not fully account for the observed deviations. The next step was taken by Swihart (1962) who replaced the simple B.C.S. constant potential with a more realistic one. This refinement met with some success but still could not account for the structure in the density of states curve. The correct formalism was finally arrived at through the realisation that the electron-electron interaction, which according to the B.C.S. model was instantaneous, was in fact retarded. This can be understood since the phonons involved with the pairing of electrons move with a phase velocity very much less than the Fermi velocity of the electrons and thus there is a time lag before the second electron "feels" the existence (or is influenced by) the first. In addition to retardation effects, lifetime effects were proposed associated with the damping of quasiparticle excitations. This approach was adopted by Migdal (1958), Nambu and Eliashberg (1960) and Eliashberg (1962) using field theoretic Greens functions (since potentials that are retarded in time cannot be treated with Hamiltonian dynamics). The results of this analysis are presented below:-

$$\phi(\omega) = \int_0^{\omega_c} d\omega' \mathrm{Re} \left(\frac{\Delta'}{(\omega'^2 - \Delta'^2)^{\frac{1}{2}}} \right) [K_+(\omega,\omega') - N(0)U_c] \qquad 2\text{-}64$$

$$\omega[1 - Z(\omega)] = \int_0^{\omega_c} d\omega' \mathrm{Re} \left(\frac{\omega'}{(\omega'^2 - \Delta'^2)^{\frac{1}{2}}} \right) K_-(\omega',\omega) \qquad 2\text{-}65$$

where

$$K_{\pm} = \sum_{\lambda} \int_{0}^{\infty} d\nu\, \alpha_{\lambda}^{2}(\nu) f_{\lambda}(\nu) [(\omega' + \omega + \nu + i0^{+})^{-1} \pm (\omega' - \omega + \nu - i0^{+})^{-1}]$$

Equations 2-64 and 2-65 are referred to as the strong-coupling gap equations. A third relationship is introduced in the form:-

$$\Delta(\omega) = \phi(\omega)/Z(\omega) \qquad 2\text{-}66$$

ω_c represents a cut off energy usually taken to be $\simeq 10\omega_D$, U_c is the Coulomb pseudopotential characterising the short range repulsive force between electrons and $Z(\omega)$ is a renormalisation function given by:-

$$\varepsilon(k,\omega) = \varepsilon/Z(\omega)$$

where ε represents a single particle energy (Bloch state).

We can see that these coupled equations for Δ are complex as is Δ itself in the general case. Clearly Δ is also a function of energy. It may be written in the form

$$\Delta(\omega) = \Delta_1(\omega) + i\Delta_2(\omega) \qquad 2\text{-}67$$

The $\alpha_{\lambda}^{2}(\nu)$ represents a coupling function associated with the electron phonon interaction whilst the function $f_{\lambda}(\nu)$ takes account of the specific nature of the phonon spectrum of the particular material under investigation. Thus we see some marked differences in this formalism from the B.C.S. approach although in the weak coupling limit the quantity $\Delta(\omega) \rightarrow \Delta(0)$ enabling us to identify $\Delta(\omega)$ with the superconducting energy gap still. To obtain $\Delta(\omega)$ we must first solve the integral equations 2-64 and 2-65 self consistently and then apply equation 2-66. An example of the form of the gap function is shown below for the case of lead due to McMillan and Rowell (1969)

Real (——) and imaginary (...) parts of the computed energy gap function $\Delta(\omega)$ for Pb vs. $\omega-\Delta(0)$.

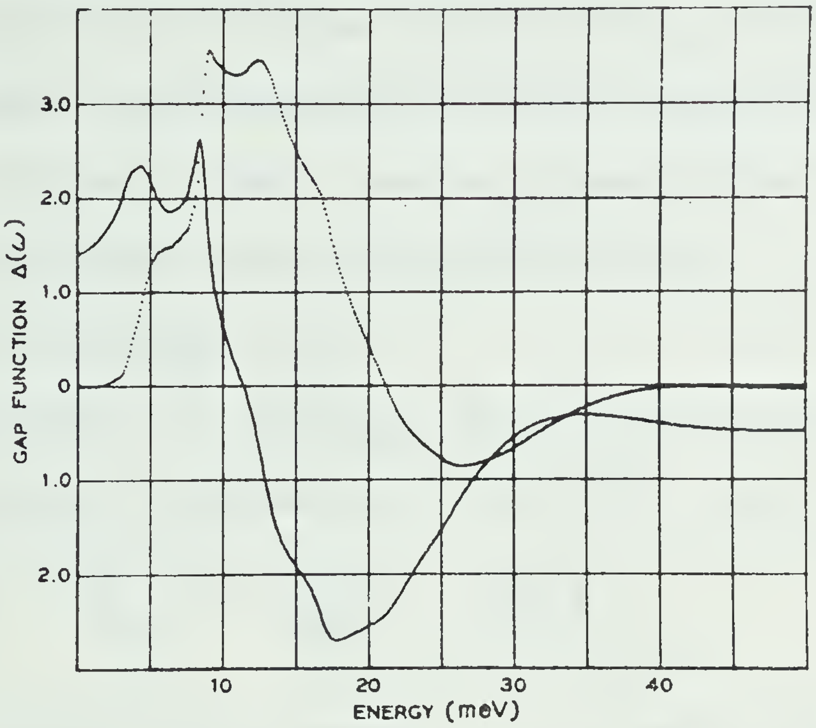

The gap function assumes a constant value at some given energy which is consistent with the minimum energy necessary for pair creation. The point at which this occurs is known as the gap edge and is the place at (or below) which the gap value is usually measured.

We saw earlier that in the weak coupling approximation of $DV \simeq 10^{-1}$ that a universal constant of 3.53 resulted for the ratio $2\Delta(0)/k_BT_c$ and whilst this approximation is not valid for strong coupling superconductors by definition, it is used instead as a guide to the strength of coupling; the higher its value the stronger the coupling is presumed to be. Clearly since both Δ and T_c have the same functional dependence on the product DV, then we would not expect there to be any deviation in $2\Delta(0)/k_BT_c$ as a result of increasing coupling strength DV. Lead for example, however exhibits a value of 4.47 for $2\Delta(0)/k_BT_c$. This is thought to be due to

inelastic phonon processes causing damping of quasiparticle states and although this would reduce both $\Delta(0)$ and T_c, the effect on T_c would be greater since there would be more thermal phonons present at T_c (as T_c for lead is high). Such a calculation has been carried out for lead on this basis by Wada (1964) with a prediction of $2\Delta(0)/k_BT_c = 5.2$

An expression for $2\Delta(0)/k_BT_c$ has been derived for strong coupling superconductors by Geilikman and Kresin (1965) given by

$$\frac{2\Delta(0)}{k_BT_c} = 3.52\left[1 + \frac{5.3T_c^{\,2}}{\omega_0^{\,2}}\left(\frac{\omega_0}{T}\right)\right] \tag{2-68}$$

where ω_0 is the limiting frequency of longitudinal phonons.

Another indicator as to the strength of the coupling is the nature of the quantity $DV = \lambda$ which is regarded as the electron-phonon coupling strength. For weak coupling this was assumed to be of the order 10^{-1} whilst for the system under consideration here it is of the order unity. The quantity λ is given by

$$\lambda = 2\int_0^\infty \frac{d\omega\alpha^2(\omega)F(\omega)}{\omega} \tag{2-69}$$

and $$1 + \lambda = \frac{m^*}{m} \tag{2-70}$$

where m* is the effective mass of the electron. A further indicator is associated with α, the coupling function appearing in the gap equation, which is usually expressed as an average given by:-

$$\langle\alpha^2\rangle = \int_0^\infty \alpha^2(\omega)F(\omega)d\omega\Big/\int_0^\infty F(\omega)d\omega \tag{2-71}$$

Increases in the values of λ, $\langle\alpha^2\rangle$ and $2\Delta(0)/k_BT_c$ are associated with increases in the coupling strength. In the experiments that were conducted Δ and T_c were directly measured whilst λ and $\langle\alpha^2\rangle$

(together with other microscopic parameters such as μ^* the Coulomb pseudopotential) were obtained indirectly by a process of inversion of the strong coupling gap equations. The inversion program will be discussed in more detail in a later chapter.

An expression for the transition temperature of strong-coupling superconductors has been proposed by McMillan (1968) in the form

$$T_c = \frac{\langle\omega\rangle}{1.20} \exp\left[- \frac{1.04\ (1 + \lambda)}{\lambda - \mu^*(1 + .62\lambda)} \right] \qquad 2\text{-}72$$

If we differentiate this expression we get (assuming $d\mu^*/dp = 0$):-

$$\frac{d\ln T_c}{dp} = \frac{d\ln\langle\omega\rangle}{dp} + 1.04 \left[\frac{1 + .38\mu^*}{(\lambda - \mu^* - .62\lambda\mu^*)^2} \right] \frac{d\lambda}{dp} \qquad 2\text{-}73$$

Those quantities on the right hand side of this equation are derivable from the inversion process whilst T_c is directly measurable and we are thus able to check the overall "quality of the inversion" technique against experiments.

Scalapino, Schrieffer and Wilkins (1963, 1966) applied the principles of strong-coupling theory to the calculation of the normal metal superconductor tunnelling current and showed that the expression 2-63 still holds in the following form:-

$$\frac{\sigma_{NS}}{\sigma_{NN}} = \frac{\mathrm{Re}\,|eV|}{\left\{(eV)^2 - \Delta^2(\omega)\right\}^{\frac{1}{2}}} \quad \left(= \frac{D(E)}{D(\varepsilon_f)} \right) \qquad 2\text{-}74$$

Using a very simple form for the phonon spectrum of lead which they approximated by two lorrentzians situated at ≃4.4 meV and 8.5 meV, Schrieffer, Scalapino and Wilkins (1963) calculated the gap function and then the normalised conductivity for the NS case at non zero temperature. These results are shown in the diagram on page 30 (fig. ①) in which we can see that there is excellent qualitative agreement with the

experimental observations of Rowell et. al. (1969).

8. Observation of Phonon Structure by Tunnelling

We have now seen that inclusion of the form of the phonon spectrum leads to structure in the normalised density of states curve obtained by tunnelling (from the results of Rowell et. al. for example). That this is plausible can be shown by examining the form taken by the expression for the normalised conductivity $\sigma = \sigma_{NS}/\sigma_{NN}$ in the light of the strong-coupling theory

$$\sigma = \frac{\mathrm{Re}|\omega|}{(\omega^2 - \Delta^2(\omega))^{\frac{1}{2}}} \qquad \text{where} \quad \omega = eV \tag{2-75}$$

expanding by the binomial theorem and using equation 2-67 we get

$$\sigma = 1 + \frac{\Delta_1{}^2(\omega) - \Delta_2{}^2(\omega)}{2\omega^2} + \ldots\ldots\ldots \tag{2-76}$$

Since $\Delta(\omega)$ clearly depends on $F(\omega)$ (inherent in the strong-coupling equations) then the normalised conductivity that we monitor in electron tunnelling experiments must also be influenced by the phonon spectrum of the metal. Quasiparticles whose energies coincide with the predominant phonon modes of a given metal have a high probability of phonon emission with subsequent decay to the peaked region in the density of states (at the gap edge). We therefore observe larger changes in the conductivity at these points. Scalapino and Anderson (1963) have shown that such resonances in $F(\omega)$ give rise to points of inflection in the density of states. This can also be seen by careful study of the effects of Δ_1 and Δ_2 on using 2-76. We are therefore provided with a powerful tool for

resolving principle phonon peaks of a metal since differentiation of the conductivity curve will give rise to maxima and minima at these inflection points.

For the lead-indium system under investigation the principle phonon peaks are those of the lead lattice but with the addition of an extra peak at the high energy end of the spectrum. This extra peak is associated with inclusion of a small amount of indium impurity in the host lattice. Justification for its existence is the subject of the next section.

9. The Localised Mode

To verify the existence of a localised mode of vibration in a solid which contains a light substitutional impurity let us consider the simple one dimensional case below:-

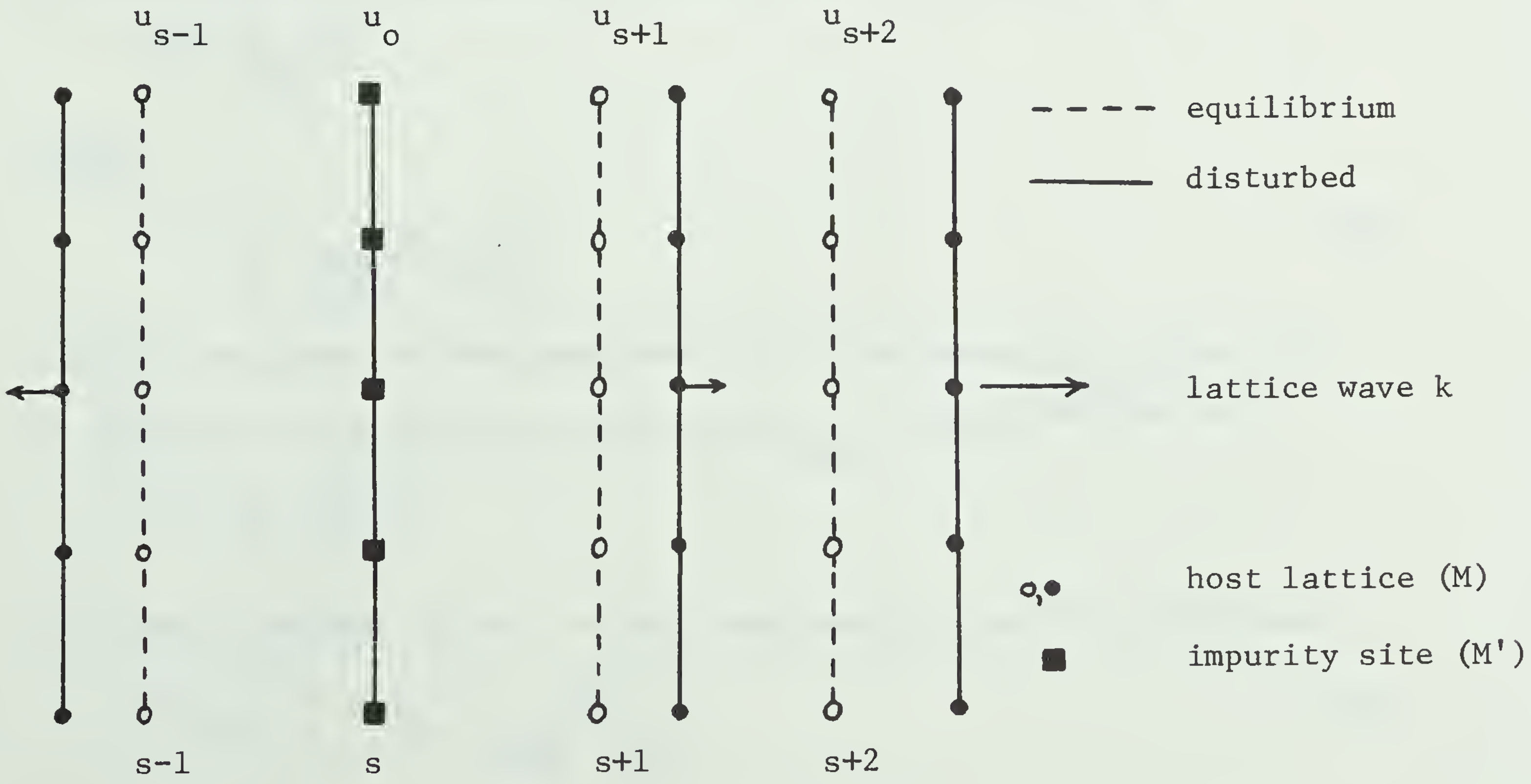

We now consider the dynamical problem arising when one row of atoms M is replaced by the light impurity M' as a longitudinal wave passes through the crystal. Assuming only nearest neighbour interactions and further that the force constant c for these interactions is constant (unchanged by the prescence of M') we have for the equations of motion of the s plane of atoms

$$M'\frac{d^2u_o}{dt^2} = c(u_1 + u_{-1} - 2u_o) \qquad 2\text{-}77$$

and for the (s + 1) plane

$$M\frac{d^2u_1}{dt^2} = c(u_2 + u_o - 2u_1) \qquad 2\text{-}78$$

where the u represent displacements of the planes of atoms from their undisturbed positions. Using a trial solution of the form

$$u_s = u_o(-1)^s e^{-i\omega t} e^{-|s|\alpha} \qquad 2\text{-}79$$

a self consistent solution is obtained for 2-77 and 2-78 if

$$e^{\alpha} = \frac{2M - M'}{M'}$$

hence

$$\omega^2 = \frac{4c}{M}\left(\frac{M^2}{2MM' - M'^2}\right) \qquad 2\text{-}80$$

Similar treatment of the case when M = M' (no impurity) yields, for a travelling wave solution of the form $u_{s+p} = u(0)e^{i(s+p)ka-i\omega t}$

$$\omega^2 = \frac{4c}{M}\,\text{Sin}^2ka$$

This has a maximum value $\omega^2 = 4c/M$ thus substituting in 2-80 we get

$$\omega^2_{\text{local}} = \omega^2_{\text{max}}\frac{M^2}{2MM' - M'^2} \qquad 2\text{-}81$$

as the predicted frequency for the local mode of vibration.

For the case at hand of indium in lead we can treat the indium as such a light impurity. Indium (face centred tetragonal) alloys with lead (face centred cubic) to concentrations of up to 65 atomic % In to give a substitutional f.c.c. structure. To obtain an approximate value for ω_{local} we put $M = 207.2$, $M' = 114.8$ (the atomic weights of Pb and In respectively) and take ω_{max} to be the cut off in the Debeye spectrum of lead and we get that

$$E_{\text{local}} \simeq 9.83 \text{ meV}$$

This prediction is in fact in excellent agreement with that observed as will be seen. Whilst it is realised that such agreement is fortuitous in the light of the assumptions made it is noteworthy that the more complex Greens function approach using Dysons equation yields an expression identical to that of equation 2-81.

CHAPTER III

EXPERIMENTAL APPARATUS

1. The Cryostat

A conventional double glass dewar system was used to cool the main body of the cryostat, a cross section of which is shown in figure 1. The original design and construction of the cryostat was carried out by Franck and Keeler (1968) for their work on pure lead and was used, after extensive modification, for this work. The cryostat basically consisted of three self contained systems.

The first of these was a beryllium-copper chamber (which will be referred to hereafter as the bomb) in which the tunnel junctions to be studied were actually mounted. Commercially supplied high pressure capillary tubing (Harwood Eng. Co. 3M series) was used to connect the bomb to a gas compressor.

The second system consisted of a small copper chamber (~150 ml) attached to the lower end of the bomb by a large copper securing nut and washer. Quick connection of this chamber to the needle valve and a roughing pump were made using swagelock couplings (not shown in diagram). By first admitting liquid helium into this chamber and subsequently lowering its vapour pressure by pumping, temperatures in the region of 1K → 2K could be attained. An indication that such temperatures could be realised can be seen in figure 2 which shows a double gap in a tunnel characteristic obtained from a lead-insulator-aluminium junction. The presence of this double gap is

FIGURE 1

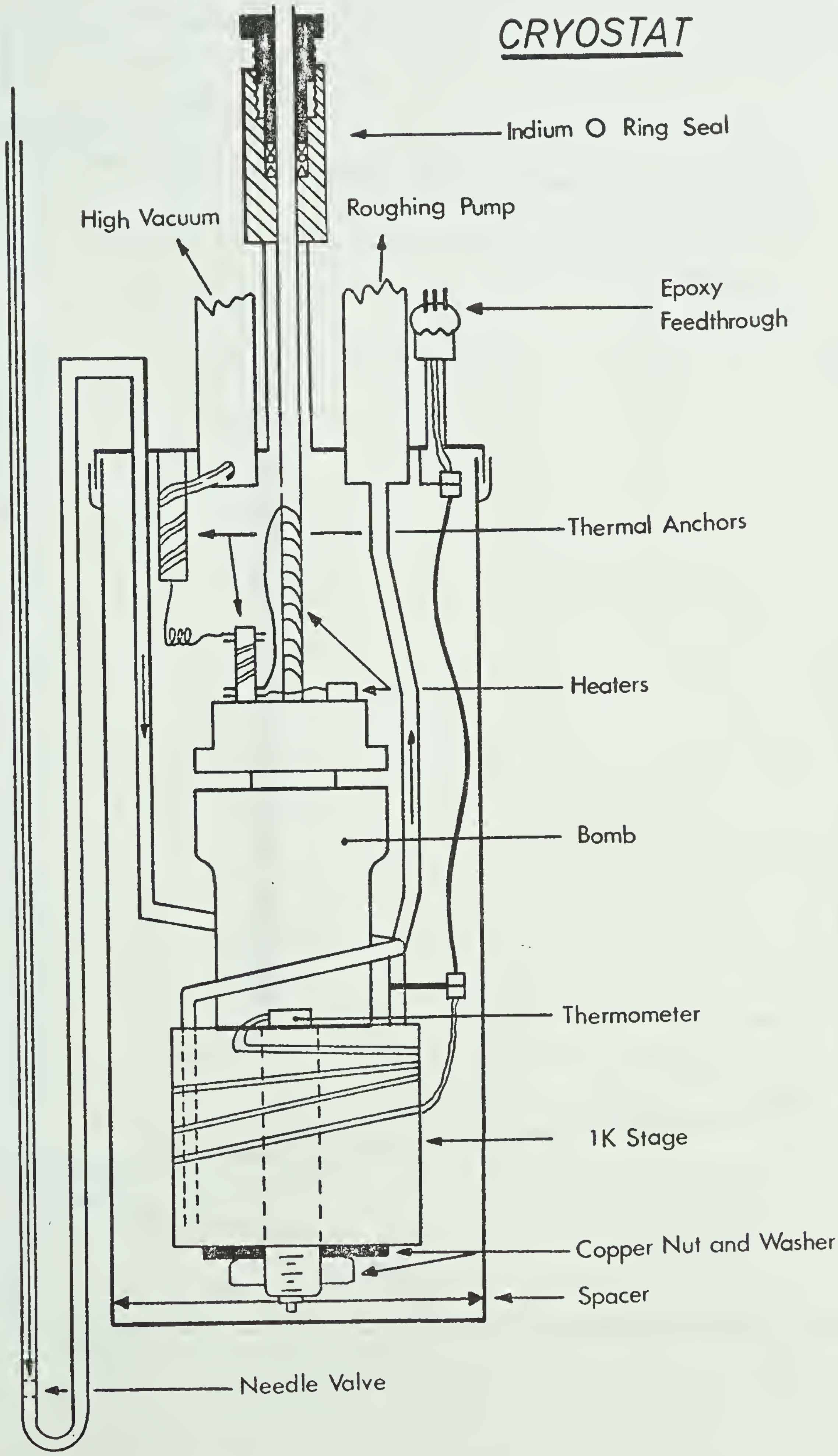
CRYOSTAT
Indium O Ring Seal
High Vacuum
Roughing Pump
Epoxy Feedthrough
Thermal Anchors
Heaters
Bomb
Thermometer
1K Stage
Copper Nut and Washer
Spacer
Needle Valve

FIGURE 2

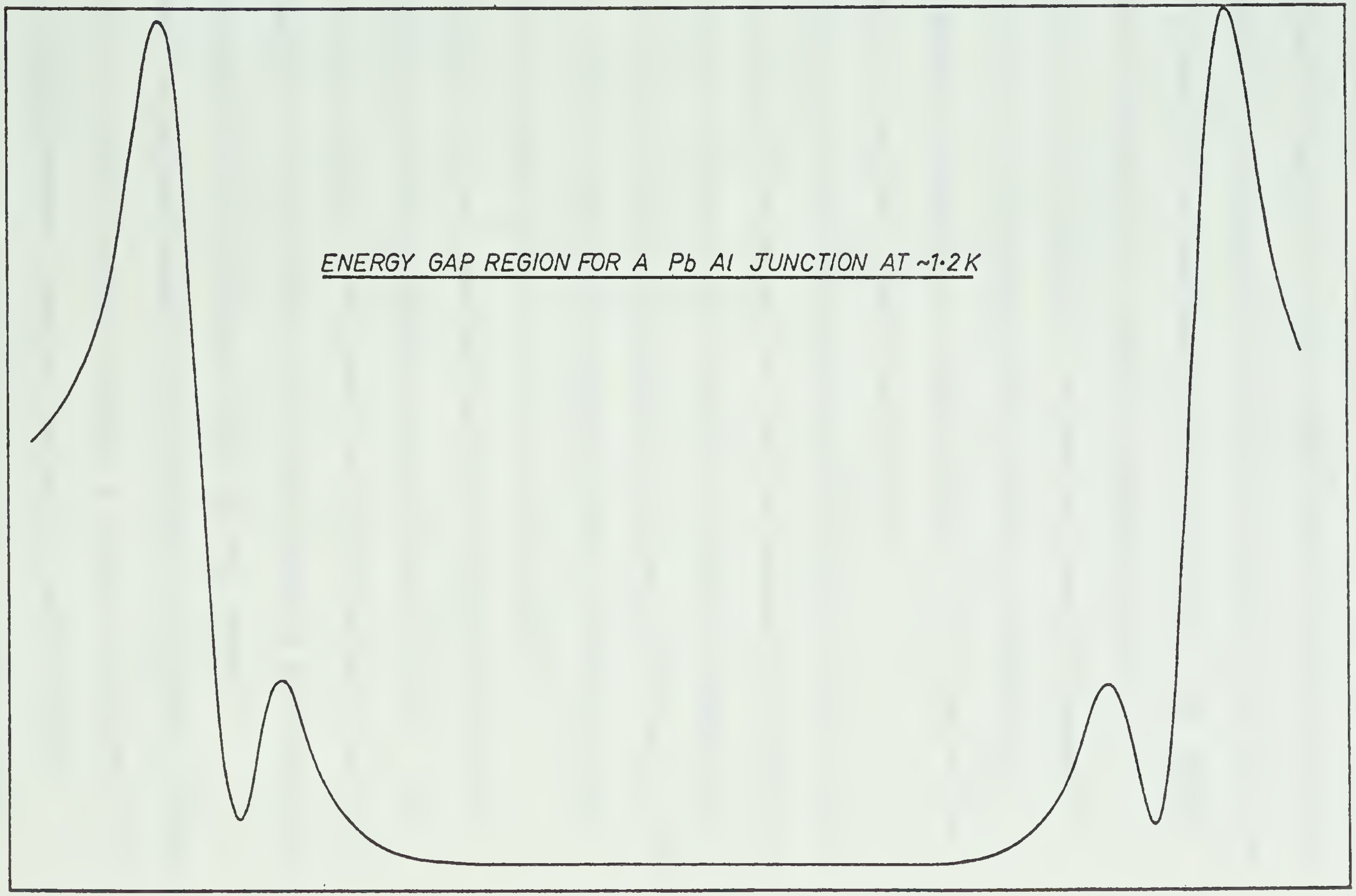

ENERGY GAP REGION FOR A Pb Al JUNCTION AT ~1·2 K

attributed to the onset of superconductivity in the aluminium film (T_c = 1.2K) and although it is appreciated that thin film effects can cause a rise in T_c to perhaps 2K, this is not thought to be the case here since a temp ~1K was confirmed by the thermometry. To obtain the excellent thermomechanical contact necessary for such low temperatures the lower surface of the bomb was carefully lapped to the upper surface of the chamber using a series of Exolon Al_2O_3 lapping compounds and smearing the mated surfaces with a suspension of copper powder in Apiezon N type vacuum grease.

The third self contained system took the form of a large copper can (main vacuum can) enclosing the other two systems and connected to a high vacuum oil diffusion pump. Except when using exchange gas, the pressure inside this can was maintained in the range 10^{-6} torr → 10^{-7} torr and provided therefore the necessary thermal isolation of the bomb from the cryogenic fluid in which it was situated.

An indium O ring seal was used to retain the high vacuum at the exit point of the high pressure capillary from this can. This seal was located several inches above the top of the can to provide an extra degree of thermal isolation for the pressure tube and thus reduce the possibility of blockage caused by cold spots.

In order to further minimise the occurrence of blockage, heaters were placed at strategic points including a manganin resistance wire inside the actual pressure tube and running its entire length. Temperature regulation was also effected in part by these heaters.

Relocation of the needle valve from the can top to its present

position permitted the use of the very simple design shown which was not only leak tight but since it was always totally immersed in the liquid helium, was not susceptible to icing up.

Wires for the heater circuits were admitted to the can through the high vacuum tube (via a room temperature epoxy feedthrough) and thermally anchored by winding several inches of their length on a copper post and securing them tightly with varnish. Two such thermal anchors were employed, one at 4K situated at the can top and the other at ~2K and located at the bomb top. The 2K anchor was constructed in such a way as to be removable in the event of failure of the main wiring (to be described).

After passing through the liquid helium bath, the thermometer leads were led into the high vacuum can via an epoxy feedthrough of the type described by Anderson (1968). From here they were then connected to the 1K pumping stage using a jumper cable wired to Amphenol miniplugs (for quick connection) at which point they were firmly anchored, again using varnish.

The cryostat was used over a temperature range of from 1K → 40K. That such elevated temperatures were necessary can be appreciated from the phase diagram (figure 3) in which it can be seen for example that in order to form a solid at 3.5 kbar temperatures $\gtrsim$35K are required.

2. The Bomb

Figure 4 shows a cross-sectional view of the bomb and low temperature pumping stage. The bomb itself was machined from an alloy

FIGURE 3

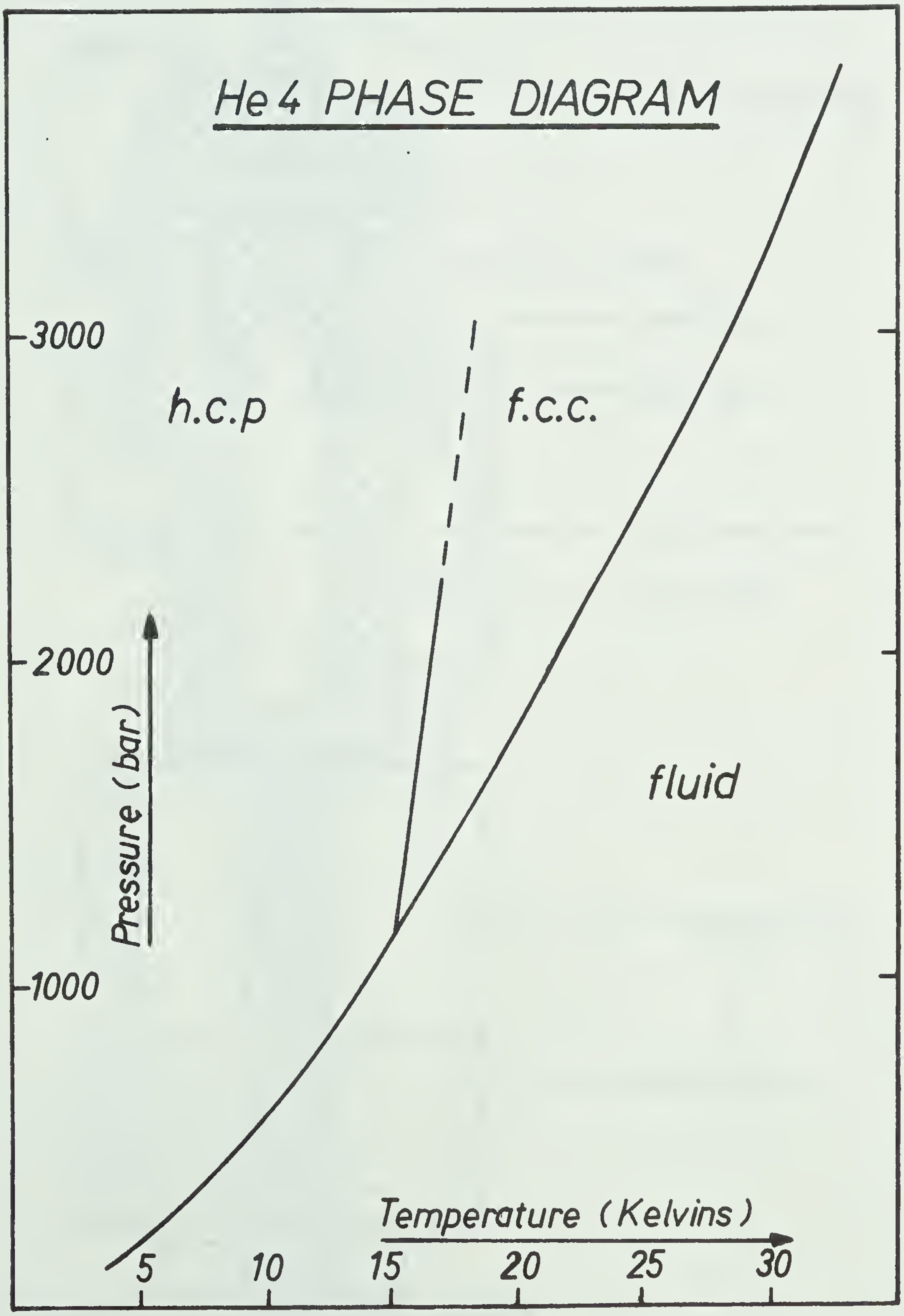
He4 PHASE DIAGRAM
3000
2000
1000
Pressure (bar)
h.c.p
f.c.c.
fluid
Temperature (Kelvins)
5
10
15
20
25
30

FIGURE 4

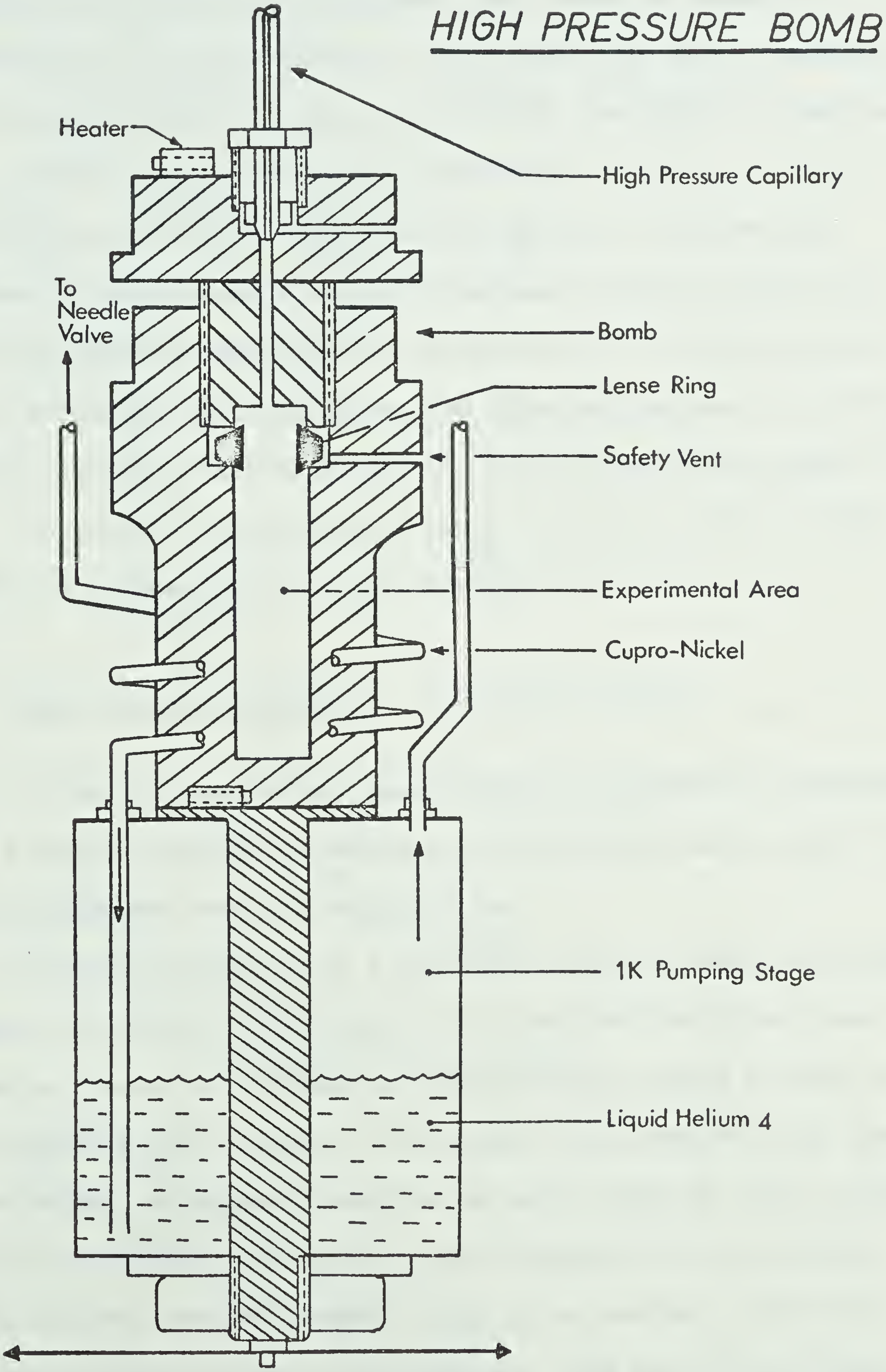
HIGH PRESSURE BOMB
Heater
High Pressure Capillary
To Needle Valve
Bomb
Lense Ring
Safety Vent
Experimental Area
Cupro-Nickel
1K Pumping Stage
Liquid Helium 4

containing approximately 98% copper and 2% beryllium (with traces of Co and Ni) which after heat treatment had a tensile strength of ~ 200,000 p.s.i. The advantages of this alloy are that it exhibits good thermal conductivity and has a strength comparable to stainless steel without embrittling at low temperature.

The gas tight seal between the two halves of the bomb was achieved by compressing a specially designed stainless steel ring (lense ring) whose edges had been bevelled at 37°. This particular method provides a self tightening seal since any increase in internal pressure serves to further force the ring onto the sealing edges of the bomb. The core of the bomb was machined to ½" dia. and to a depth of ~2½" to accommodate the sample housing.

3. Sample Housing and Holder

In order to maximise the useable space in the bomb's experimental area a special housing was designed and constructed and is shown in figure 5 together with the sample holder.

The housing consisted of a thin wall stainless steel tube (whose diameter was chosen to be a close fit in the bomb) which had been milled as shown. A thin capillary tube was then swaged slightly at each end and silver soldered to the back of this tube to allow passage of the wires. An Amphenol miniplug was next turned to size, relieved so as to accommodate the capillary and then epoxied into position as illustrated. Having attached a lid to the top end, this device was then secured in place in the bomb top. The use of this housing

FIGURE 5

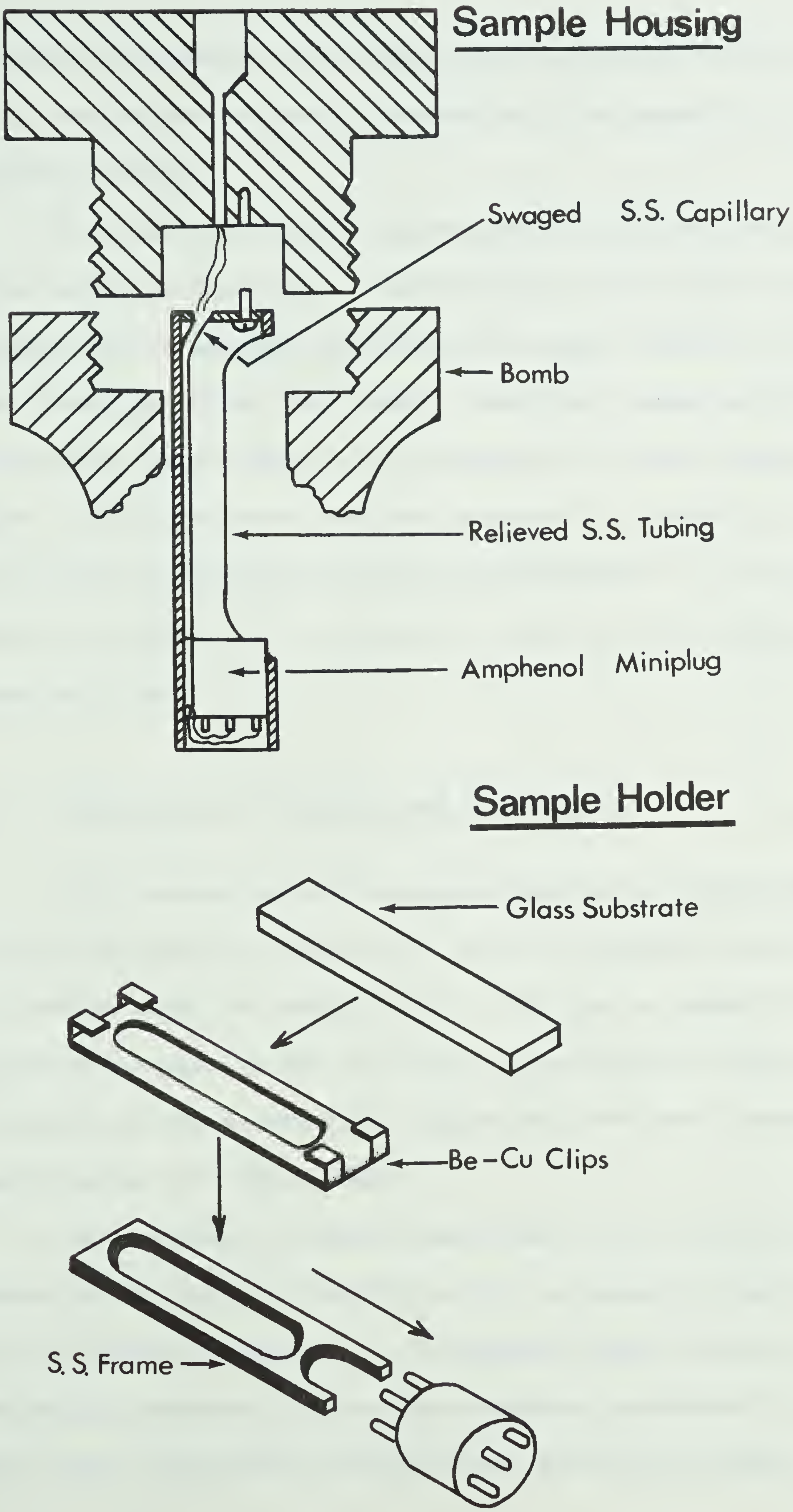
Sample Housing
Swaged S.S. Capillary
Bomb
Relieved S.S. Tubing
Amphenol Miniplug
Sample Holder
Glass Substrate
Be-Cu Clips
S. S. Frame

allowed the passage of the wires to the bottom end of the plug where they were secured in such a fashion as to be completely safeguarded against breakage.

The sample holder was constructed by first fabricating the base from stainless steel and silver soldering to this the beryllium copper clip arrangement which holds the glass substrate (on which the tunnel junctions are formed). Beryllium copper was chosen for the clips since cold working of stainless steel leads to breakage in this case. This arrangement was then soldered to a compatible plug. The two greatest advantages of this set-up were that it was very fast to mount a specimen whilst eliminating completely the handling of the specimen itself.

4. High Pressure Production and Measurement

High pressure production was achieved using a Harwood Eng. Co. compressor specially adapted for use with gaseous helium four. From an initial supply at 800-1000 p.s.i. the gas was pumped in three successive stages to the 3.5 kilobar range used for these measurements. Isolation of the experimental chamber from the final compressor stage was effected by a needle valve.

Three methods of pressure measurement were employed namely a Heise Bourdon gauge (0-100,000 p.s.i.), a manganin gauge and the tunnel junctions themselves. The manganin gauge supplied with the compressor monitored the pressure dependent resistance of a manganin wire using a Wheatstone bridge circuit and was supposedly accurate

to 1%. This gauge and the Heise Bourdon gauge were used to calibrate the tunnel junction by recording its zero bias resistance as a function of pressure. The final frozen in pressure was always determined using the junction itself since the two other methods would then only monitor external pressure. This method is to be discussed in more detail in a later chapter. Experiment showed that the temperature dependent resistance change of a sample was <.5% for a ΔT of 70K and thus no correction to pressures was applied in this regard.

5. The High Pressure Electrical Feedthrough

In conducting experiments at high pressures using gaseous helium as the pressure transmitter one is faced with the problem of introducing electrical wires into the experimental chamber without loss of pressure. To overcome this, a seal was constructed based on the frozen oil method employed by Dugdale and Hulbert (1957) and is illustrated in figure 6. An oil-epoxy feedthrough which incorporates this principle has been described by Goree et. al. (1965), in which heavy emphasis is placed on the role of the epoxy which separates the gas-oil interface. This particular seal was found to be extremely difficult to construct and its failure rate in service found to be high, both of these drawbacks being attributed to the presence of the epoxy. Furthermore a close examination of the defunct feedthroughs revealed that the epoxy had in fact not penetrated the pressure tube to any appreciable extent. This latter problem was due in part to the fact that in the experiments described herein, 6-9 wires were necessary

FIGURE 6

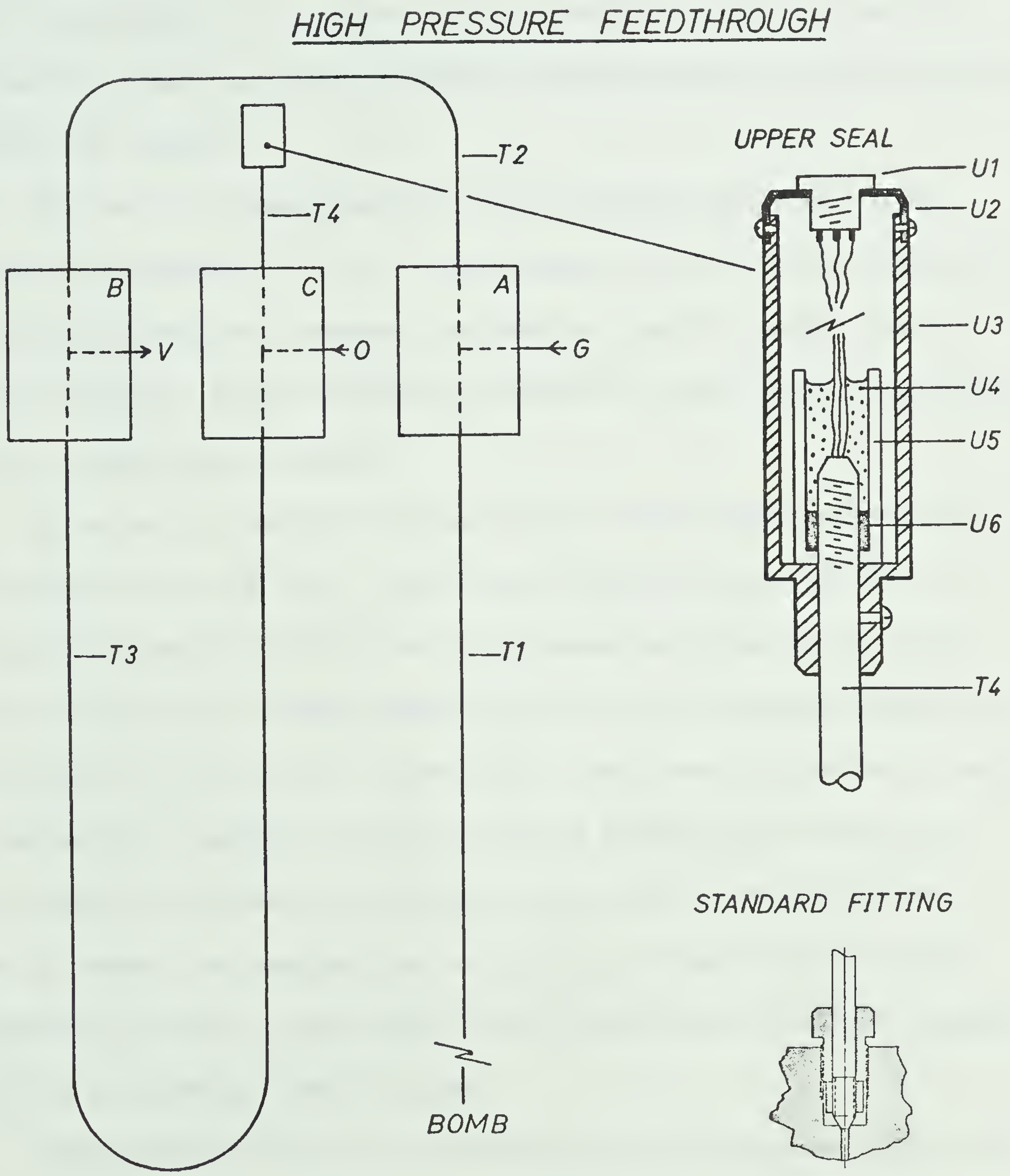
HIGH PRESSURE FEEDTHROUGH
T2
T4
B
C
A
V
O
G
T3
T1
BOMB
UPPER SEAL
U1
U2
U3
U4
U5
U6
T4
STANDARD FITTING

thus providing a major constriction in the pressure tubing.

To this end, a feedthrough was devised for use with large numbers of wires which did not employ the use of epoxy filled tubes. This feedthrough is in comparison very easy to construct and refillable as well as incorporating a plug designed to protect wires from accidental damage.

Subject to a specifically ordered filling procedure which prevents contamination of the experimental chamber, the feedthrough illustrated not only survived the test of time but vented itself of oil when the liquid nitrogen level fell; again without contamination of the experimental chamber.

In order to construct the particular seal shown, approximately twelve feet of 3/16" O.D., .0025" bore stainless steel pressure tubing (Harwood 3M series) was first coned and threaded (for use with the standard fitting shown) and cut to the desired lengths for the tubes T1, T2, and T3. These tubes were then laid out on a long clean surface together with the junction blocks and fittings in a development which would ultimately lead to the final form shown. Having passed the required number of wires through the system and allowing an excess at each end, the fittings were carefully tightened and the feedthrough bent to shape.

The principle involved in retaining the gas pressure with such an arrangement would be to fill the tube T3 with oil by admitting it through O in block C and then immersing T3 in liquid nitrogen. In order to prevent the preferential leakage of oil at the top of block

C during filling it was necessary to block T4. To this end a re-usable device (upper seal in illustration) was constructed which not only blocked T4 but accommodated a plug so that the wiring could be accessed without exposure to possible breakage. Since T4 was never called upon to withstand more than two or three thousand p.s.i. oil pressure, a slightly larger - but still standard - pressure tube was used having an o.d. of 1/4" and a bore of 1/16" (Harwood 4L series).

To assemble the upper seal, the main body of machined brass (U3) and the the stainless steel cup (U5) were first slid onto the tube followed by the standard threaded collar (U6). The stainless steel cup was held in position and filled with Stycast 2850 G.T. epoxy which was allowed to cure. Some of this epoxy is also expected to enter T4 and, although favourable, is not essential to the operation of the seal. The protruding wires were then attached to an Amphenol miniplug (U1) housed in the machined brass cap (U2). Finally the main body was raised into position and locked onto the tube and the cap secured.

To fill the seal, very low pressure helium gas was pumped into block A through G and allowed to leak slowly from the vent V. Simultaneously, oil was pumped at low pressure into block C through O and thus through tube T3 to block B and also allowed to leak from V. It was felt that the steady stream of gas in T2 would prevent the slight possibility of oil leaking into this tube. Having established a continuous bubble free flow of oil from the vent, the tube T3 was immersed in liquid nitrogen. When the oil ceased to

flow, the oil pressure was reduced to zero and the vent valve V tightened whereupon the system pressure was observed to rise as expected. The bomb remained in position throughout the filling process. The system described is now ready for use and will remain so if the nitrogen level is maintained.

When not in active use (or when deliberately venting the oil seal) the bomb was kept in place containing a few hundred p.s.i. of gas pressure while the oil supply line O remained vented. This practice ensured that if the nitrogen trap was left untended the melted oil would be ejected from O and eliminate any possibility of contamination of T1 via T2. Should this occur it would be necessary to recharge the seal by repeating the above procedure.

6. Vacuum Deposition

The tunnel junctions were formed by evaporation in a customised Norton Research Company 3115 model high vacuum system. Masks were fashioned from stainless steel to give the required film geometry and an enlarged contact area and located in a carousel which allowed up to six different source-mask combinations to be used. The carousel was enclosed in a large glass tube, with quartz glass divisions to prevent mutual contamination of sources and masks.

An arrangement compatible with the sample holder described previously was incorporated in the carousel design in such a way as to allow any desired mask to be raised into contact with the substrate. Since the back of the sample holder had been machined away, it was

possible (with the aid of a prism) to view the film during formation.

7. Temperature Measurement

Temperatures were measured with the aid of a commercially supplied calibrated germanium resistance thermometer (Cryocal), the calibration range being from 1.5K to 40K.

The 1.5K to 2.0K readings were based on the Helium Vapor Pressure Scale of 1958 with an accuracy of 0.003K while the 2.25K to 13K readings are traceable to the National Bureau of Standards Provisional Scale of 1965 (2-20°K) through secondary standards maintained by CryoCal, Inc. with an accuracy of 0.005K from 2K to 5K and 0.01K from 5K to 13K.

The 14K to 40K readings are traceable to the International Practical Temperature Scale of 1968, again through secondary standards maintained by CryoCal, Inc. with an accuracy of 0.01K from 14K to 20K and 0.04K from 22K to 40K.

Resistance values were obtained to better than .1% using potentiometric techniques.

Standard curve fitting procedures were employed for interpolation (and extrapolation where necessary) with excellent reliability.

CHAPTER 4

ELECTRONIC DETECTION TECHNIQUES

1. The Principle of the Measurement

It was shown earlier (Chapter 2) that the quasiparticle density of states in a superconductor was in one to one correspondence with the normalised dynamic conductance σ_{NS}/σ_{NN} as measured in a normal-superconductor (NS) tunnel junction. Measurements of this quantity were made using standard harmonic detection techniques by applying a small constant a.c. signal across the tunnel junction and monitoring its a.c. response. Considering the idealistically simple circuit shown below

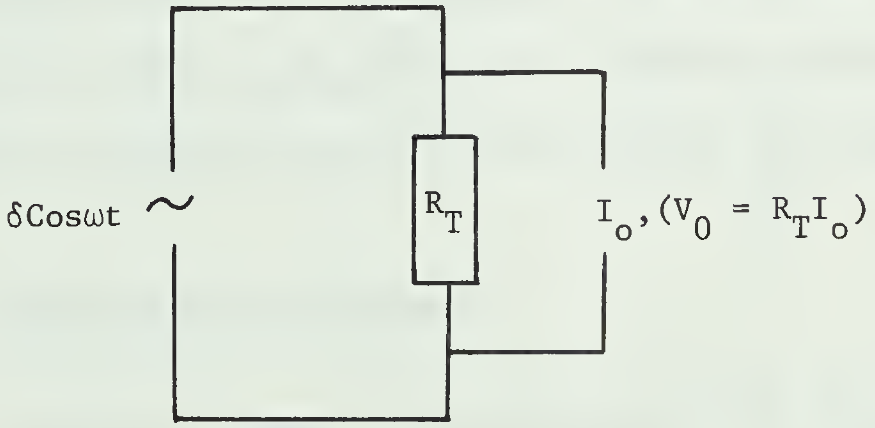

where a constant a.c. signal $\delta \mathrm{Cos}\omega t$ (current or voltage) is applied across the sample R_T together with a d.c. bias current I_o. The signal developed across the sample resistance R_T therefore may be expressed using a Taylor series expansion as:-

$$V(I) = V(I_o + \delta \mathrm{Cos}\omega t) = V(I_o) + \left(\frac{dV}{dI}\right)_{I_o} \delta \mathrm{Cos}\omega t + \frac{1}{4}\left(\frac{d^2V}{dI^2}\right)_{I_o} \delta^2 \times (1 + \mathrm{Cos}2\omega t) + \ldots\ldots \qquad 4\text{-}1$$

where $\delta \mathrm{Cos}\omega t$ here represents a constant a.c. current supply.

If we now let $\delta \mathrm{Cos}\omega t$ represent instead a constant voltage supply we obtain in a similar manner:-

$$I(V) = I(V_o + \delta \mathrm{Cos}\omega t) = I(V_o) + \left(\frac{dI}{dV}\right)_{V_o} \delta \mathrm{Cos}\omega t + \frac{1}{4}\left(\frac{d^2I}{dV^2}\right)_{V_o} \delta^2 \times (1 + \mathrm{Cos}2\omega t) + \ldots\ldots \qquad 4\text{-}2$$

where in both equations 4-1 and 4-2 use has been made of a trigonometric identity. Thus we can see that if we can measure the components of the signal across R_T that are proportional to ω and 2ω we are in fact measuring quantities directly proportional to the dynamic resistance (or conductance) and its derivative. The component proportional to ω is used to yield σ_{NS}/σ_{NN} whilst the component proportional to 2ω is used to resolve structure in the density of states.

2. Detection of the Harmonics

In order to measure the amplitudes of the components of ω and 2ω, phase sensitive detection techniques were employed using the circuit logic shown in figure 7.

An a.c. signal is applied across the tunnel junction which is incorporated as one arm of a bridge circuit. By so doing we are able to balance out the large component of fundamental and observe only the small non linear changes associated with dV/dI etc. The

FIGURE 7

CIRCUIT LOGIC

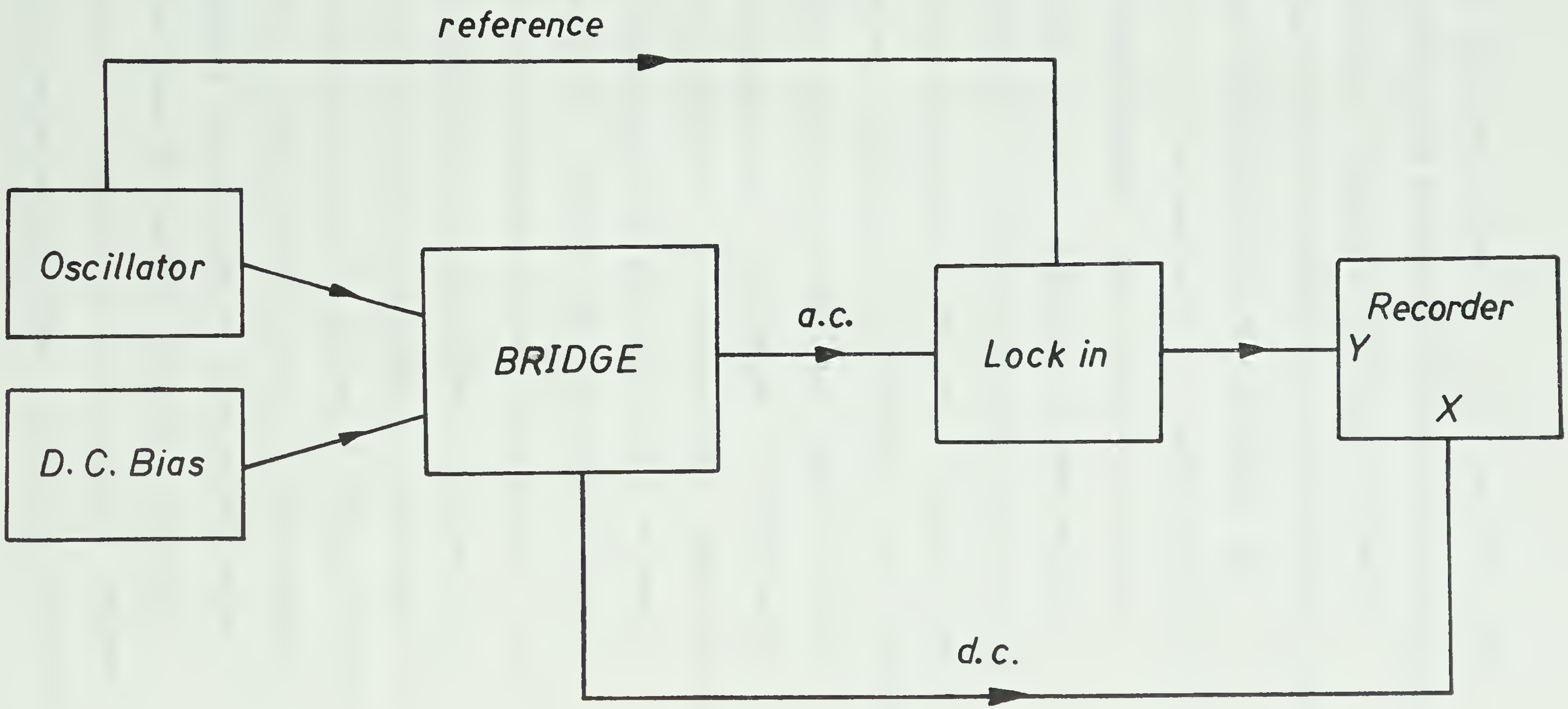

response of the tunnel junction is then fed to the input of a phase sensitive lock-in amplifier (P.A.R. HR8) whose phase is set initially to zero and whose band pass is centred on the source frequency. Simultaneously a reference signal from the same source is fed to the lock-in amplifier and in this way we are able to observe the component proportional to ω. The source of a.c. supply should be as stable in amplitude as possible and, less critically, stable in frequency. Variations in oscillator amplitude are most serious since not only do they manifest themselves directly at the lock in output, but sweep times associated with each curve traced might range up to an hour in duration. Slight drift in frequency is not so serious (depending on the band pass) since the reference supply is derived from the source. The bridge circuit is balanced by minimising the output from the lock-in amplifier (for a specific d.c. bias condition) both resistively and capacitively, in the latter case the phase at the lock-in is shifted by 90°. Having done this (and returned the phase of the detector to zero) unbalancing of the capacitive circuit should cause no appreciable effect on the output of the lock in. Finally while locked onto the resistive component of the sample the d.c. bias is changed slightly causing an unbalanced bridge condition and corresponding output signal from the lock-in. Fine adjustments of the phase and frequency are then made to maximise this output.

The system is thus tuned for maximum response to the first harmonic content. In order to detect the second harmonic component it is only necessary to change the oscillator frequency to $\omega/2$ while

leaving the lock-in tuned to ω.

The output from the lock-in is then fed to a recorder where it is plotted as a function of applied d.c. bias using an X - Y recorder. The desired amplification required is achieved by the combined effect of the variable gains of lock-in and pen recorder.

3. Circuit Design Considerations

Since the tunnelling experiments carried out were in the Fermi surface region it is essential that the measuring technique itself should not interfere with the Fermi surface shape. The temperature dependence of the Fermi surface shape is often alluded to as thermal smearing, an effect which becomes less pronounced as the temperature decreases. At 1K for example the thermal smearing is $\simeq 86\mu eV$ r.m.s. To this end it is essential that the a.c. level (modulation) applied across the tunnel junction by the circuit be as small as possible and less than the thermal smearing at the temperature of the measurements.

In the expansions given by equations 4-1 and 4-2, the component of the first harmonic is already small compared to that of the fundamental but with the further restriction of low applied signal levels and the fact that the tunnel junction response is only weakly non linear, it is necessary to incorporate the tunnel junction in a bridge circuit in which the large fundamental component can be balanced out.

Two such bridge circuits were employed for this purpose one

being a constant current device of the type used by Adler and Jackson (1966) and the other a constant voltage device due to Rogers (1970). These circuits are shown in detail in Figures 8 and 9 respectively, the former showing the support systems which were used for both.

The constant voltage bridge was used for measurements in the immediate energy gap region where the sample resistance approaches ∞. This avoids the problem of over modulation associated with the constant current bridge and consequent smearing of data. Both bridge circuits allowed four terminal measurements to be made and included large resistors to swamp the normal state resistance of the film electrodes. The detailed circuit for d.c. biasing (sweep) is shown in figure 10.

4. The Constant Current Bridge

The diagram below shows a simplified form of the resistance bridge circuit used in which R_T represents the sample and R_D the bridge balancing components.

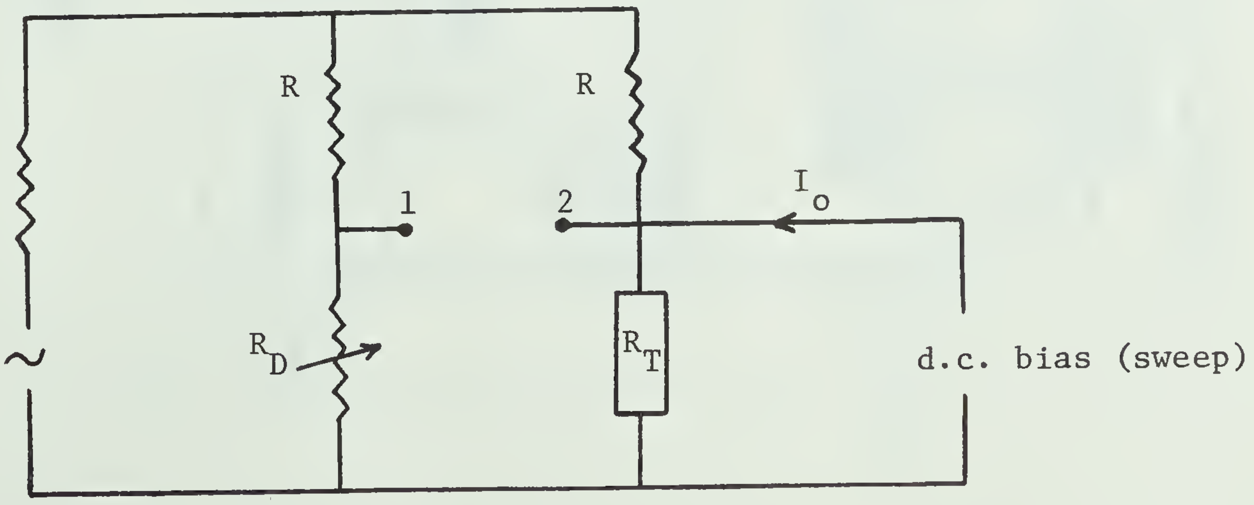

FIGURE 8

CONSTANT CURRENT BRIDGE (and support systems)

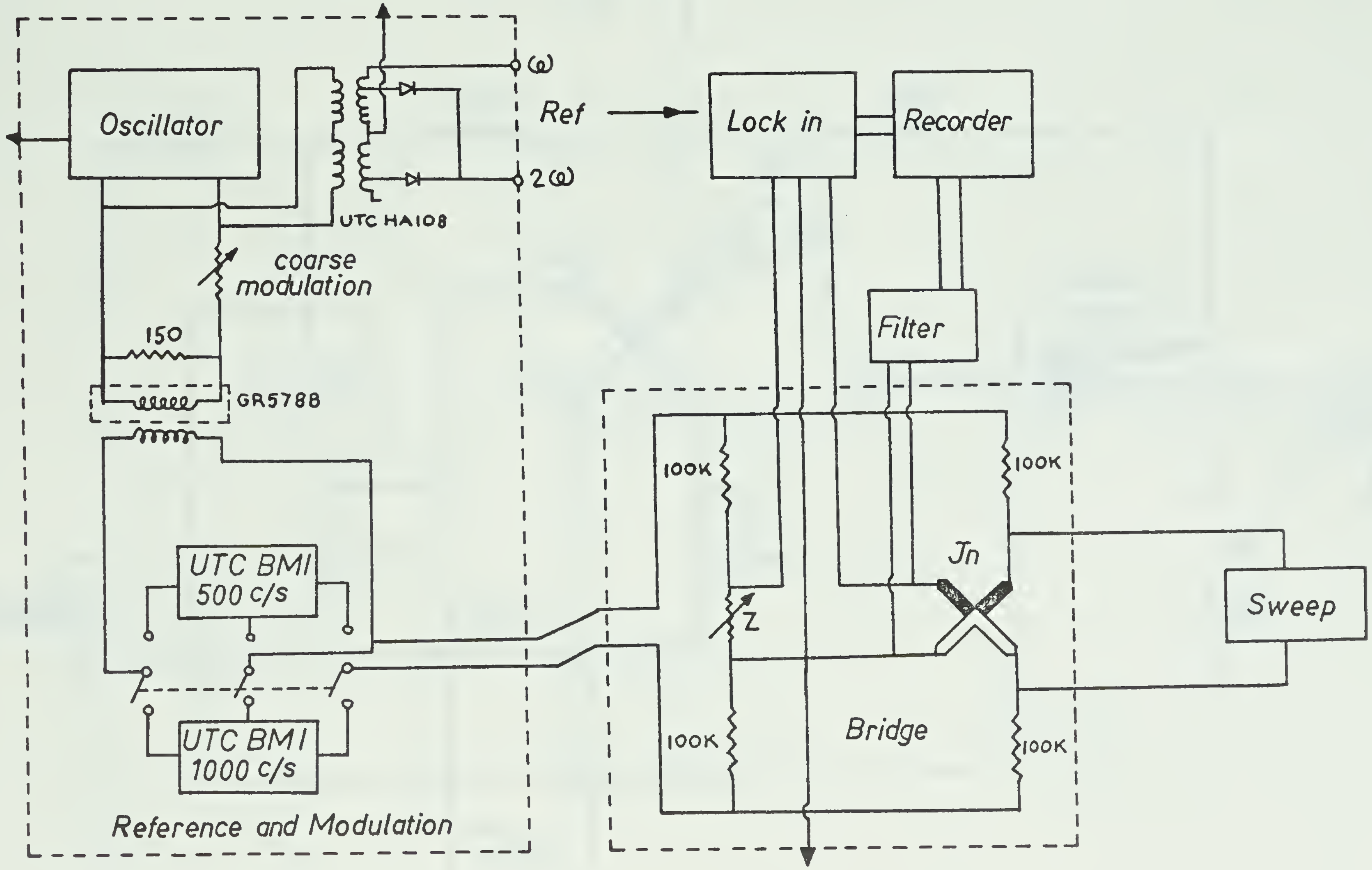

FIGURE 9

CONSTANT VOLTAGE BRIDGE

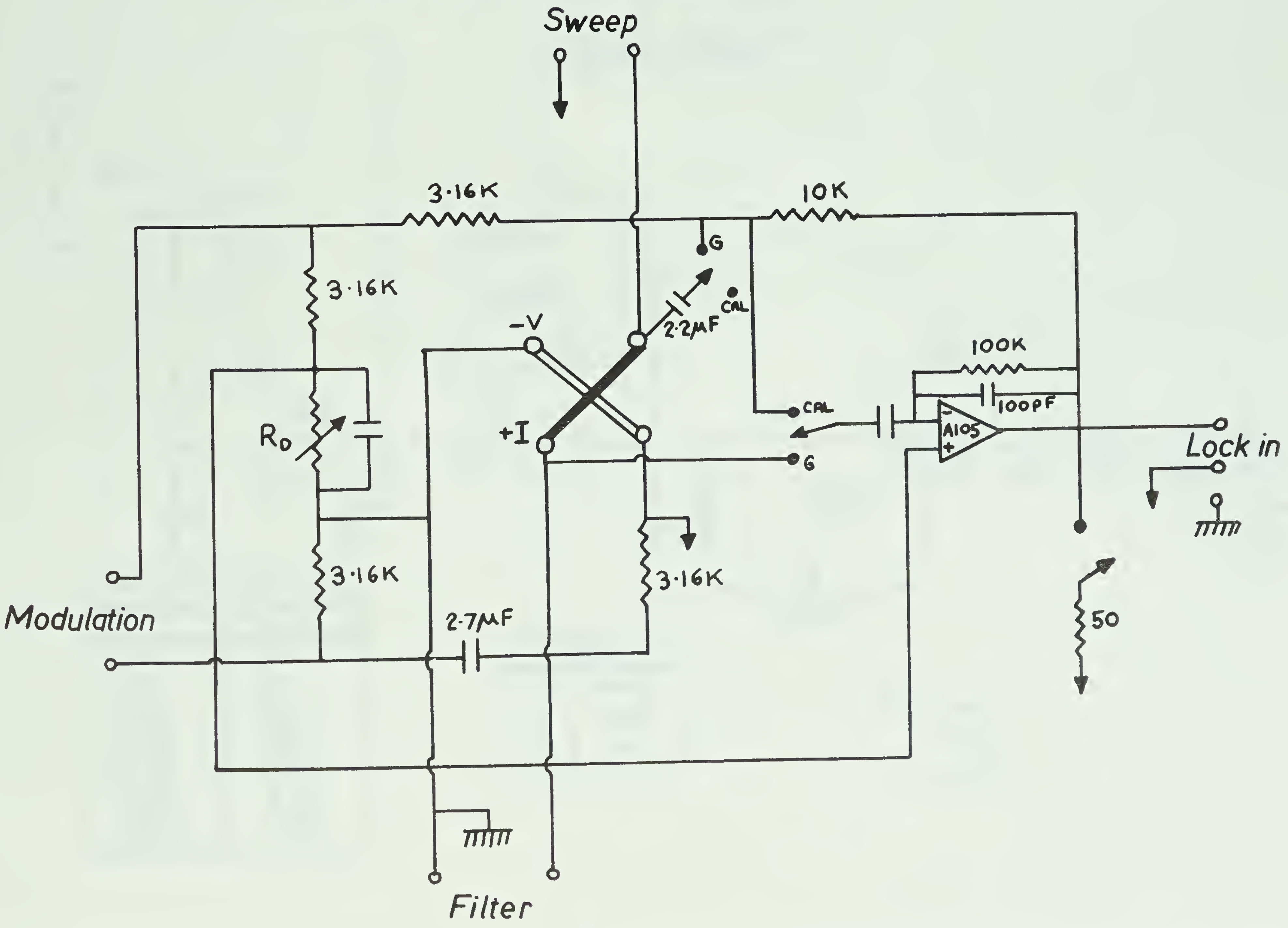

FIGURE 10

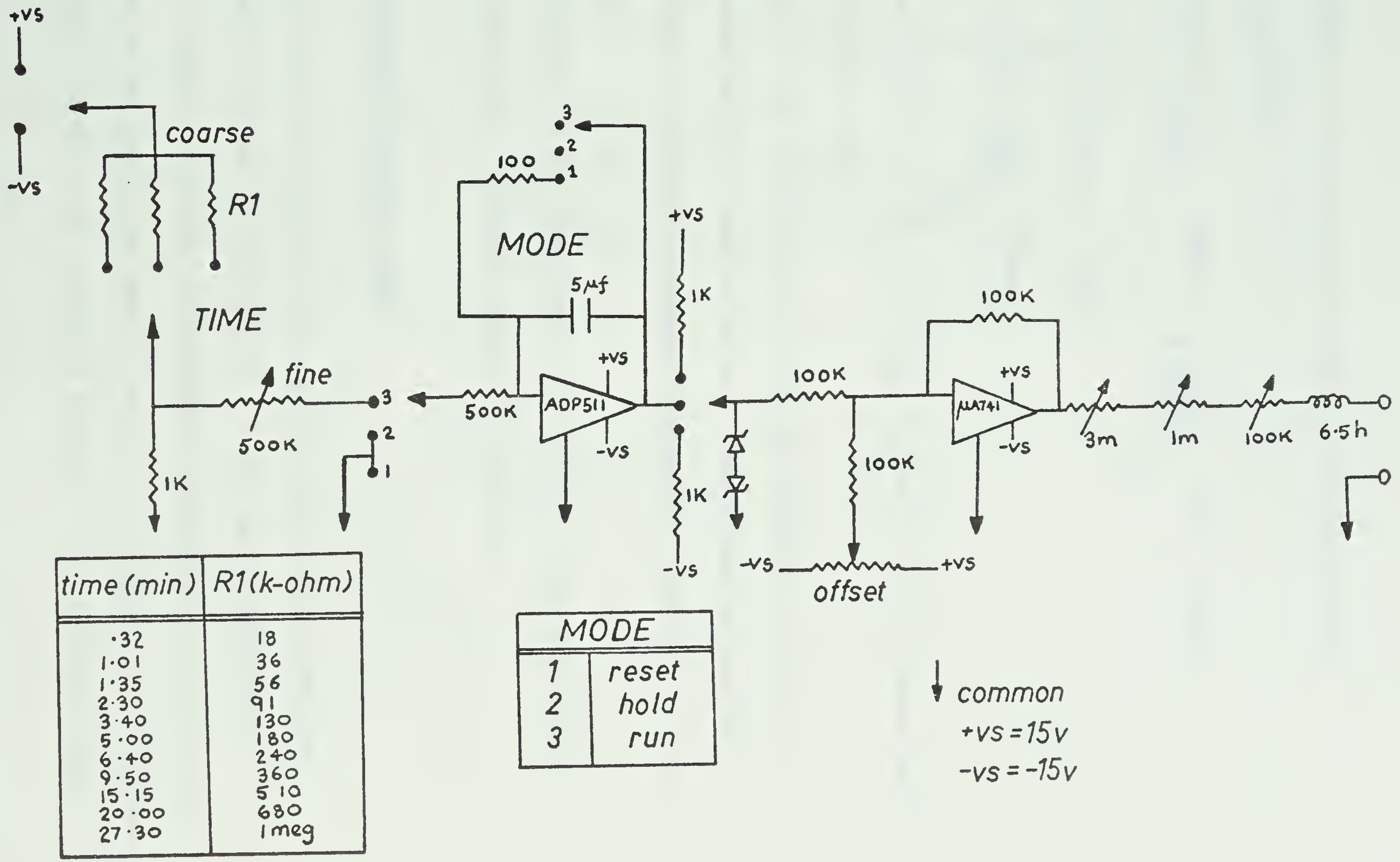

SWEEP CIRCUIT

time (min)	R1 (k-ohm)
·32	18
1·01	36
1·35	56
2·30	91
3·40	130
5·00	180
6·40	240
9·50	360
15·15	510
20·00	680
27·30	1 meg

MODE	
1	reset
2	hold
3	run

If the current in each arm of the bridge is $\delta\text{Cos}\omega t$ then

$$V_1 = R_D\ \delta\text{Cos}\omega t$$

$$V_2 \simeq I_oR_D + \left(\frac{dV}{dI}\right)_{I_o} \delta\text{Cos}\omega t + \frac{1}{4}\left(\frac{d^2V}{dI^2}\right)_{I_o} \delta^2(1 + \text{Cos}2\omega t) + \ldots\ldots$$

where $R_D = R_T$ at balance. Thus:-

$$V_{12}(\omega) = \delta\left[R_D - \left(\frac{dV}{dI}\right)_{I_o}\right]\text{Cos}\omega t$$

We see therefore that detecting $V_{12}\propto\omega$ is in fact measuring the required quantity $dV/dI = \sigma$

Furthermore it can be seen that the bridge response is linear as would be expected in a passive device. This bridge is claimed by its authors to be able to measure resistance changes of a few parts in 10^5.

Calibration of the characteristics obtained can be achieved by replacing R_T by a standard variable resistance.

5. The Constant Voltage Bridge

This circuit is of the active variety and actually measures conductance as opposed to resistance. A high gain operational amplifier is used to provide the necessary inversion to do this. A fraction of the output voltage, α say, is fed back so as to maintain a zero signal condition at the input subject to the condition that $\alpha A >> 1$ where A is the gain.

Conductance measurements of a few parts in 10^5 are obtainable to

an accuracy of 1% and the response of the circuit is linear to .1%. Since the circuit contains an active component a proof of its linear response is given.

The constant voltage bridge may be represented in simplified form as shown below.

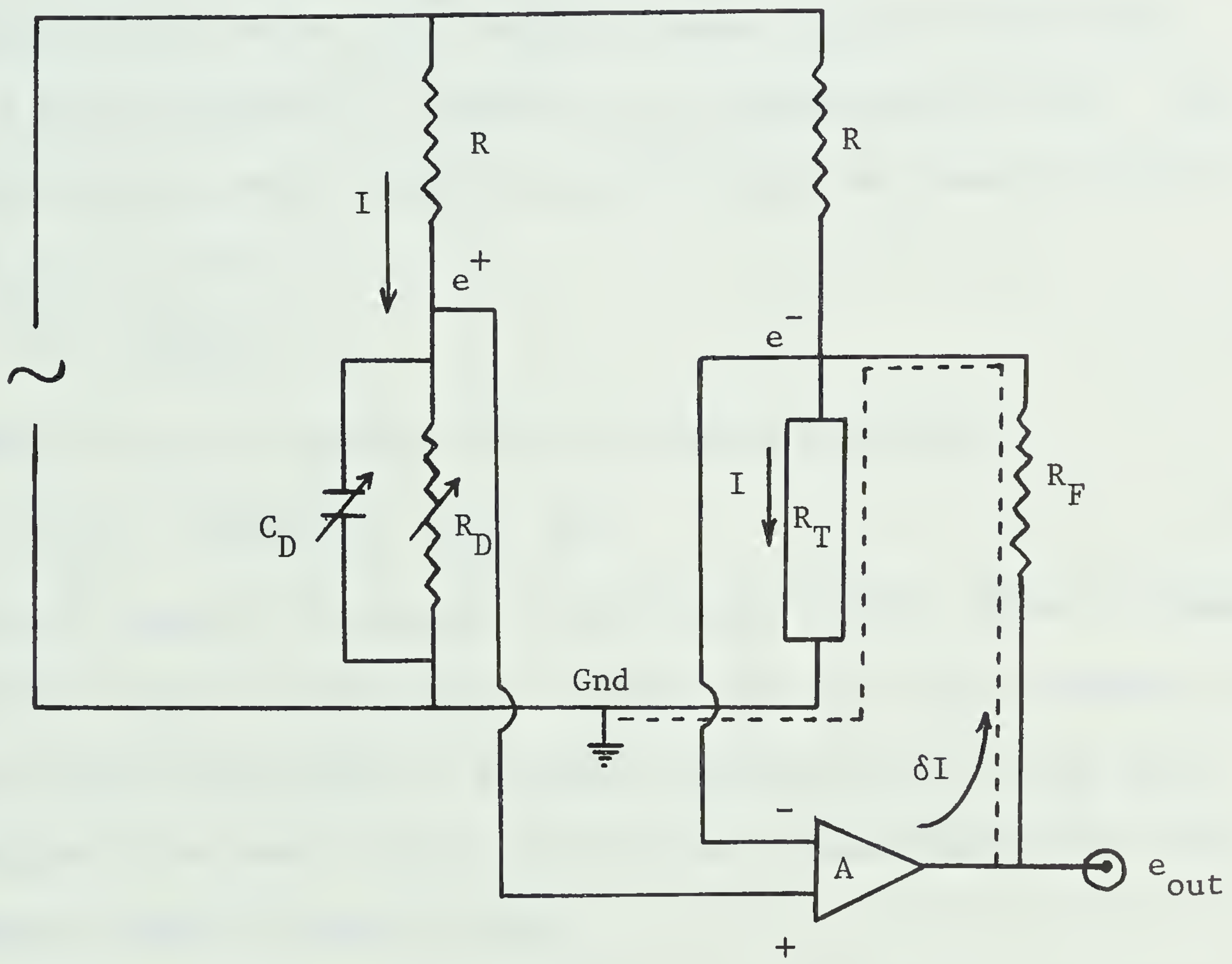

By definition

$$e_{out} = Ae_{IN} = A(e^+ - e^-) = A(IR_D - IR_T - \delta IR_T) \tag{4-3}$$

According to the dotted path to ground we can see that

$$e_{out} = \delta IR_F + (I + \delta I)R_T = \delta I(R_F + R_T) + IR_T \tag{4-4}$$

equating 4-3 and 4-4 gives after simplification

$$\delta I = I \left(\frac{R_T(-1-A) + AR_D}{R_F + R_T + AR_T} \right) \qquad 4\text{-}5$$

Extracting a factor $\beta \equiv R_T/(R_F + R_T)$ we can write 4-5 as:-

$$\delta I = \frac{\beta A}{1 + \beta A} \left(\frac{-1}{A} - 1 + \frac{R_D}{R_T} \right) I \qquad 4\text{-}6$$

If the feedback resistor R_F had a value of 10^5 ohm with the amplifier gain being $\simeq 10^5$ then for tunnel junction resistances $R_T \gtrsim 10$ the prefactor in equation 4-6 is approximately unity. Thus neglecting the small quantity 1/A and writing the tunnel conductance $1/R_T$ as G_T we have

$$\delta I = I[R_D G_T - 1] \qquad 4\text{-}7$$

substituting into equation 4-4 and simplifying yields:-

$$e_{out} = (IR_D R_F)G_T + I(R_D - R_F) \qquad 4\text{-}8$$

Clearly therefore the output of this bridge is also linear in response but this time in conductance. To calibrate the curves obtained, two points only are required. The most convenient points being those obtained in an open circuit condition (zero conductance) and at the balance condition where $G_T = 1/R_D$.

The condition imposed upon allowable sample resistances by R_F and A were well satisfied in the experiments performed.

CHAPTER 5

EXPERIMENTAL METHOD

1. Sample Fabrication

Prior to the fabrication of the tunnel junction itself, alloys containing various known atomic concentrations of indium in lead were produced in a cleaned environment from extremely high purity constituents (69 purity) which were supplied commercially (Cominco Co.). The tunnel junctions formed from these alloys were of the traditional metal-insulator-metal type prepared by vacuum deposition. Aluminium was chosen for the second electrode for two main reasons. First, it does not itself exhibit any appreciable structure which might cloud observation of the alloy in the energy range of interest and second, it oxidises readily thereby providing a very convenient method of producing the insulating barrier.

A 1" by 1/4" section was cut from a standard glass microscope slide and after being cleaned and fire polished was mounted in the sample holder previously described. This provided the substrate for the tunnel junction and from this point onward it was never necessary to touch the slide again. The sample holder was then constrained in a jig while indium metal contacts were applied to the surface of the glass in places predetermined by the evaporator geometry. Six such contacts were made and wired to the amphenol plug in order to allow four terminal measurements to be made on two junctions simultaneously.

The sample holder was placed in the evaporator which was

pumped to a pressure of better than 1 x 10^{-7} torr before depositing the aluminium electrode from a multistranded tungsten filament. The sample was then removed from the evaporator and placed in a Fisher Isotemp oven in order to form an oxide layer on the aluminium. Oxidation temperatures used ranged from 100°C to 130°C and were applied for durations of from 1 minute to 5 minutes. This resulted in final tunnel resistances of from 50 ohm to 300 ohm. Several attempts were made to control the oxidation process within the evaporator, one of these consisting of a glow discharge in low pressure oxygen and while the glow discharge method was very reproducible the oxide layers so produced did not in general survive the application of pressure. Having returned the sample to the evaporator, the alloy electrodes were deposited using a molybdenum boat. Both the alloy and aluminium electrodes had an approximate width of 1/16" with the latter running the length of the substrate.

2. Mounting Procedure

After filling the oil seal, a slow steady stream of helium gas was allowed to pass through the compressor to the experimental area. Simultaneously the electronic detection system was readied for an immediate check on tunnel resistance. The sample was then removed from the evaporator and, subject to a satisfactory visual inspection of the films, was plugged into the specially designed housing whereupon it was possible to check instantly the approximate tunnel resistance. This was achieved by presetting the modulation level for

a nominal 100 ohm sample and noting the change upon sample contact. The bomb was then screwed loosely into place while being flushed with helium during which time a more accurate check of the tunnel resistance was made.

After tightening the bomb into place the helium pumping chamber was secured (as shown in figure 4) and thermometer connections established. The vacuum can was then soldered into place using Woods metal and evacuated to a pressure of approximately 10^{-5} torr at which point the system was cooled to liquid nitrogen temperature. Pumping of the system was then continued to the lowest attainable pressure in order to provide good thermal isolation between the cryogenic fluid and the bomb.

3. Validity Checks

Before collecting all of the data required from a sample, certain checks were made both on the sample itself and the system. At liquid nitrogen temperature a tunnel characteristic was recorded for $E = +\ 30$ meV to $E \simeq -\ 30$ meV in order to check for major abnormalities and noise levels. Pressure approaching that used for actual measurements was then applied while monitoring the zero bias resistance of the sample to establish reproducibility in this respect. In addition this provided a check on the pressure system itself including the feedthrough. Between the cool down from liquid nitrogen to liquid helium temperatures, the needle valve operation was checked. The transition temperature was also recorded during this process.

The sample was then further cooled to the ultimate limit attainable and examined for the existence of the localised mode. This was most easily resolved by observing the second derivative curve d^2V/dI^2. At this temperature the resistance in the gap region at zero bias was checked in comparison to its normal state value. Since by requiring that this ratio be $<10^{-3}$ at ~1K we can safely neglect any non-tunnelling contribution to the current.

4. An Experimental Run

Having established the validity of a given sample and that support systems were operating efficiently the various low temperature zero pressure characteristics of the sample were recorded. The cryostat was then left until the level of the He_4 bath was just below that of the vacuum can. It was usually found that this practice resulted in a temperature slightly in excess of that predicted by the Simon equation (1937 and 1953) for working pressures of approximately 50,000 p.s.i.g. During the actual pressurisation process, heaters around and inside the pressure tubing were used to insure against capillary blockage. Monitoring of the zero bias tunnel resistance as a function of pressure was also carried out at this time for the prime purpose of determining the final frozen in pressure although it was also possible to detect the occurrence of capillary blockage since when this occurred the external pressure rose while the sample resistance remained constant.

Freezing at constant pressure was then achieved by opening the needle valve while simultaneously maintaining the external pressure

at a constant value. In view of the location of the 1K cooling stage it was expected that the solid would form from the bottom of the bomb upwards.

On the occasions when both junctions on the same substrate were useable it was possible to determine the pressure at two points in the solid separated by ≃ ½". The pressure variation over this distance was found to be of the order of 1% and greatly supports the belief that the technique used did in fact produce pressures which were hydrostatic. With the sample now suspended in solid helium at constant pressure, the liquid helium was restored to a level several inches above the indium O ring seal and the cryostat allowed to cool to the region of 1K, at which point the finite pressure characteristics were recorded.

The penultimate stage of each experimental run provided the challenge of releasing the pressure without destroying the sample and the wiring. It was naturally not possible to attain the temperature necessary to do this while the level of the helium was high and so heaters were employed to boil off the helium to a level below the can. Heat was then applied to the bomb and the high pressure capillary. When the temperature reached a value just below that at which freezing in occurred, the external pressure was raised to just above the frozen in pressure and heating continued. When the fluid phase was realised the pressure indicated by the Heise Bourdon gauge showed a sudden change in value corresponding to the equalisation of pressures. This change was also noted at the sample itself via the zero bias resistance. Early attempts to

release the pressure at temperatures slightly above the melting temperature resulted in destruction of both sample and wiring. This was thought to be due to the retention of a plug of solid helium high in the capillary tube which itself is evidence that the cryostat temperature is non uniform during this process. An alternative method of de-pressurisation would be to wait until the helium level fell naturally to the desired level but since the cryostat must be full duing the actual measurements, this would always be an extremely lengthy wait. In contrast, the method used involved the use of elevated temperatures, a disadvantage which was tolerated subject to the careful monitoring of the process.

After returning the system pressure to zero again a further check on the reproducibility was made both on the resistance value and the observed structure location.

5. Determination of Sample Composition

Despite the fact that the sample was formed from an alloy whose composition was known, the final composition of the evaporated electrode remained to be determined since the vapour pressures of the elements differ widely (see for example Nesmayanov (1963)). To do this, residual resistance ratio techniques were employed (see for example Rosenberg) in which the ratio R_{293}/R_4 for the samples was compared to a calibration curve of the same quantity that had been obtained by measuring a series of alloys of known composition. Several pieces of each known alloy were taken from various places

on the ingot and rolled out to ≃ .001" in thickness. The same sample holder that was used for the tunnelling measurements (figure 5) was used to mount these speciments but with a slight variation. A plain glass slide was first placed in the holder and four indium contacts were soldered across its width. Wires were then attached to these contacts at the edges and also to the plug. Pieces of the rolled ingot were then cut to slightly less than the size of this glass slide and placed on top in such a way as to cover the raised indium contacts. A second slightly smaller glass slide was then placed on top (thereby sandwiching the sample onto the contacts) and held in place with masking tape.

The sample holder was then placed in a dipstick arrangement wired for a four terminal resistance measurement. Resistance measurements were then made using a Cambridge Instruments high resolution potentiometer both at room temperature and at liquid helium temperature. The latter measurement was made by placing the sample at the centre of a Westinghouse 21 Kilogauss superconducting magnet and applying the necessary field to induce the normal state. All measurements were carried out for currents in both directions and averaged over all samples from an ingot of a particular concentration. It was in fact found in this way that the original alloys were homogeneous. The calibration curve obtained by this procedure is shown in figure 11.

A determination of the ratio R_{293}/R_4 for the pure lead from which the alloys were made yielded a value of ≃ 21,000 thereby

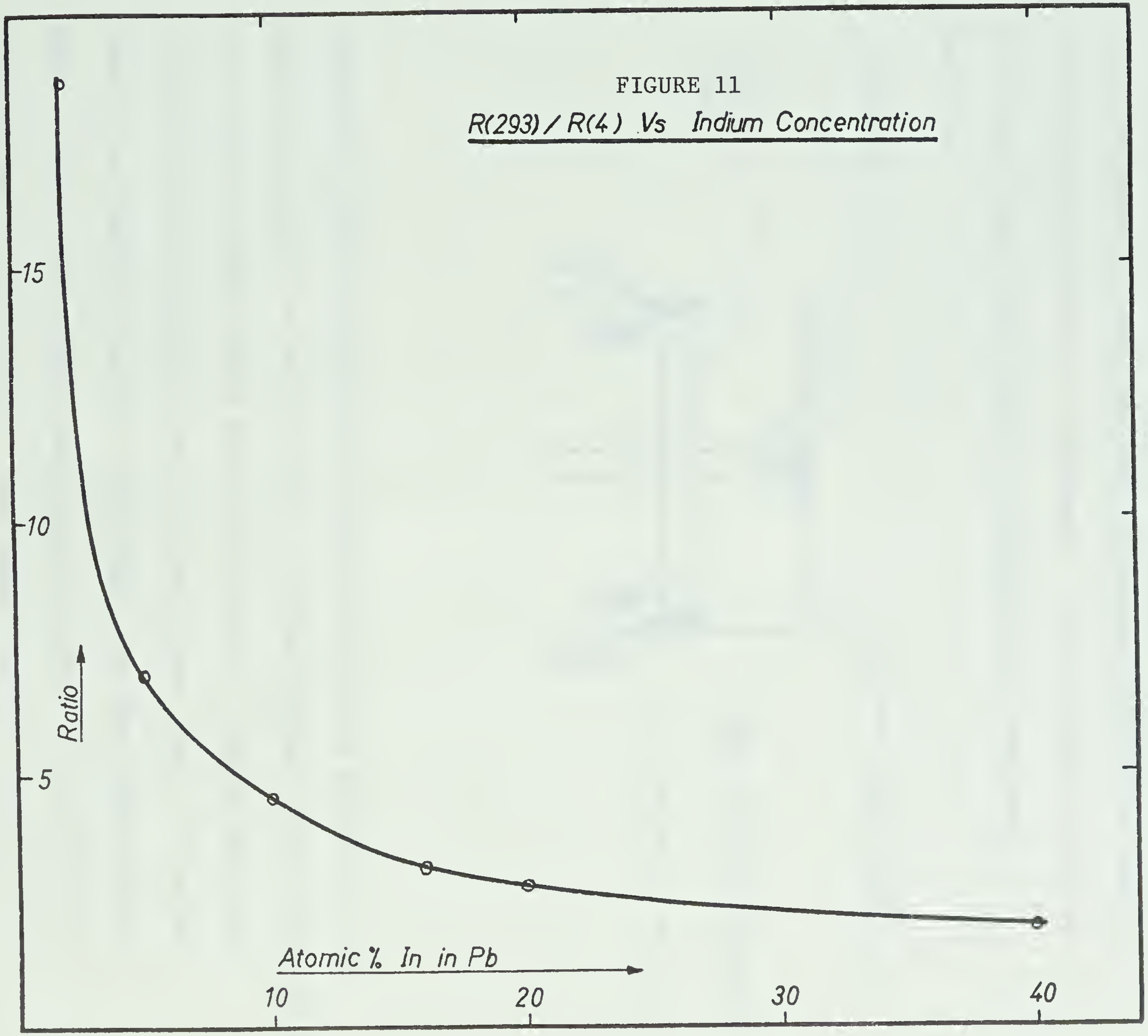

FIGURE 11

R(293) / R(4) Vs Indium Concentration

attesting to its high degree of purity. Before the ratio R_{293}/R_4 for the actual films that were tunnelled through could be determined it was necessary to apply two more contacts to the film to enable a four terminal resistance measurement. This was done as shown in the diagram below which shows an enlarged view of one tunnel junction.

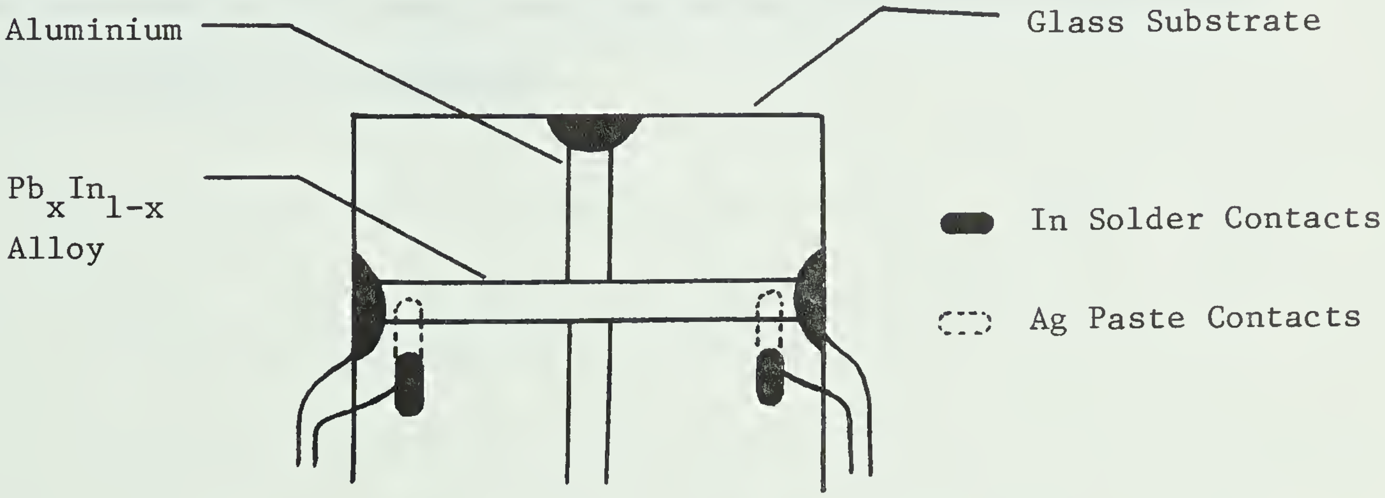

Indium was first deposited at two places as close as possible to the existing contacts and wires attached. Bridges between these points and the film itself were then formed using silver paste. Several such coats of silver paste resulted in very low resistances from A - B of the order of a fraction of an ohm. Once again the same sample holder was utilised. Indium metal was chosen throughout for contacting purposes due to its ability to "wet" glass, however, for this particular application it was essential not to attempt to solder to the film itself with indium since not only would the film probably not survive the process but more importantly if it did, it would not

be possible to say with any certainty that indium from this source had not itself diffused into the film. Contacts using silver paste alone to secure the wires were tried but found to be unreliable at low temperature.

It was very reassuring to notice during these experiments that the potential difference across the alloy films vanished (as would be expected) as the superconducting state was realised regardless of the nature of the contacts.

CHAPTER VI

EXPERIMENTAL RESULTS AND DISCUSSION

1. Introduction

It has been observed by several workers (see Adler (1967) for example and Sood (1971)) that the major properties of interest do not differ significantly over samples whose impurity concentrations vary by ~2 at % which, coupled with the inability of a large proportion of the samples to withstand high pressure, led this author to limit investigations to the concentrations $Pb_{64}In_{36}$ and $Pb_{88}In_{12}$. Such a choice offers the advantage of being able to group together data from samples whose impurity concentrations vary by the above mentioned tolerance (2%) while still being indicative of any trends in the data which are concentration dependent (as a consequence of the ~25 at % difference). Except where specifically mentioned therefore, results quoted henceforth indicate averages for the particular compositions over those samples whose concentrations (as determined by the residual resistance ratio methods described earlier) satisfied the above condition.

The capacitance of each sample was determined in order to estimate the thickness of the oxide layer (which constituted the barrier). These values ranged from 0.038μF to 0.051μF over nine samples which included both the $Pb_{88}In_{12}$ and $Pb_{64}In_{36}$ samples (since the oxide layer is dependent only on the oxidation conditions of the aluminium electrode which is common to both alloys). Assuming

the tunnel junctions to be simple parallel plate capacitors of area $2.25 \times 10^{-6} m^2$ and obeying the relationship $C = \varepsilon A/d$, the barrier thickness is estimated to be ~50Å where the dielectric constant of the Al_2O_3 has been taken as 9.34 from Gray (1972).

By measuring the resistance of the alloy electrodes (which were of the order 1.5 ohm - 2 ohm) and assuming the value of 21μohm cm for the resistivity of lead, as taken from Meaden (1965), the thickness of the alloy electrodes is estimated to be from 4400Å - 5800Å.

2. Pressure Dependence of the Transition Temperature

The development of the energy gap in the electronic quasiparticle density of states of the superconducting electrode of the tunnel junctions provided a very convenient method of determining the transition temperature of the alloys under investigation. This method involved monitoring the tunnel conductance of the samples at zero bias (in the middle of the energy gap region) and noting the temperature at which the sample conductance exhibited a sharp decrease. Although the width of the superconducting transition has been shown by Adler et al (1965) to be $\sim 5 \times 10^{-2}$K for the lead-indium alloy system (up to 26 at % In), the transition temperatures measured in this way are still very accurate (better than ± 10 mK). This is so since the conductance undergoes a very large change over this temperature and is readily observable with the high gain detection system that was employed for the whole of

the tunnelling experiments performed.

The measurement of the transition temperature for each sample was repeated at least five times and averaged. Experimental accuracy of this data was limited mostly by the resolution of the electronic circuitry associated with the germanium resistance thermometer and to a lesser extent by the uncertainty in the pressure determination.

Included in Table 1, which contains the numerical averages obtained, are average values for the ratio of room temperature resistance to liquid helium temperature resistance of the alloy films (R_{293}/R_4) for the respective compositions. By referring to figure 11 a more precise value for the average sample concentration could be obtained than the nominal 12 at % and 36 at % figures which have been rounded to the nearest one percent and which will be used henceforth.

TABLE 1

Pressure Dependence of the Transition Temperature

Concentration (at % In in Pb)	$\frac{R_{293}}{R_4}$	T_c(P=800 p.s.i.) (K)	$\frac{dT_c}{dp}$ (10^{-5}K bar^{-1})	$\frac{d\ln T_c}{dp}$ (10^{-6} bar^{-1})
12	3.69	7.110 ±.008	-3.19 ±.16	-4.48 ±.22
36	2.18	6.75 ±.008	-3.06 ±.15	-4.53 ±.23

For comparison purposes, Table 2 lists the values of T_c determined by other workers at zero pressure (for impurity concentrations as close as possible to those of interest here).

TABLE 2

Comparative Transition Temperatures (at Zero Pressure)

Authors	Concentration (at % In in Pb)	T_c(P=0) (K)
Adler et al (1967)	12	7.097
Farrel et al (1969)	10	7.05
Farrel et al (1969)	40	6.57
Adler et al (1967)	40	6.63
Wu (1967)	40	6.65*

*Theoretical

Several factors can affect the critical temperature of a superconductor when determined from a thin film sample. The most important of these being effects of structure, impurity content and stress.

For samples which are formed at room temperature the crystalline structure is generally not that different from that of the bulk, providing the film is sufficiently thick, and critical temperatures measured in this case are indicative of those for the bulk material. The transition temperature of superconductors deposited at low temperatures however can exhibit considerable enhancement as for the case of aluminium for which transition temperatures up to 2.5K have been observed. The underlying reason is that at low deposition temperatures the atom mobility of the condensate is low and the crystalline growth is inhibited yielding an amorphous structure. An extreme example of this effect, observed by Lazaren et al (1957)

is that of beryllium which in its normal crystalline state is a non superconductor whilst if deposited at low temperature exhibits a transition temperature of 8K. If annealed, the transition temperature of a sample exhibiting this kind of T_c enhancement reverts to that of the "bulk" state. Since the samples used in these experiments were produced at room temperature and a finite time necessarily elapsed before cooling, structure enhanced T_c's are not expected.

Impurities constitute a more significant effect on the transition temperature by generally decreasing the value of T_c linearly with decreasing electronic mean free path. According to Mathiessen's rule the decrease in T_c in this regard is linear and given by:-

$$\Delta T_c = K\rho_{res}$$

where K is a constant associated with the solute-solvent pair and ρ_{res} is the residual resistance. Since the samples used were produced by vacuum deposition, the main source of unwanted impurities would be gaseous in nature. Doping of indium with oxygen for example depresses its transition temperature. Depression of the transition temperature due to the inclusion of impurities was minimised however by depositing the films from extremely pure source materials after first attaining the highest possible vacuum. A liquid nitrogen trap was employed to assist in the pumping as well as to reduce the backstreaming of oil from the diffusion pump.

Stress effects as a result of differential contraction between the substrate and the film have the effect of enhancing the transition

temperature. This problem has been investigated by Toxen (1961) for the case of indium on fused quartz substrates who calculated an expression for the change in transition temperature given by:-

$$\Delta T_c = \frac{52}{d} - \frac{750}{d^2}$$

where d is in Angstroms. For a film of thickness 5000Å this amounts to an increase in T_c of ~10mK.

It is difficult to make a quantitative assessment of the net effect of the previous factors although for thick films (>3000Å) bulk values of T_c for lead at least seem to be in close agreement with those obtained using tunnelling techniques (see Franck & Keeler (1967)).

It can be seen from Tables 1 and 2 that there is good agreement between the values obtained here for the alloys with those of other workers. The last column in Table 1 has been included for referral purposes in a later section since it provides a convenient form for theoretical comparison.

3. The Energy Gap and its Dependence on Pressure

Determination of the superconducting energy gap was less direct than was the determination of the transition temperature. At the finite temperatures employed here, the conductivity does not exhibit a sharp discontinuity at biases close to the energy gap region but appears as a smooth continuous function. Consequently a criterion has to be established for deciding at which point to

evaluate the gap. Figure 12 shows typical characteristics of a $Pb_{64}In_{36}$ junction both at low and high pressure recorded at a temperature of ~2.5K in which it can be seen that although a large decrease in conductance occurs, no one obvious point is in evidence for the gap determination.

One such criterion which is widely used is that proposed by McMillan & Rowell (1969) for example in which one makes the measurement from zero applied bias to the mid-point of the current jump in the current voltage characteristic of the superconductor. On the conductance curves that were recorded here this point corresponds to the inflection point on the low energy side of the conductance maximum.

The normalised conductance of a B.C.S. superconductor at finite temperatures has been tabulated by Bermon (1964) as a function of the reduced parameters (bias/energy gap) and (energy gap/k_BT) where k_B is Boltzman's constant and T the temperature in Kelvins. By comparing the conductance plots obtained in these experiments with this tabulation and identifying the one which most closely approximates the experimental curve the value of the latter reduced parameter was identified and since the temperature of the experimental determination was known, it was possible to calculate the gap. In employing this procedure, emphasis was placed on the curve matching procedure in the higher energy region where the gap edge might be expected and where the error in the conductance measurements was least. The criterion of McMillan and Rowell is implicit in this approach if, when the parameter

FIGURE 12

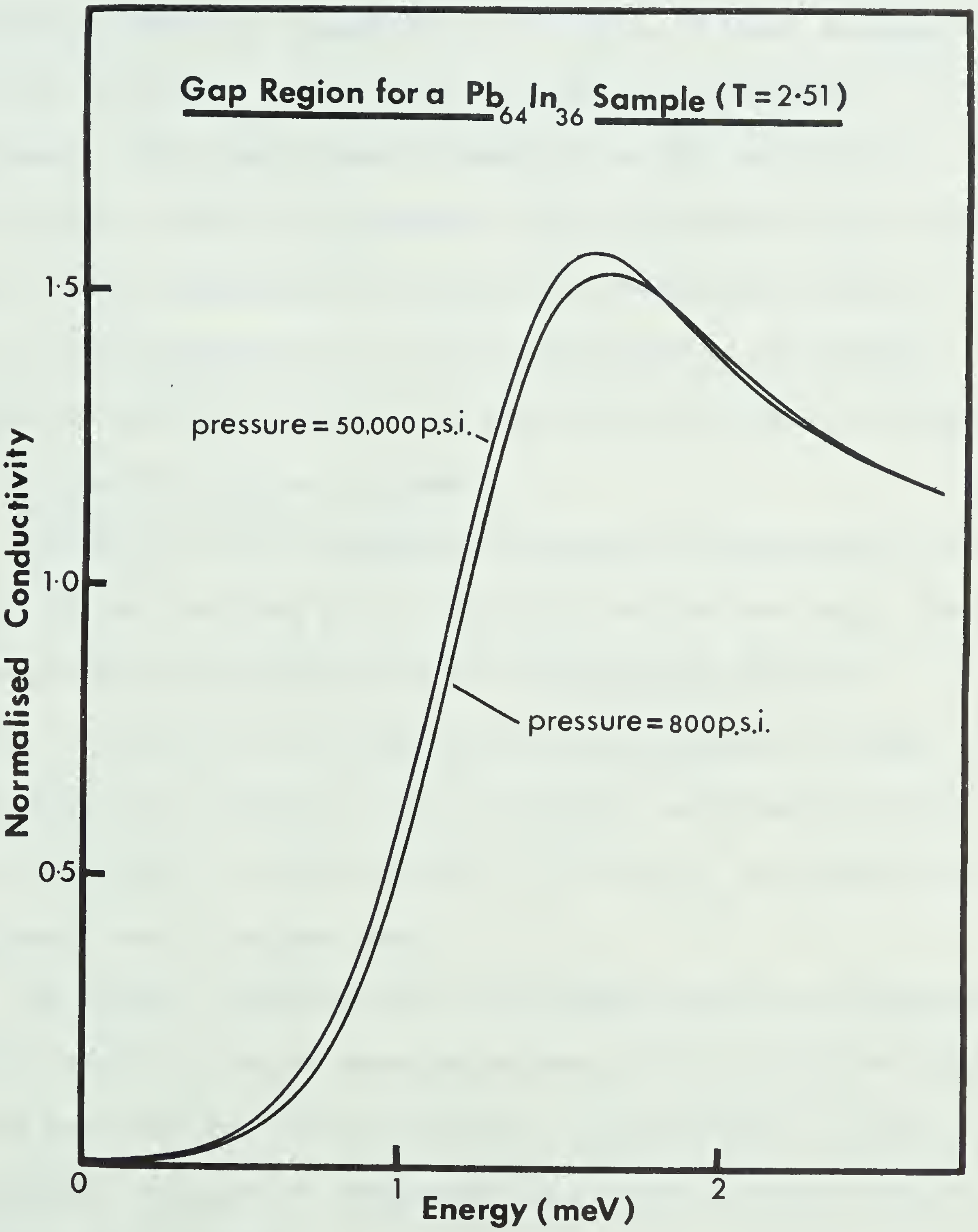
Gap Region for a $Pb_{64}In_{36}$ Sample (T = 2·51)
pressure = 50,000 p.s.i.
pressure = 800 p.s.i.
Normalised Conductivity
1·5
1·0
0·5
0
1
2
Energy (meV)

bias/Δ assumes the value unity, the experimental and tabulated conductance values correspond.

For the example of figure 12 this procedure yielded a value of $\Delta = 1.230$meV. Since it would be difficult to compare gaps measured at different temperatures with those of other workers it is usual to convert these values to their zero temperature analogues. This can be done by referring to the tabulation of Mühlschlegel (1959) which expresses the relationship between the gap at finite temperature to that at zero temperature again, for a B.C.S. type superconductor. At the temperature of this example (2.51K) an increase of 1% in Δ is predicted and we have, therefore, $\Delta = 1.243$meV for the case at hand.

The whole of the foregoing has assumed the superconductor to be of the weak coupling B.C.S. type which was not the case. For strong coupling superconductors the energy gap is given by $\Delta = \Delta_1 + i\Delta_2$ where both Δ_1 and Δ_2 are also functions of energy. The above method is, however, still an excellent approximation since as will be seen in a later section, $\Delta_2 \simeq 0$ and Δ_1 is constant for energies close to the gap edge.

The pressure induced shift in the energy gap was obtained more readily and with greater expected accuracy than the absolute value of the gap since for curves recorded at approximately the same temperature the point of comparison can be seen to be non critical over a wide range of energy.

Table 3 summarises the results obtained for the pressure

dependence of the energy gap.

TABLE 3

Pressure Dependence of the Energy Gap

Concentration (at % In in Pb)	$\Delta(P=0)$ (meV)	$\frac{d\Delta}{dp}$ (10^{-6}meV bar^{-1})	$\frac{d\ln\Delta}{dp}$ (10^{-6} bar^{-1})
12	1.32	$-8.14 \pm .40$	$-6.16 \pm .30$
36	1.242	$-8.57 \pm .43$	$-6.90 \pm .36$

Taking the logarithm of the B.C.S. gap ratio expression we have that:-

$$\frac{d\ln\left(\frac{2\Delta}{k_B T_c}\right)}{dp} = \frac{d\ln\Delta}{dp} - \frac{d\ln T_c}{dp}$$

substituting the average values of $\frac{d\ln\Delta}{dp}$ and $\frac{d\ln T_c}{dp}$ from Tables 3 and 1 respectively in the above expression gives:-

$$\frac{d\ln\left(\frac{2\Delta}{k_B T_c}\right)}{dp} = -1.68 \pm .52 \text{ for } Pb_{88}In_{12}$$

and $$\frac{d\ln\left(\frac{2\Delta}{k_B T_c}\right)}{dp} = -2.37 \pm .59 \text{ for } Pb_{64}In_{36}$$

Both of these results indicate a trend towards weaker coupling as a function of applied pressure but apparently to a lesser extent than that found for pure lead by Franck & Keeler (1968). The comparitive rate of change of the gap and transition temperature can also be estimated from the data of Tables 1 and 3 which give:-

$$\frac{d\ln\Delta}{d\ln T_c} = 1.375 \pm .53 \text{ for } Pb_{88}In_{12}$$

and $$\frac{d\ln\Delta}{d\ln T_c} = 1.523 \pm .58 \text{ for } Pb_{64}In_{36}$$

Table 4 lists the values of other workers which are relevant to those parameters determined here. In contrast to Table 2, however, we are now able to compare the pressure dependence of our data with the very recent work of Hansen et al (1973) and Galkin et al (1973)

TABLE 4

Comparative Pressure Dependence of the Energy Gap

Authors	Concentration (at % In in Pb)	$\Delta(P=0)$ (meV)	$\frac{d\Delta}{dp}$ (10^{-6}meV bar^{-1})	$\frac{d\ln\Delta}{dp}$ (10^{-6} bar^{-1})
Adler et al (1967)	12	1.33		
Hansen et al (1973)	12	1.351	-10.3 ±.06	-7.63 ±.48
Galkin et al (1973)	12	1.34		-8.8 ±.60
Adler et al (1967)	40	1.21		
Galkin et al	40	1.22		-7.9 ±.60

Hansen et al do not appear to have measured T_c although in their publication they allude to a $d\ln T_c/dp$ for $Pb_{88}In_{12}$ of $-5.4 \pm 2.6 \times 10^{-6}$ bar^{-1} as being an experimental value. Using this value (which pertains to Pb) with their experimentally determined $d\ln\Delta/dp$ however yields a value of

$d\ln\Delta/d\ln T_c = 1.413 \pm 3.1$ which, regardless of the large tolerance, is in excellent agreement with the value obtained by this author.

The decrease in the B.C.S. gap ratio in strong coupling superconductors subjected to hydrostatic pressure (indicative of a trend towards weaker coupling) has been explained in a series of publications revolving around the numerical solution of the Eliashberg equations. The Eliashberg equations (as was pointed out in Chapter II) allow provision for the explicit form of the phonon spectrum of a given metal wherein lies the crux of the problem.

Using a Born-von Kármán force constant fit to the dispersion curves obtained from inelastic neutron scattering experiments to obtain information on the lattice vibrations and combining this with the Coulomb pseudopotential term, Carbotte and Dynes (1968) calculated the form of the electron-phonon interaction (essential to the superconducting state) and from this calculated a form for $\alpha^2F(\omega)$ for use in the Eliashberg equations which led to a value of $\Delta = 1.49$ for lead.

These calculations were then extended to finite pressure by Trofimenkoff and Carbotte (1969) who, for the $\alpha^2F(\omega)$ at finite pressure, simply scaled the zero pressure $\alpha^2F(\omega)$ upward in energy by the observed average change in sound velocities. By incorporating the experimental evidence of Franck & Keeler for lead that T_c decreases according to $\sim(\Delta)^{\frac{1}{2}}$ they were able to predict qualitatively the observed reduction of T_c with pressure.

Still within the framework of the calculations of Carbotte and Dynes, Trofimenkoff and Carbotte (1970) again solved the Eliashberg

equations this time for Δ and T_c at zero and at finite pressure but with a new scaling procedure for producing the pressure dependent $\alpha^2F(\omega)$. This scaling, again concerned with the electron-phonon interaction, consisted of shifting of the phonon frequencies to higher energy by an amount implied by an average Grüneisen parameter and the calculation of a re-screened pseudopotential. Beside the prediction of pressure dependences of the energy gap and transition temperature which were in excellent agreement with the experimental results Franck & Keeler,(through the relation $d\ln\Delta/d\ln T_c$) they also note that the repulsive Coulomb part of the electron-phonon interaction is fairly insensitive to pressure and can be accounted for by a simple scaling factor. Trofimenkoff & Carbotte further predict a certain degree of pressure dependence in $d\ln\Delta/d\ln T_c$ as can be seen in Table 5 which lists their values together with those obtained from experiment.

TABLE 5

Relative Rate of Change of the Energy Gap and Transition Temperature

Authors	Concentration (at % In in Pb)	$\frac{d\ln\Delta}{d\ln T_c}$
Trofimenkoff & Carbotte (1970)	0	1.92 2.18 (P ~ 24.4 kbar)
Franck & Keeler (1968)	0	2.06 ± .3
Hansen et al (1973)	12	1.413 ± 3.1
This work	12	1.375 ± .53
This work	36	1.523 ± .58

There would appear to be very good agreement therefore of these experiments with theoretical predictions. Carbotte and Vashishta (1971) have extended these calculations to finite temperatures and carried them out with greater numerical precision although their findings for the case of strong coupling lead do not differ significantly from those of Troffimenkoff and Carbotte.

The choice of scaling the finite pressure phonon spectrum to higher energy stems from the work of McMillan (1968) who defined a parameter λ as a measure of the coupling strength and showed that $\lambda \propto \frac{1}{\omega^2}$ where ω represents the frequency of the phonons responsible for the electron-phonon coupling.

The results obtained for the alloys also indicate a decrease in gap ratio (and hence coupling strength) as a function of concentration with typical values of $2\Delta/kT_c$ being 4.32 and 4.28 for the $Pb_{88}In_{12}$ and $Pb_{64}In_{36}$ alloys respectively. This is not too surprising since the electron/atom ratio has decreased in each case resulting in a reduction in the screening of the ion sites and thus a corresponding reduction in the strength of the electron-phonon interaction.

Further effects on the gap, T_c and the gap ratio include those effects mentioned in the previous section (for T_c) and possible gap anisotropy effects. The transition temperature can also be dependent on crystal alignment in the film. The net effect of these latter factors is, for all intents and purposes, inestimable.

4. Pressure Dependence of the Phonon Spectrum

A great deal of information regarding the phonon spectra of the alloys can be obtained from the tunnel conductance characteristics some of which, namely the location and pressure shifts of the principle phonon modes (and hence the associated Grüneisen parameters), is observable in a very direct manner.

Further information can be obtained somewhat less directly in a procedure (to be described) which involves the numerical solution of the Eliashberg equations. This latter approach involves extensive computation but produces as a result an overall view of the phonon spectrum, the renormalization function and the gap function as well as such important parameters as λ, (the coupling strength) and μ^* (the Coulomb pseudopotential term).

The two different approaches employed in dealing with the data of this section, therefore, suggest a natural subdivision for its analysis.

a. Directly Observed Principle Phonon Characteristics.

It was shown in Chapter II that the normalised tunnel conductance was in one to one correspondence with the electronic quasiparticle density of states and further that structure in the density of states was a reflection of the phonon characteristics of the metal in question. Since phonon structure is measured from the gap edge, the tunnel characteristics and their derivatives appearing henceforth

are displayed so that their gap edge energies coincide. In this way, shifts in phonon energies are directly observable. Figures 13 and 14 show characteristics for typical $Pb_{88}In_{12}$ and $Pb_{64}In_{36}$ tunnel junctions together with their B.C.S. weak coupling counterparts (which do not contain the specific nature of the phonon spectrum). The general decrease in the sharpness of the structure of these curves with increasing indium concentration is consistent with the trend towards weaker coupling that was observed previously in the gap ratio at zero pressure. Critical points in the phonon spectrum corresponding to the predominant phonon modes, manifest themselves in the conductance curves as points of inflection which can be easily resolved by differentiation whereupon each point of inflection gives rise to a peak.

The phonon structure observed in this way was found to be sharper with decreasing temperature and thus the lowest temperatures that could be maintained fairly constant were employed in these determinations. With decreasing temperature however the possibility of instrumental smearing of the data becomes more prevalent. A temperature of 1.4K for example, corresponds to a thermal smearing of ~120μV of the Fermi surface and thus to ensure that the smearing of data was thermally rather than instrumentally limited, applied modulation signals should be as small as possible and certainly less than that corresponding to the temperature at which the measurements are to be made. For the second derivative measurements here (and also for the gap determinations) applied modulation signals were of the order of 10μV - 20μV r.m.s. It is note worthy that during the measurement

FIGURE 13

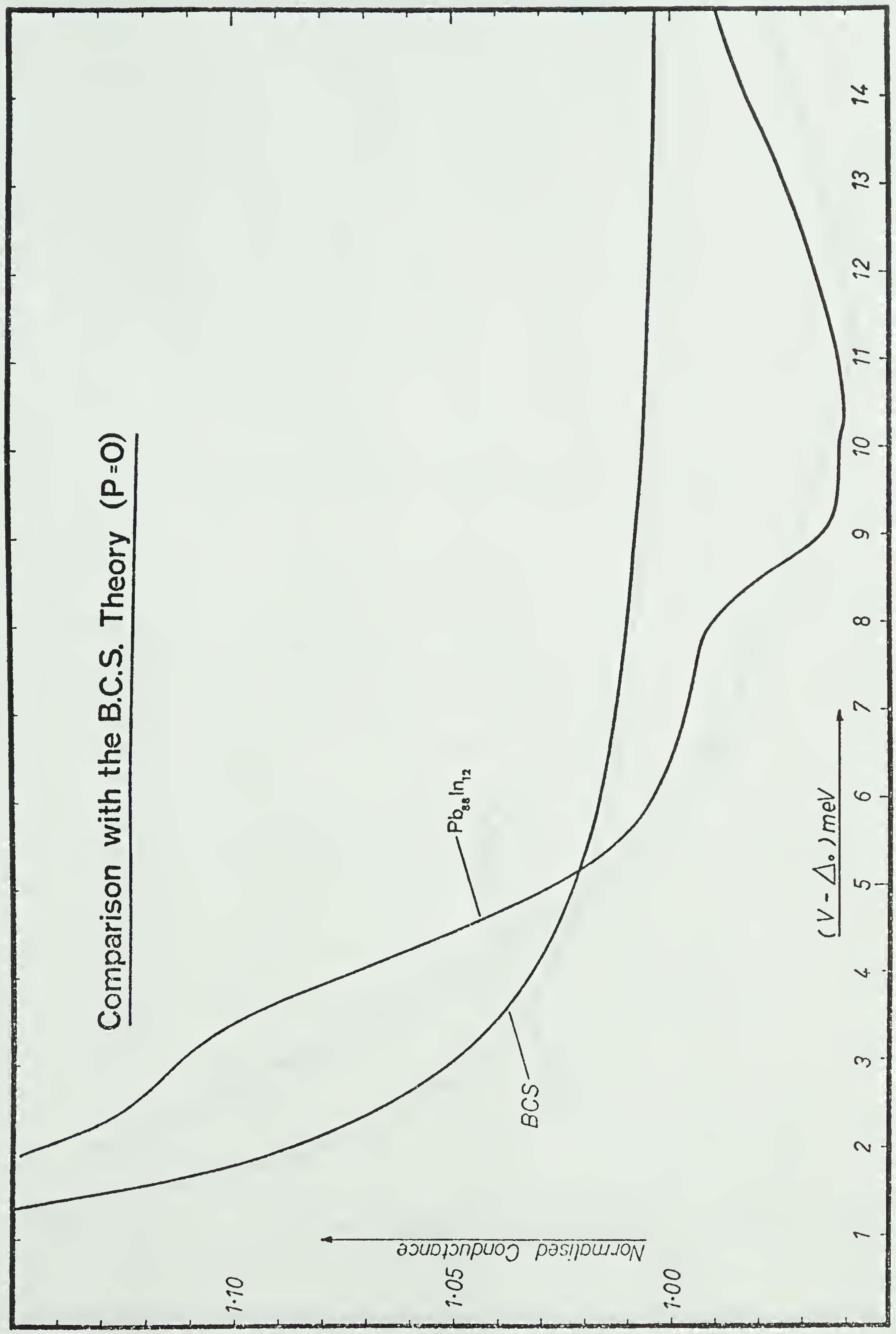

Comparison with the B.C.S. Theory (P=O)

FIGURE 14

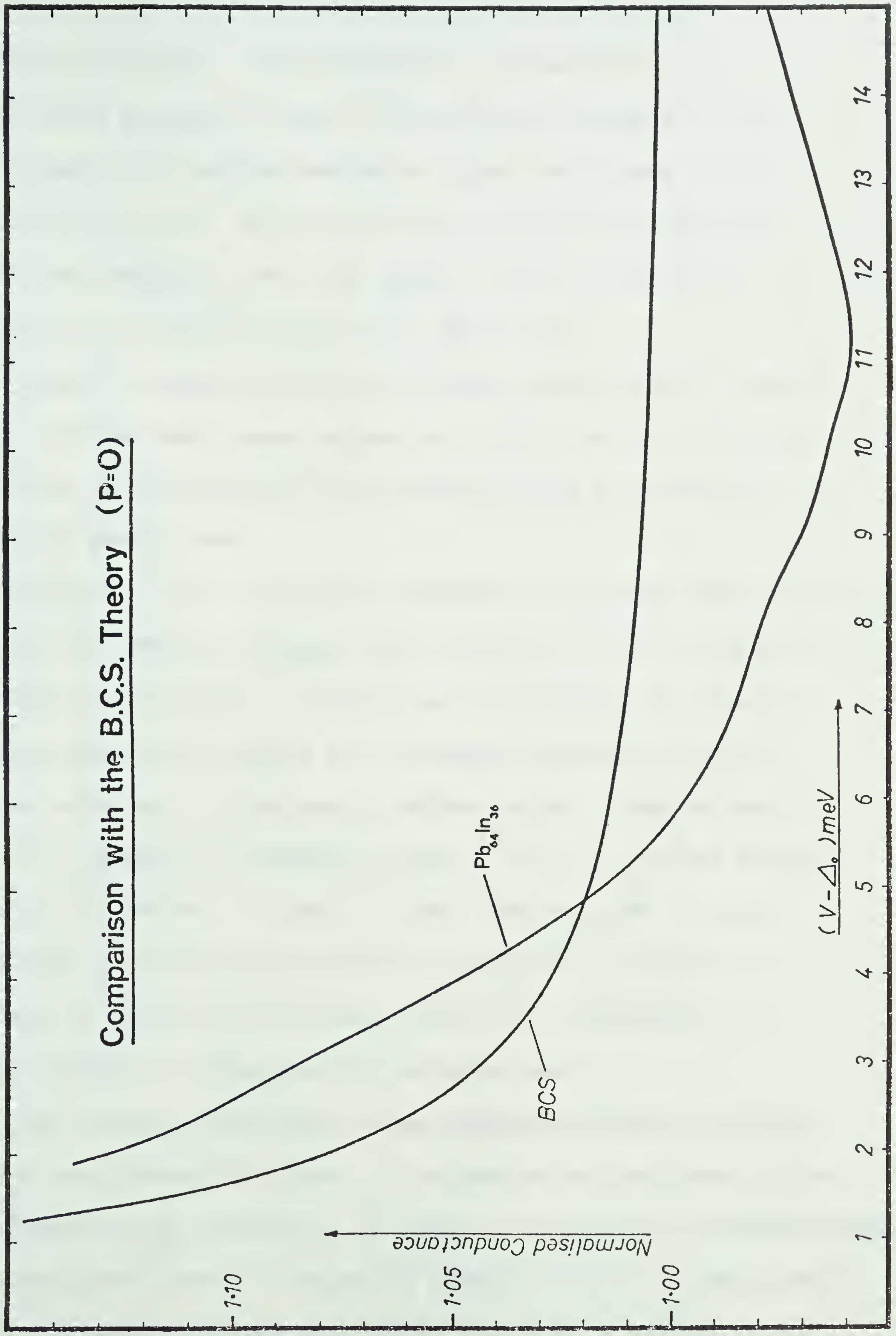
Comparison with the B.C.S. Theory (P=O)
Normalised Conductance
1·10
1·05
1·00
$Pb_{64}In_{36}$
BCS
$(V-\Delta_o)$ meV
1
2
3
4
5
6
7
8
9
10
11
12
13
14

of the energy gaps, it was observed by this author that the conductance maximum (at least) was definitely dependent on the magnitude of the applied modulation signal for signals in the range >100μV r.m.s. At the particular point of observation the shift was observed to be of the order .4% for an increase in modulation of 70μV r.m.s. above the 100μV level.

Figure 15 shows a typical conductance characteristic together with the associated second derivative in this case for a $Pb_{64}In_{36}$ sample as an illustration of the general method of locating the principle phonon peaks.

Figures 16 and 17 show the normalised conductance characteristics for typical samples of $Pb_{88}In_{12}$ and $Pb_{64}In_{36}$ that were obtained as a function of pressure. By comparing qualitatively the figure 17 with the figure 16 we again see the general washing out of the phonon structure with increasing indium content. Less obvious, but still apparent, by examining figures 16 and 17, is the general shift in the phonon spectrum to higher energies. The structure amplitude reduction which occurs as a function of pressure (as opposed to indium concentration) is not easily observable from these curves as a consequence of the scale used.

The principle difference in the phonon spectrum of the lead-indium alloy system from that of pure lead is the existence of the localised mode of vibration. The power of the method of differentiating the conductance curve to locate the phonon structure is emphasised in figure 18 which shows the high energy region for a typical $Pb_{64}In_{36}$

FIGURE 15

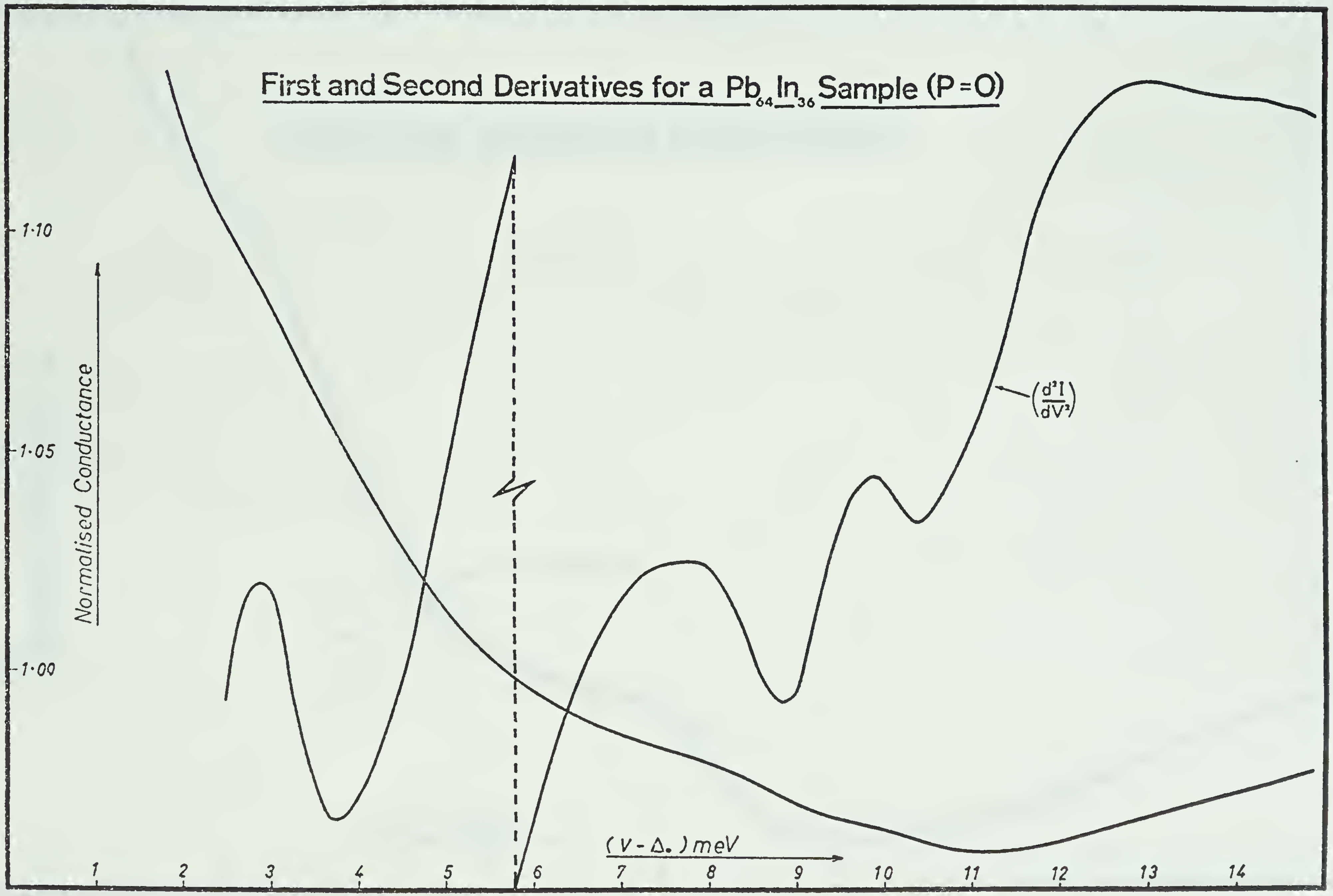

First and Second Derivatives for a $Pb_{64}In_{36}$ Sample (P=O)

FIGURE 16

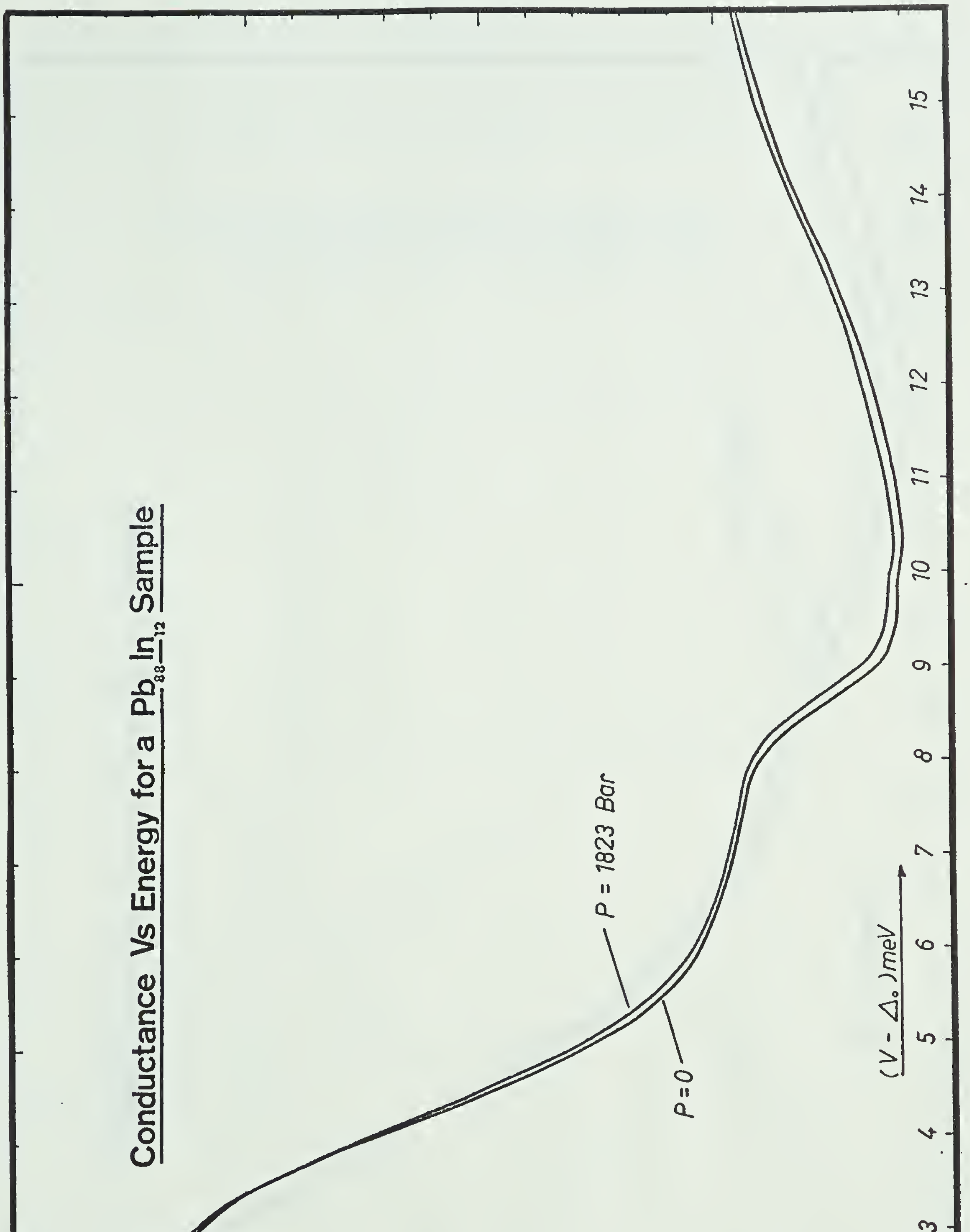
Conductance Vs Energy for a $Pb_{88}In_{12}$ Sample
Normalised Conductance
1·10
1·05
1·00
P = 1823 Bar
P = 0
(V - Δ_0) meV
1
2
3
4
5
6
7
8
9
10
11
12
13
14
15

FIGURE 17

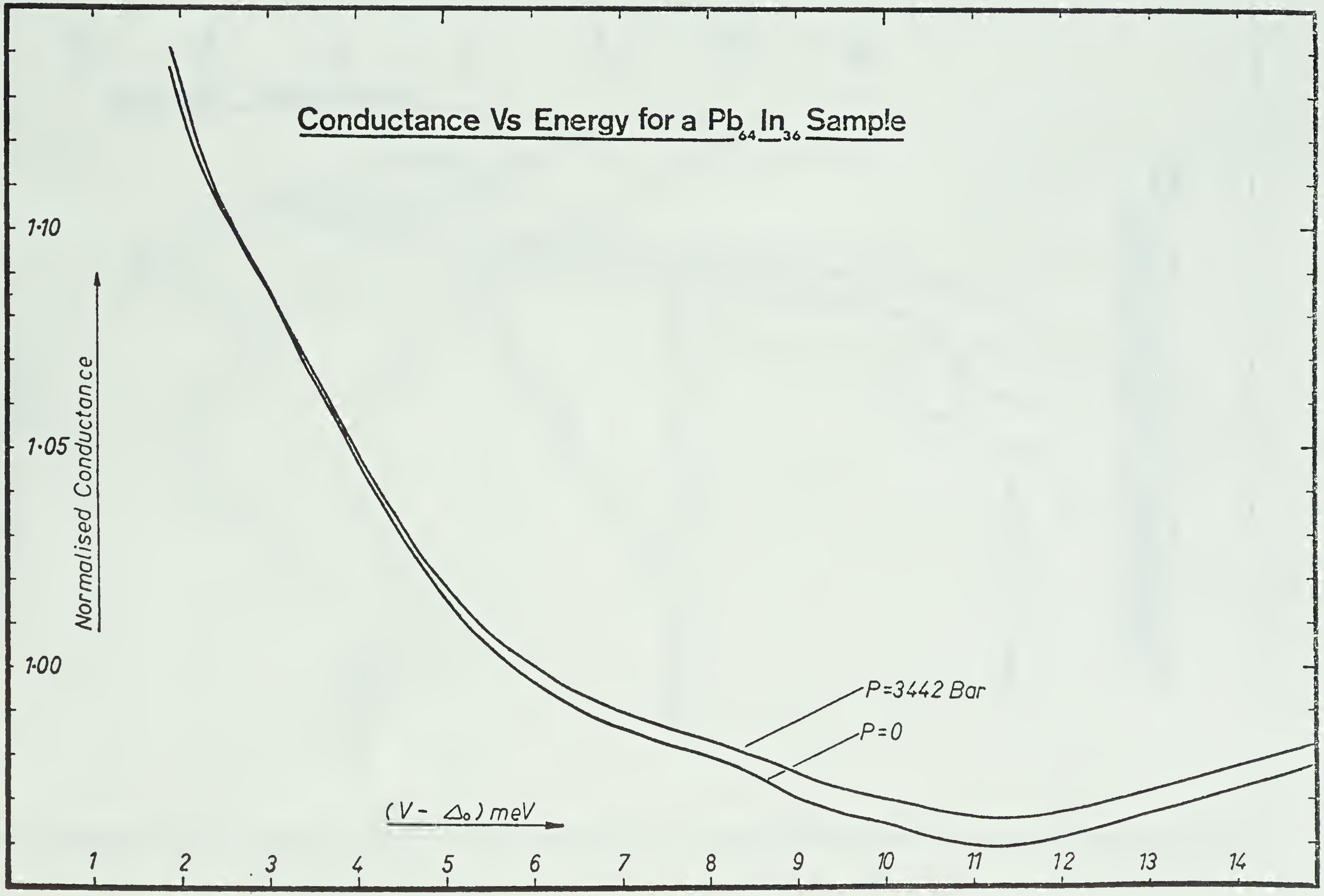

Conductance Vs Energy for a $Pb_{64}In_{36}$ Sample

FIGURE 18

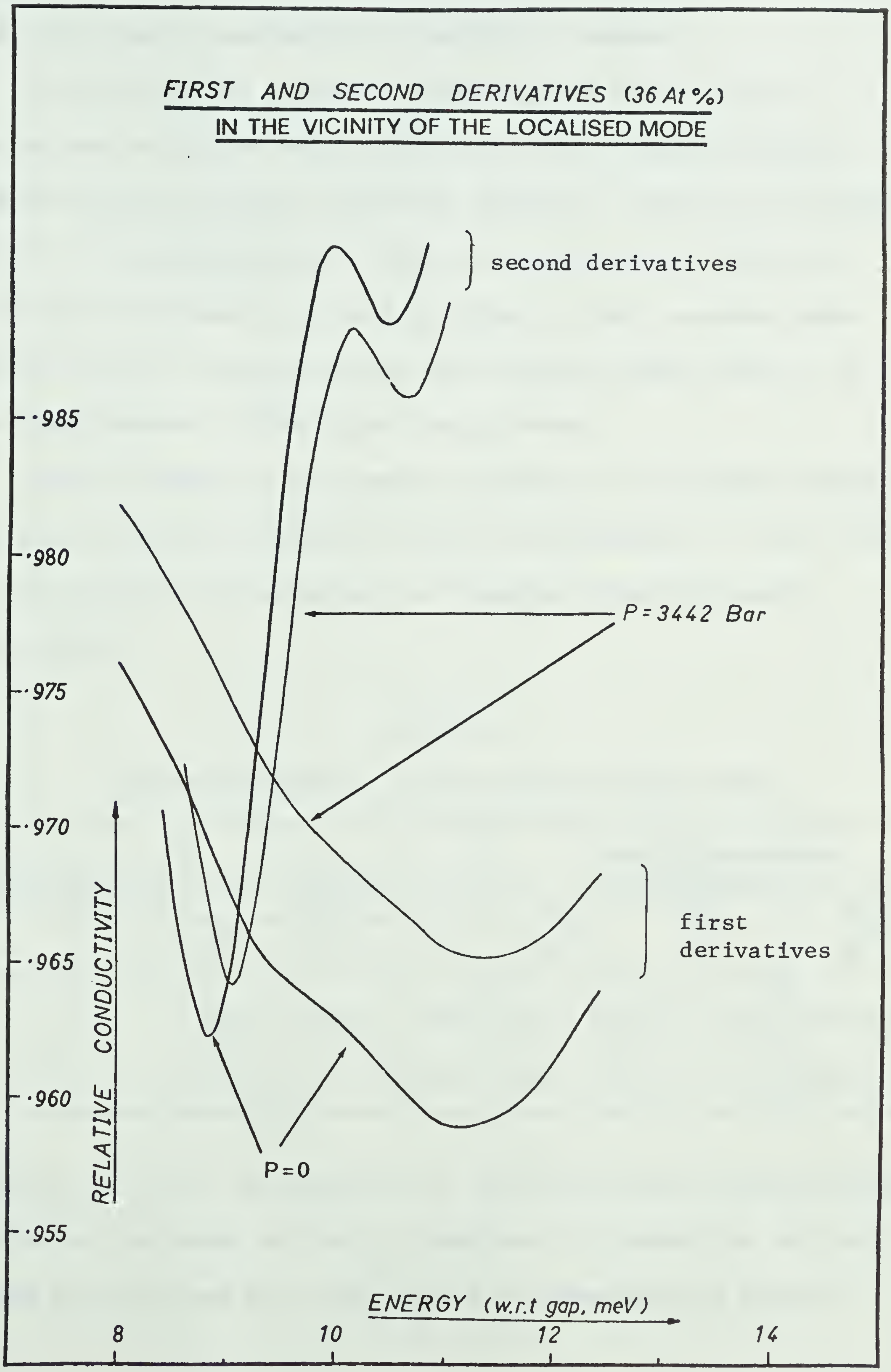
FIRST AND SECOND DERIVATIVES (36 At %)
IN THE VICINITY OF THE LOCALISED MODE
second derivatives
first derivatives
P = 3442 Bar
P = 0
RELATIVE CONDUCTIVITY
·985
·980
·975
·970
·965
·960
·955
ENERGY (w.r.t gap, meV)
8
10
12
14

sample. In this figure the shifts in the longitudinal and localised modes are clearly resolved as a function of pressure.

In resolving the predominant phonon peaks a difficulty is encountered in the low energy region where two transverse phonon branches exist at slightly different energies. This has the overall effect of broadening the peak while also adding slight structure. By using the minimum in the peak obtained for the transverse mode (as was done for the longitudinal and localised modes) what has in fact been measured is the higher energy branch.

Table 6 summarises the results pertaining to the phonon energies and their pressure dependence in which the subscripts t, l and i refer to the transverse, longitudinal and localised (impurity) modes respectively.

TABLE 6

Pressure Dependence of the Principle Phonon Peaks

Concentration (at % In in Pb)	Peak Location (P=0) (meV)			Pressure Dependence (10^{-5}meV bar^{-1})		
	ω_t	ω_l	ω_i	$\frac{d\omega_t}{dp}$	$\frac{d\omega_l}{dp}$	$\frac{d\omega_i}{dp}$
12	4.30	8.65	9.86	2.74 ±.69	5.21 ±.52	4.33 ±.65
36	3.67	8.79	10.43	2.24 ±.56	4.97 ±.50	4.01 ±.6

Hansen et al (1973) and Galkin et al (1973) have very recently obtained results on the phonon shifts as a function of pressure for the lead-indium alloy systems and their results are summarised in Table 7.

TABLE 7

Comparative Pressure Dependence of the Principle Phonon Peaks

Author	Concentration (at % In in Pb)	Peak location (P=0) (meV)				Pressure Dependence (10^{-5}meV bar^{-1})			
		ω_{tl}	ω_{tu}	ω_{l}	ω_{i}	$\frac{d\omega_{tl}}{dp}$	$\frac{d\omega_{tu}}{dp}$	$\frac{d\omega_{l}}{dp}$	$\frac{d\omega_{i}}{dp}$
Hansen et al	12		4.409	8.699	9.89		3.34 ±.26	5.1 ±.15	4.57 ±.22
Galkin et al	12	3.48	4.25	8.61	9.73	3.17 ±.35	3.06 ±.43	5.34 ±.27	5.45 ±.27
Galkin et al	40	2.9		8.73	10.72	2.18 ±.28		4.89 ±.64	2.89 ±.75

By reaching lower temperatures (at which the aluminium electrode was superconducting) Galkin et al have been able to resolve the two transverse modes through increased sensitivity. Their results were recorded for pressures between 9kbar and 11kbar which suggests (using the data cited by Trofimenkoff and Carbotte (1969)) that the temperature of their investigations was in the neighbourhood of ~0.7K. The general agreement between the results obtained here and those of Hansen et al and Galkin et al is excellent.

Attention is now turned towards the calculation from Table 6 of the relevant Grüneisen constants. The Gruneisen rule states that at low temperatures:-

$$\gamma_G = \frac{V\alpha}{KC_V} \qquad 6\text{-}1$$

where V is the volume, α the thermal expansion coefficient, C_V the specific heat at constant volume and K the compressibility. If we consider this in terms of the normal modes of vibration of the substance it can be expressed as:-

$$\gamma_G = \frac{\sum_i \gamma_i C_{vi}}{\sum_i C_{vi}} \qquad 6\text{-}2$$

where γ_i are the individual mode gammas defined by:-

$$\gamma_j = -\frac{d\ln\omega_i}{d\ln V} = \left(\frac{\delta\omega_i}{\delta p}\right)\frac{B}{\omega_i} \qquad 6\text{-}3$$

where the ω_i are now the frequencies associated with the normal modes of vibration and B is the bulk modulus defined by $B = -\,dp/d\ln V$. The Grüneisen constants for the predominant phonon modes can

therefore be determined and are given in Table 8.

TABLE 8

Grüneisen Gammas of the Predominant Phonon Modes

Concentration (at % In in Pb)	Grüneisen mode γ's		
	γ_t	γ_l	γ_i
12	3.11 ±.78	2.94 ±.29	2.14 ±.32
36	2.98 ±.75	2.76 ±.28	1.88 ±.28

The data of Bridgman (1954) obtained at room temperature shows that the bulk modulus of $Pb_{75}In_{25}$ is not significantly different from that of pure lead and thus, in the absence of any data for the alloy at low temperatures, the Grüneisen gammas have been determined here using a value of 4.88×10^5 bar for the bulk modulus of pure lead at 4K as determined by Waldorf and Alers (1961).

Listed in Table 9 are the values for the Grüneisen γ's as calculated from the data of Galkin et al.

TABLE 9

Grüneisen Gammas Calculated from the Data of Galkin et al (1973)

Concentration (at % In in Pb)	Grüneisen mode γ's		
	γ_t	γ_l	γ_i
12	3.90 ±.49	3.03 ±.24	2.73 ±.25
40	3.66 ±.48	2.73 ±.34	1.32 ±.34

Agreement of the results obtained here is also very good and always within the experimental error. It is noteworthy that for the 40 at % sample of Galkin he no longer was able to resolve two transverse modes and that the structure he observed in the second derivative became unduly washed out which leads this author to believe that perhaps the concentration was higher than that assigned.

b. Inversion of the Eliashberg Gap Equations.

By guessing the parameters $\alpha^2(\omega)$ and $F(\omega)$, relating to the phonon spectrum of the metal, it is in principle possible to solve the Eliashberg coupled integral equations described in Chapter II for $\phi(\omega)$ and $Z(\omega)$ and hence obtain the gap function $\Delta(\omega)$ through the relationship:-

$$\Delta(\omega) = \phi(\omega)/Z(\omega) \qquad 2\text{-}66$$

Subsequently one can use this to calculate the normalised density of states for a superconductor using the relationship:-

$$\frac{D(E)}{D(\varepsilon_f)} = \frac{\mathrm{Re}|eV|}{[(eV)^2 - \Delta^2(\omega)]^{\frac{1}{2}}} \qquad 2\text{-}74$$

Since the normalised density of states was earlier shown to be in 1:1 correspondence with the normalised tunnel conductance, the results of such a calculation can be compared directly with experiment. This procedure was carried out by Rowell and Kopf (1965) and others with excellent results.

McMillan (1965 and 1969) and Rowell however have devised an

innovative approach to solving the Eliashberg equations (and also using equation 2-74) which uses experimentally obtained input data for the energy gap and density of states and yields (after considerable computation) the form of the phonon spectrum and associated parameters. Because the aim of this procedure is to gain information regarding the phonon spectrum rather than the density of states (as was the previous method of solution) it has come to be known as an inversion process.

Briefly the method is as follows. A zero order guess is first made for the function $\alpha^2(\omega)F(\omega)$, U_c (the Coulomb pseudopotential) and Δ. The first two of these parameters are based on intelligent insight while the initial input for Δ is the gap at the gap edge as obtained from experiment. On the basis of this information, the gap equations are first solved by iteration for $\Delta(\omega)$ from which the density of states is calculated. This calculated density of states is then compared with that obtained by experiment and, depending on the difference between the two, a revised guess is made for $\alpha^2(\omega)F(\omega)$. This procedure is repeated as many times as is necessary until the agreement between the calculated and experimental densities of states is acceptable at which time the best form of $\alpha^2(\omega)F(\omega)$ will have been arrived at. Between successive iterations for $\Delta(\omega)$, the parameter U_c is adjusted so that the calculated gap function (at the gap edge) is consistent with the experimental value.

Output from this kind of analysis includes the form of the Coulomb pseudopotential μ^* (note $\mu^* = N(0)U_c$) as well as of course

$\alpha^2(\omega)F(\omega)$ (from which the electron phonon coupling strength λ and various average phonon energies can be derived).

Such an analysis has been carried out for the $Pb_{64}In_{36}$ system. As input data to the computer programme the function $(\sigma/\sigma_{B.C.S.})-1$ was required where the σ refer to normalised conductances and in particular:-

$$\sigma_{B.C.S.} = \frac{|V|}{(V^2 - \Delta^2)^{\frac{1}{2}}}$$

In obtaining σ for the alloy from $(\sigma_{NS}/\sigma_{NN})$, it was first necessary to apply a correction to the absolute value of σ_{NN} before obtaining the low pressure data. This arose from the fact that σ_{NS} and σ_{NN} were determined at slightly different pressures. At the present time it is sufficient to say that this correction is entirely justified and will be dealt with in greater detail in the following section (5).

Figure 19 shows the input data used for the inversion programme while figures 20, 21 and 22 show the resulting phonon spectrum, gap function and re-normalisation function respectively.

To the knowledge of this author, no other pressure dependent data is available with which to compare the results at this concentration. Wu (1967) has obtained the phonon spectrum at zero pressure for a $Pb_{60}In_{40}$ alloy which compares favourably with that of figure 20 in a qualitative sense although the localised mode appears to be sharper than might be expected (Wu's data). The gap function and re-normalisation function that have been calculated here show considerably less structure than those for lower concentration

FIGURE 19

Input to Inversion Programme for a $Pb_{64}In_{36}$ Sample

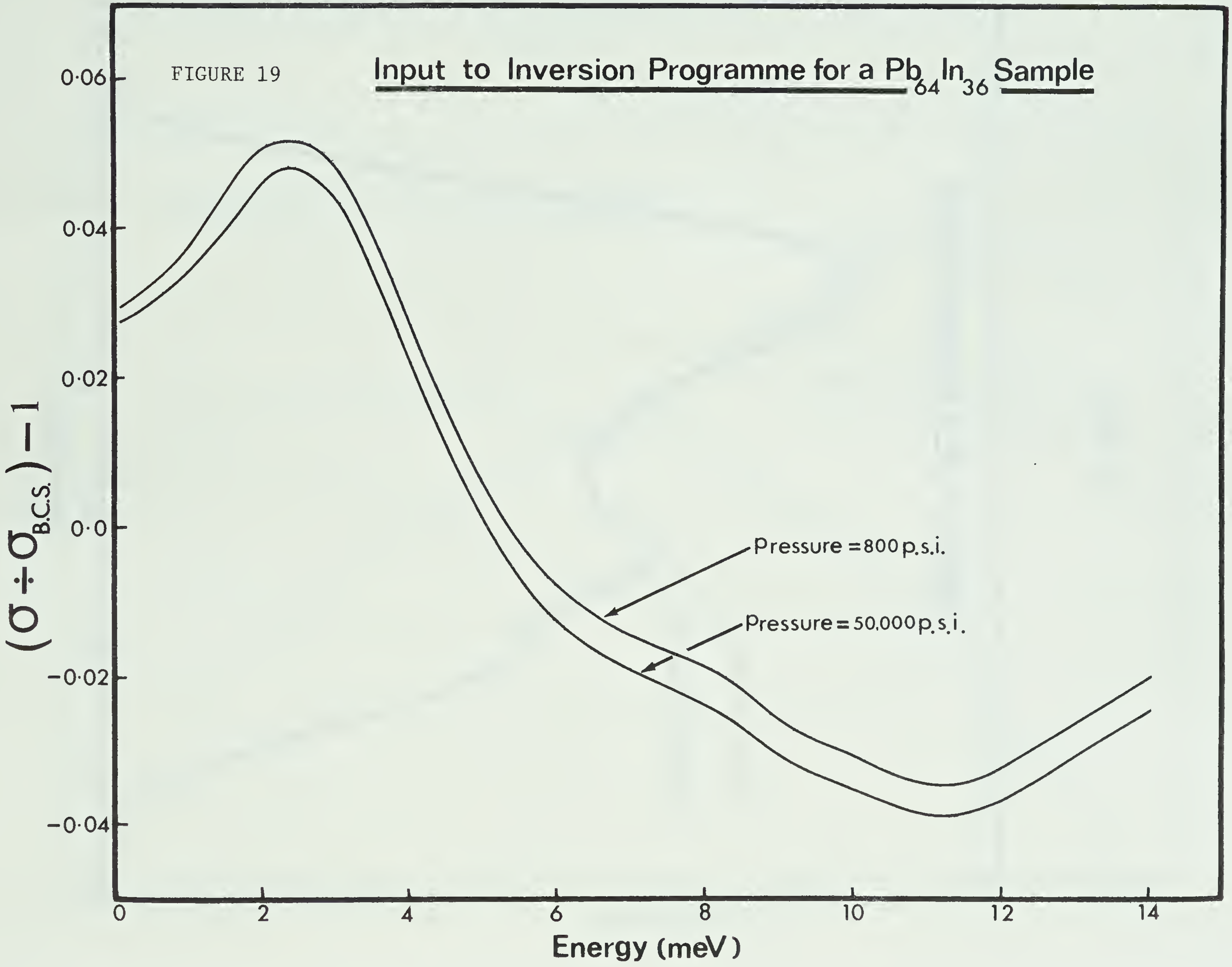

FIGURE 20

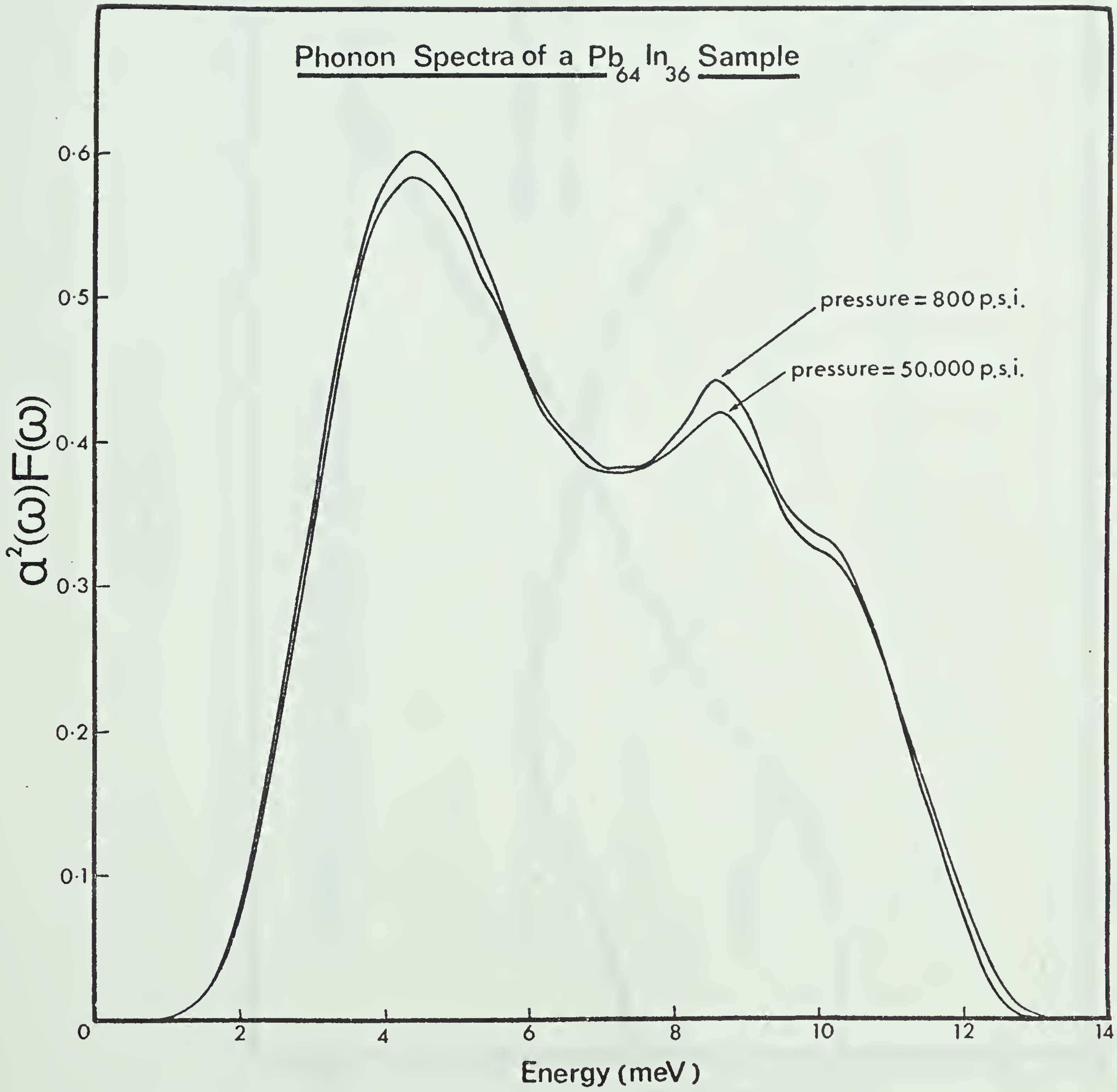
Phonon Spectra of a Pb$_{64}$In$_{36}$ Sample
$\alpha^2(\omega)F(\omega)$
0·6
0·5
0·4
0·3
0·2
0·1
0
2
4
6
8
10
12
14
Energy (meV)
pressure = 800 p.s.i.
pressure = 50,000 p.s.i.

FIGURE 21

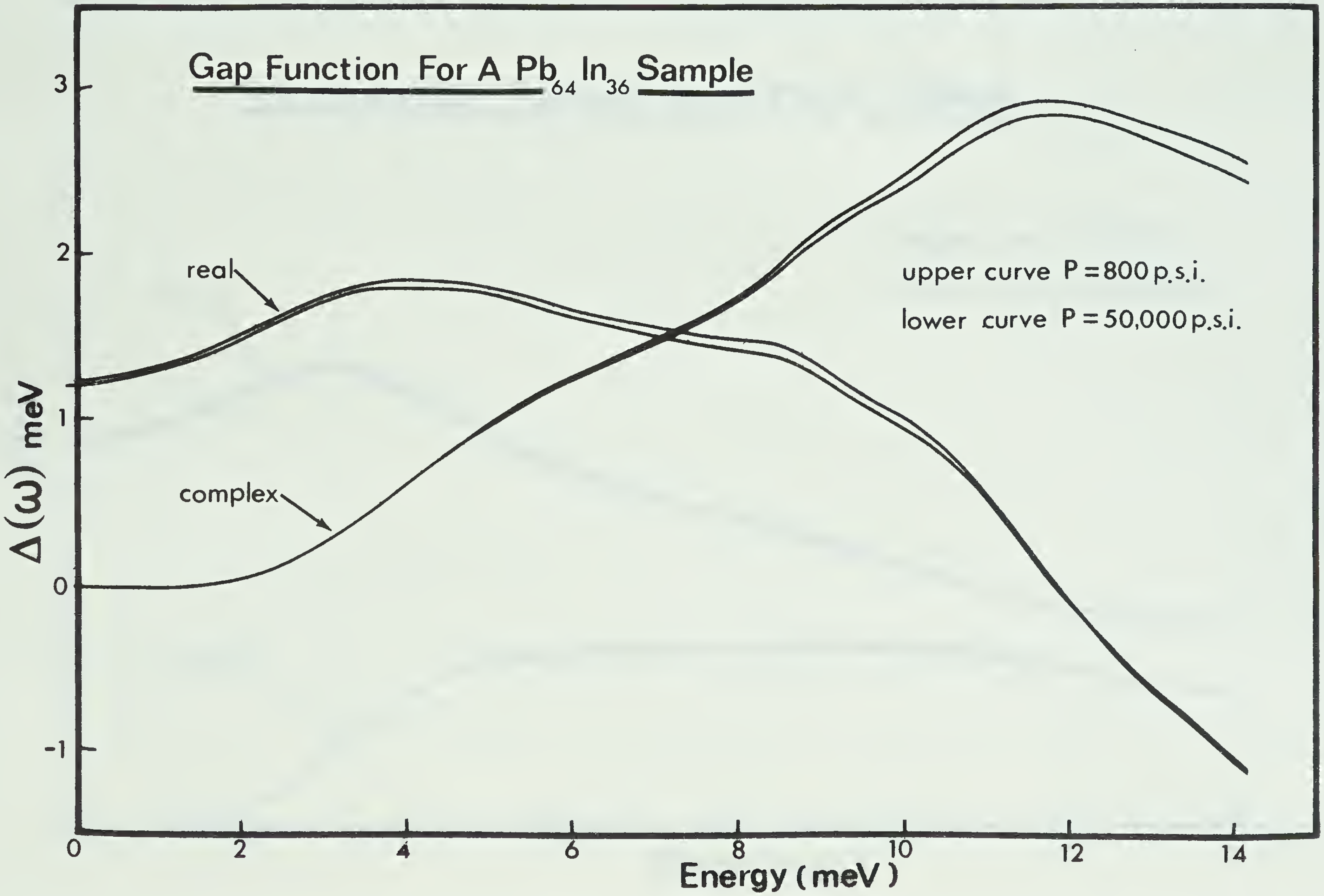

Gap Function For A $Pb_{64}In_{36}$ Sample

FIGURE 22

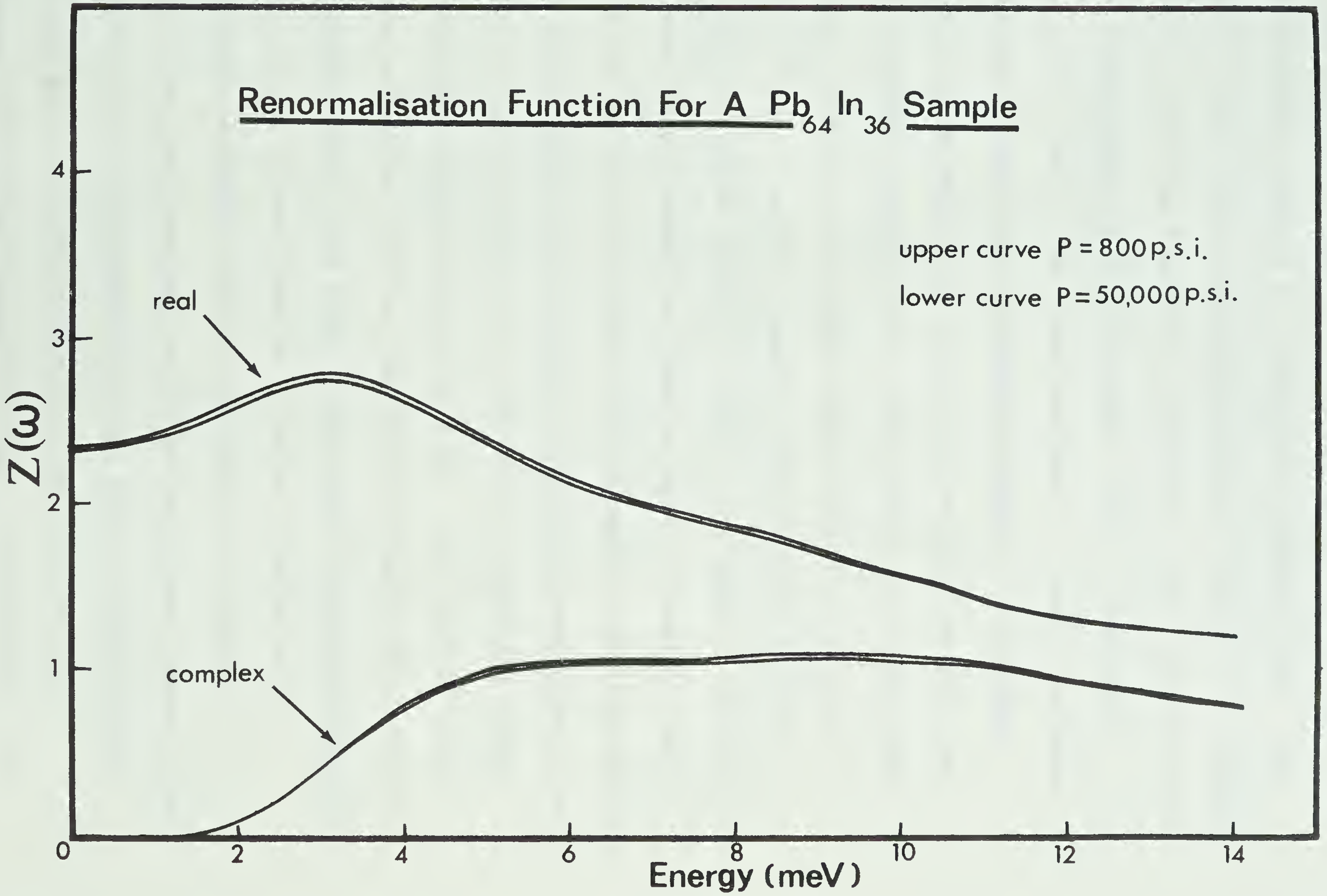
Renormalisation Function For A $Pb_{64}In_{36}$ Sample
upper curve P = 800 p.s.i.
lower curve P = 50,000 p.s.i.
real
complex
$Z(\omega)$
0
1
2
3
4
2
4
6
8
10
12
14
Energy (meV)

together with a general slight decrease in magnitude indicative of the trend to weaker coupling as a function of concentration. Also in evidence is the trend to weaker coupling as a function of pressure.

As can be seen from figure 20, the overall phonon structure has decreased in magnitude and definitiveness. This is especially noticeable in the case of the localised mode. A drastic decrease in the amplitude of this peak is evident however as the indium concentration is increased from ~12 at % to ~40 at % as can also be seen in the data of Galkin et al. Sood (1972) has investigated the effect of alloying on the phonon spectrum of $Pb_xIn_{(1-x)}$ and concludes that the localised impurity band associated with the impurity atoms of indium consists in fact of two peaks. The first of these peaks (lower energy) he finds to occur at constant energy (9.57 ±.03 meV) and with width that varies linearly with concentration while the second peak not only varies in width with concentration but also shifts to higher energies as a function of increasing indium concentration (for concentration >2 at % In). The first of these two peaks he associates with the vibration of single substitutional impurity indium atoms in the lead, lattice while the second peak is believed to be due to the vibration of pairs of indium atoms.

This effect certainly would be inherent in the lack of definition of the localised mode but to an even greater extent since not only is it a poor approximation to say that the indium atoms are localised but it becomes difficult to evaluate the effect of the change in the force constants at such a concentration. In

short it is somewhat surprising that the localised mode is observed at all.

McMillan (1968) defines a dimensionless electron phonon coupling constant as:-

$$\lambda = 2 \int_0^\infty \frac{\alpha^2(\omega)F(\omega)}{\omega}\, d\omega \qquad 6\text{-}4$$

and within the framework of the Eliashberg strong coupling gap equations derives a formula for the transition temperature for a strong coupling superconductor given by:-

$$T_c = \frac{<\omega>}{1.20} \exp[-1.04(1 + \lambda)/(\lambda - \mu^* -.62\lambda\mu^*)] \qquad 6\text{-}5$$

From equation 6-5 the following expression for the pressure dependence of the transition temperature can be derived:-

$$\frac{d\ln T_c}{dp} = \frac{d\ln<\omega>}{dp} + 1.04 \left(\frac{1 + .38\mu^*}{(\lambda-\mu^*-.62\lambda\mu^*)^2}\right) \frac{d\lambda}{dp} \qquad 6\text{-}6$$

where $<\omega>$ is an average phonon frequency defined by:-

$$<\omega> = \frac{\int_0^\infty \alpha^2(\omega)F(\omega)d\omega}{\int_0^\infty \frac{\alpha^2(\omega)F(\omega)d\omega}{\omega}} \qquad 6\text{-}7$$

For convenience we introduce the parameter $A^2 = \int_0^\infty \alpha^2(\omega)F(\omega)$ and thus equation 6-7 can be expressed as:-

$$<\omega> = \frac{2A^2}{\lambda} \qquad 6\text{-}8$$

McMillan suggests that for f.c.c. lattices a good approximation to $<\omega>$ is an average of the transverse and longitudinal phonon frequencies i.e.:-

$$\langle\omega\rangle \simeq \bar{\omega} = \tfrac{1}{2}(\omega_t + \omega_1) \qquad 6\text{-}9$$

differentiating equation 6-9 with respect to pressure gives:-

$$\frac{d\ln\langle\omega\rangle}{dp} = \left(\frac{1}{\omega_t + \omega_1}\right)\frac{d\omega_t}{dp} + \left(\frac{1}{\omega_t + \omega_1}\right)\frac{d\omega_1}{dp} \qquad 6\text{-}10$$

Table 10 summarises the data that was obtained using the inversion technique for the $Pb_{64}In_{36}$ alloy.

Using the experimental data of Table 6 in conjunction with equation 6-10 to obtain the first term in equation 6-6 and the data of Table 10 for the second term yields a value of:-

$$\frac{d\ln T_c}{dp} = -3.01 \times 10^{-6}\ \text{bar}^{-1} \qquad 6\text{-}11$$

This compares with the direct experimentally determined value of:-

$$\frac{d\ln T_c}{dp} = -4.53 \times 10^{-6}\ \text{bar}^{-1} \qquad 6\text{-}12$$

If instead we use the expression 6-8 we have that:-

$$\frac{d\ln\langle\omega\rangle}{dp} = \frac{d\ln A^2}{dp} - \frac{d\ln\lambda}{dp}$$

using this expression (with values from Table 10) in the McMillan equation 6-6 gives:-

$$\frac{d\ln T_c}{dp} = -7.18 \times 10^{-6}\ \text{bar}^{-1} \qquad 6\text{-}13$$

The agreement obtained between the experimentally determined $d\ln T_c/dp$ and that calculated using McMillan's formula is much better in the first case (equation 6-11) than in the second case (equation 6-13), the difference revolving around the definition of $\langle\omega\rangle$. In this regard it is interesting to note that better agreement was

TABLE 10

Parameters Obtained from the Inversion Programme

Concentration (at % In in Pb)	Author	μ^*	A^2 (meV)	$\frac{dA^2}{dp}$ (10^{-5}meV bar^{-1})	$\frac{d\ln A^2}{dp}$ (10^{-6} bar^{-1})	λ	$\frac{d\lambda}{dp}$ (10^{-5} bar^{-1})	$\frac{d\ln\lambda}{dp}$ (10^{-6} bar^{-1})
12	Hansen et al	.137	4.04	-1.275	-3.155	1.519	-1.204	-7.926
36	This work	.148	3.8929	-2.24	-5.75	1.42	-1.04	-7.40

obtained for the value which was less dependent on the "inversion acquired" data.

Although the McMillan equation for T_c is in itself approximate, this author attributes the major proportion of the disagreement to the inversion procedure.

The experimentally determined density of states used as input to the inversion programme is particularly inaccurate in the low energy region and thus it is usual to make some kind of assumption here. The basis for this assumption has long been the subject of some conjecture as to whether $\alpha^2(\omega)F(\omega)$ depends linearly or quadratically on ω. A very recent paper by Allen and Silberglitt (1974) suggests that at low frequency, $\alpha^2(\omega)F(\omega)$ is linear in ω.

Such factors will clearly affect the computed $\alpha^2(\omega)F(\omega)$ and μ^* upon which the parameters of Table 10 and calculations employing them depend.

5. The Tunnel Junction as a Pressure Sensing Device

For the entirity of this research work, the pressure that was ultimately applied to the samples was determined by the sample itself as alluded to earlier. So reliable and reproducible were the pressure responses of the tunnel junctions that their use as pressure gauges in their own right merits further attention.

In dealing with the theory of tunnelling (Chapter II section 6) it was shown that for the normal-normal metal case that the net tunnel current which flowed as a result of an applied potential V was given by:-

$$I \propto D^2T^2eV \qquad 6\text{-}14$$

where D^2 represents the product of the electron density of states functions (close to the Fermi surface), e the electronic charge and T some average matrix element describing the probability that an electron will in fact tunnel from one metal to the other.

By considering the simple case of one dimensional tunnelling, one can obtain an estimate of the quantity T by solving the Schrodinger equation for a simple potential barrier to find that:-

$$T \propto \exp-[(2m\{U-E\})^{\frac{1}{2}}t/\hbar] \qquad 6\text{-}15$$

where E is the kinetic energy of the electron, U is the height of the barrier and U>E; t represents the thickness of the barrier. Combining equations 6-14 and 6-15 we get:-

$$I \propto C_1V\exp[-\phi^{\frac{1}{2}}t] \qquad 6\text{-}16$$

where ϕ the work function in eV replaces (U-E), t is in $\overset{0}{A}$ and C_x are constants. Using Ohm's law the tunnel resistance is then given by:-

$$R_T \propto C_2 \exp \phi^{\frac{1}{2}} t \qquad 6\text{-}17$$

or $$\ln[R_T] \propto C_3 + \phi^{\frac{1}{2}} t \qquad 6\text{-}18$$

By applying pressure to the tunnel junctions we have been able to test the validity of this relationship since a reduction in t should produce an exponential increase in P.

Results of this investigation are shown in figures 23 and 24 for typical samples of each composition. In each case the data has been plotted linearly and logarithmically to illustrate the exponential behaviour.

Since the circuitry employed in the determination of the tunnel resistance was capable of resolving resistance changes of a few parts in 10^5, experimental uncertainty of this data lies in the pressure determinations. The smallest graduation of the Heise Bourdon gauge was 100 p.s.i. while the manganin gauge supplied with the compressor was accurate to better than 1%. The uncertainty of the pressure values is therefore estimated to be less than 1%.

It can be clearly seen from figures 23 and 24 that:-

$$\ln[R_T] \propto - C_4 P + C_5 \qquad 6\text{-}19$$

and hence using equation 6-18 that:-

$$-P \propto C_6 \phi^{\frac{1}{2}} t + C_7 \qquad 6\text{-}20$$

Equation 6-19 is precisely what one would expect assuming t to change linearly with pressure.

For the most part the tunnel junctions were used to determine the pressure in the bomb in the ~1K — 9K temperature range although their calibration (against the two external gauges) took place at

FIGURE 23

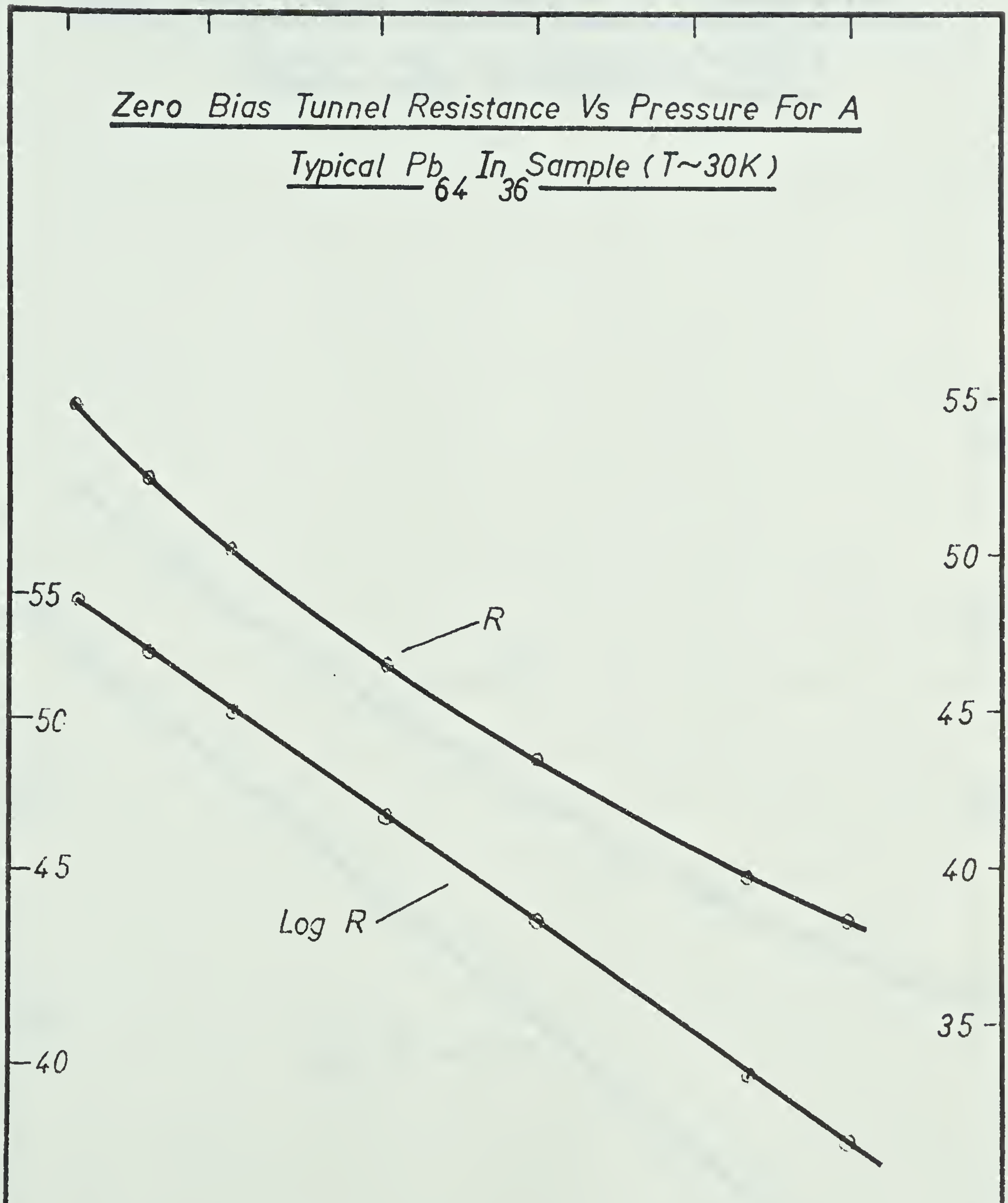
Zero Bias Tunnel Resistance Vs Pressure For A Typical $Pb_{64}In_{36}$ Sample (T~30K)
R
Log R
PRESSURE (× 1000 psig)
0
10
20
30
40
50
55
50
45
40
35
55
50
45
40

FIGURE 24

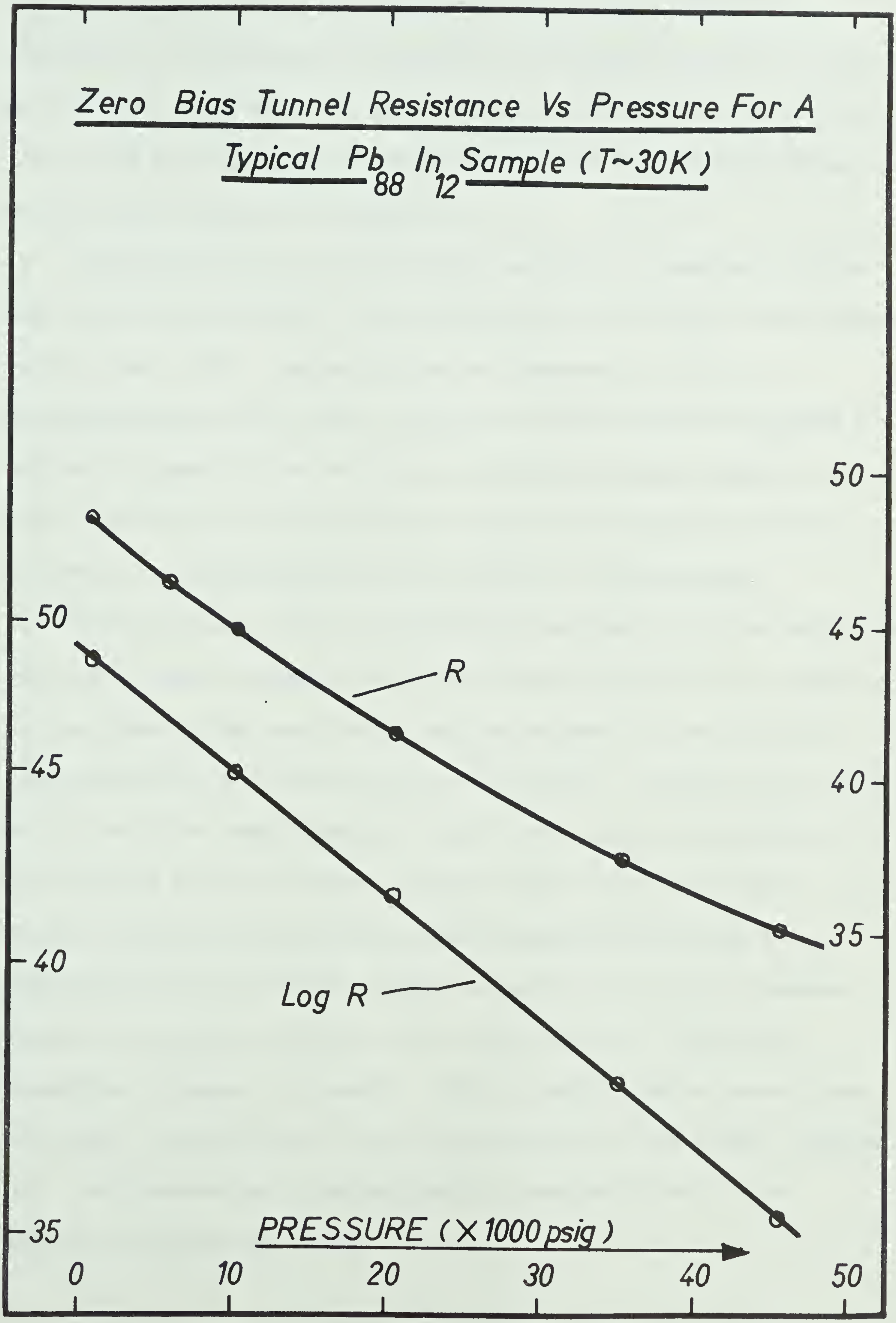

Zero Bias Tunnel Resistance Vs Pressure For A Typical $Pb_{88}In_{12}$ Sample (T~30K)

~30K. In view of this, the dependence of the zero bias tunnel resistance on temperature was checked by recording data at ~7K and also at ~77K. Variation of R_T over this range was found to be from .2% to .5% and negligible in comparison to the ~30% change invoked by a pressure change of ~50,000 p.s.i.

Reproducibility of the data when subjected to pressure cycling was found to be excellent, the tolerance after successive runs being better than ± .5%. When maintained at temperatures <77K the characteristics of the tunnel junctions tested remained unchanged for periods in excess of two weeks and although prolonged exposure of the tunnel junction to room temperature caused deterioration, the only outcome of a brief exposure was the need for re-calibration.

Beside its most widely acknowledged use therefore as an analytical tool, the tunnel junction also exhibits great potential as a sensitive pressure monitoring device with application over a wide range of temperatures and in both solid and fluid media. Throughout the course of this work the tunnel junction itself has proved an invaluable tool since having filled the sample chamber with solid helium four - and thereby rendering the external pressure gauges ineffective - it provided the only convenient method of monitoring further pressure changes (at constant volume) which might occur as a result of temperature changes for example. The following example taken from this work illustrates not only the sensitivity of the tunnel junction but its agreement with thermodynamical considerations of the pressure transmitting medium.

In order to quench superconductivity within the lead-indium alloy electrode of the tunnel junction and thereby obtain the normal-normal tunnel resistance as a function of d.c. bias, the temperature of the sample chamber was raised to ~9K whereas the superconducting normal characteristic was recorded at ~1.5K. Theoretical predictions indicate that at constant pressure and for energies well beyond the superconducting gap region these characteristics should be coincident, however, in view of the temperature difference between these two measurements (and accompanying constant volume pressure change) one might expect to observe a certain degree of non-coincidence.

Figures 25 and 26 show typical examples of these characteristics for a Pb_{64} In_{36} sample both at high pressure (~50,000 p.s.i.) and at low pressure (~800 p.s.i.). Despite the temperature difference in the measurements, it can be seen that for the high pressure case the characteristics are in fact coincident suggesting that a negligible pressure change has taken place. The helium four melting curve below taken from Spain & Segall (1970) shows that a solid formed at 50,000 p.s.i. (~3.4 K bar) remains in the solid state at 9K and also that in general, little change in pressure occurs in the solid as a function of temperature.

FIGURE 25

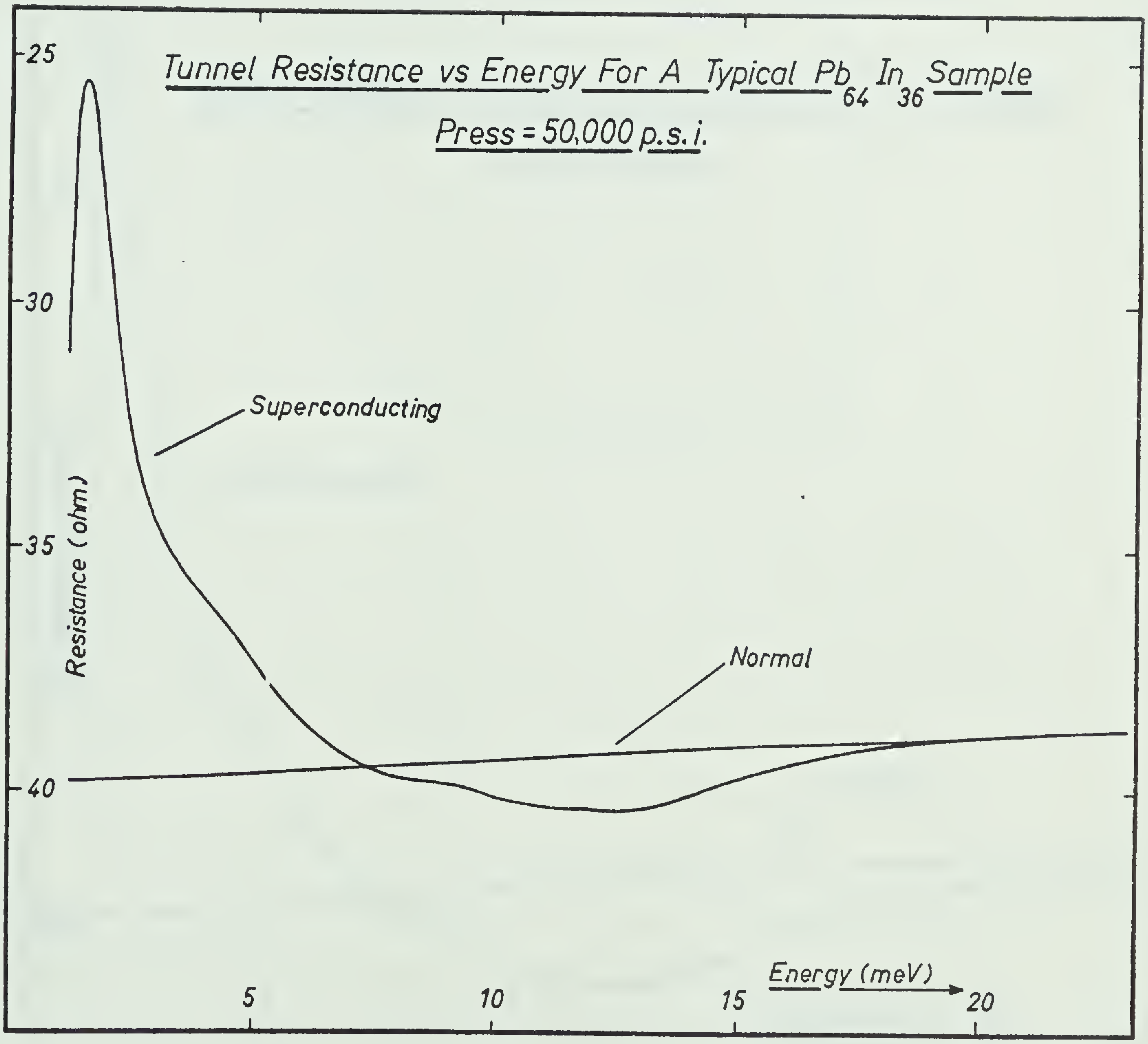
Tunnel Resistance vs Energy For A Typical $Pb_{64}In_{36}$ Sample
Press = 50,000 p.s.i.
Superconducting
Normal
Resistance (ohm)
25
30
35
40
Energy (meV)
5
10
15
20

FIGURE 26

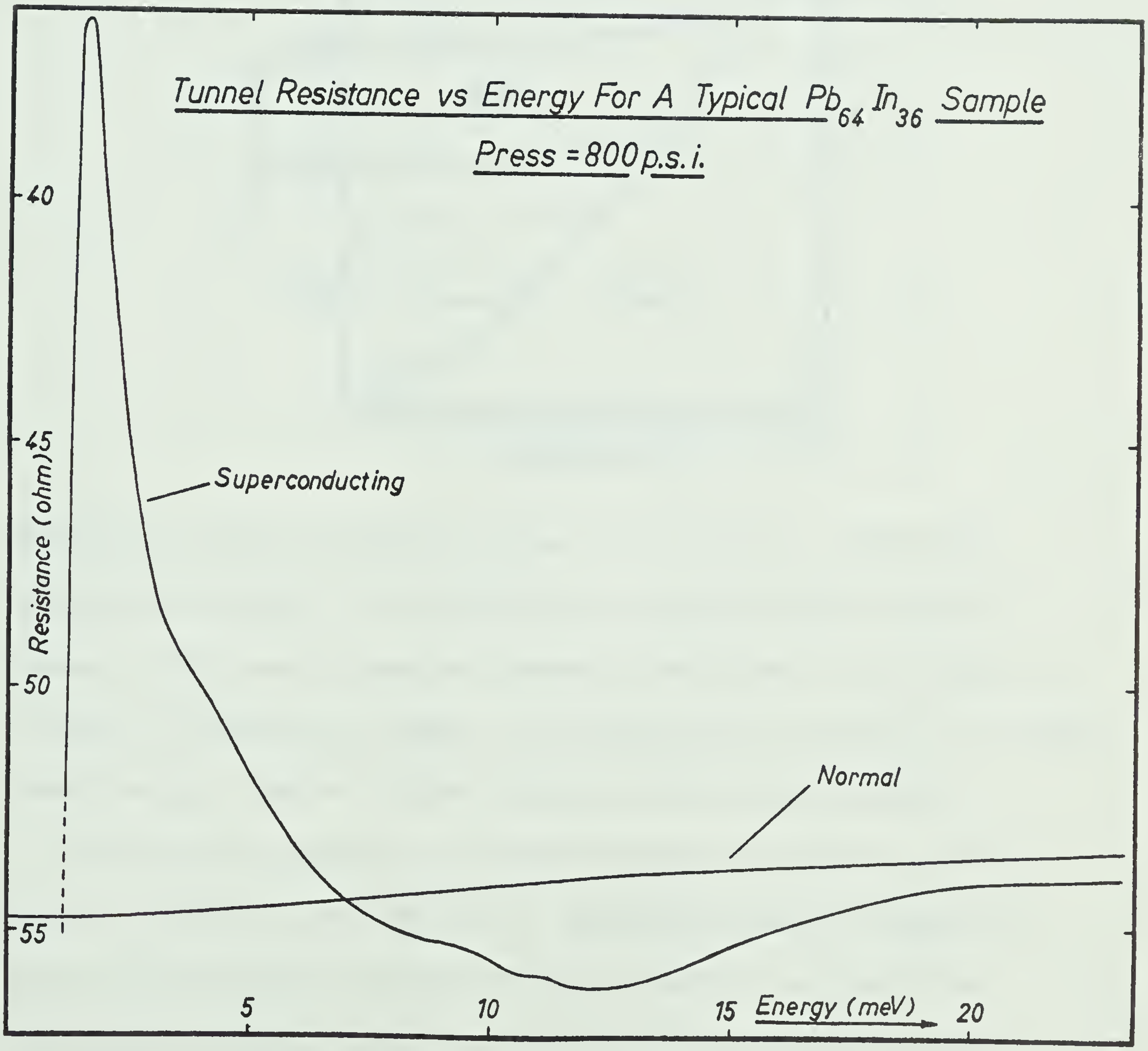
Tunnel Resistance vs Energy For A Typical $Pb_{64}In_{36}$ Sample
Press = 800 p.s.i.
40
45
50
55
Resistance (ohm)
Superconducting
Normal
5
10
15
20
Energy (meV)

Isochores of Solid He^4 at High Pressures

(figures on curves are molar volumes in cm^3)

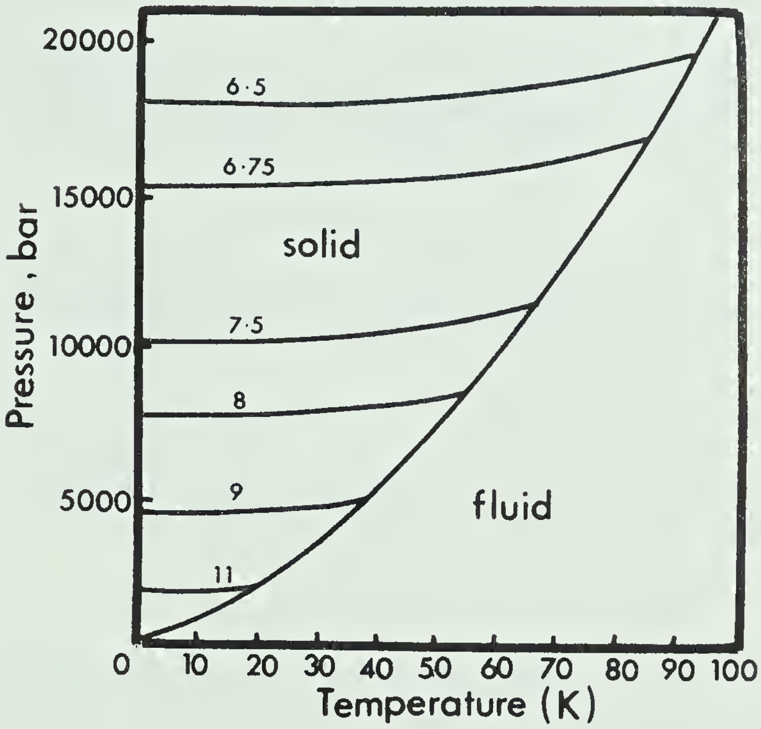

Referring to the more detailed results of table 11 , also taken from Spain & Segall, it is indicated for example that in a solid formed at 3441 bar, a pressure change of the order of .2% occurs as a result of warming the sample the necessary 9K to achieve the normal-normal state. Thus we observe exactly what would be expected.

For the low pressure measurements however, which were carried out at 800 p.s.i., the 9K rise in temperature causes a change of state of the pressure transmitter from a solid to a fluid when recording the normal-normal characteristics as can be seen from the graph below taken from Edwards and Pandorf (1965):-

TABLE 11

Temperature and Pressure Values Along Isochores of He^4 at 400 Bar Intervals Starting with the Pressure at 0 K

ρ_o	$0.2T_m$	$0.3T_m$	$0.4T_m$	$0.5T_m$	$0.6T_m$	$0.7T_m$	$0.8T_m$	$0.9T_m$	T_m
400	1.61 (400)	2.41 (400)	3.21 (400)	4.01 (400)	4.82 (401)	5.62 (403)	6.42 (406)	7.22 (410)	8.03 (416)
800	2.49 (800)	3.74 (800)	4.98 (801)	6.23 (802)	7.47 (806)	8.72 (811)	9.96 (818)	11.21 (828)	12.45 (841)
1200	3.23 (1200)	4.85 (1200)	6.46 (1202)	8.08 (1205)	9.69 (1210)	11.31 (1219)	12.93 (1232)	14.54 (1248)	16.16 (1269)
1600	3.89 (1600)	5.84 (1601)	7.78 (1603)	9.73 (1608)	11.67 (1616)	13.62 (1629)	15.56 (1647)	17.51 (1671)	19.46 (1700)
2000	4.50 (2000)	6.74 (2001)	8.99 (2005)	11.24 (2011)	13.49 (2023)	15.74 (2041)	17.99 (2065)	20.23 (2096)	22.48 (2133)
2400	5.06 (2400)	7.59 (2402)	10.12 (2406)	12.65 (2415)	15.18 (2430)	17.71 (2453)	20.24 (2483)	22.78 (2522)	25.31 (2568)
2800	5.59 (2800)	8.39 (2802)	11.19 (2808)	13.98 (2819)	16.78 (2838)	19.58 (2865)	22.38 (2903)	25.17 (2949)	27.97 (3003)
3200	6.10 (3200)	9.15 (3203)	12.20 (3209)	15.25 (3223)	18.31 (3426)	21.36 (3279)	24.41 (3323)	27.46 (3377)	30.51 (3441)
3600	6.59 (3601)	9.88 (3604)	13.18 (3611)	16.47 (3628)	19.76 (3654)	23.06 (3692)	26.35 (3743)	29.65 (3807)	32.94 (3878)

Isochores of Solid He^4 at Low Pressures

(figures on curves are molar volumes in cm^3)

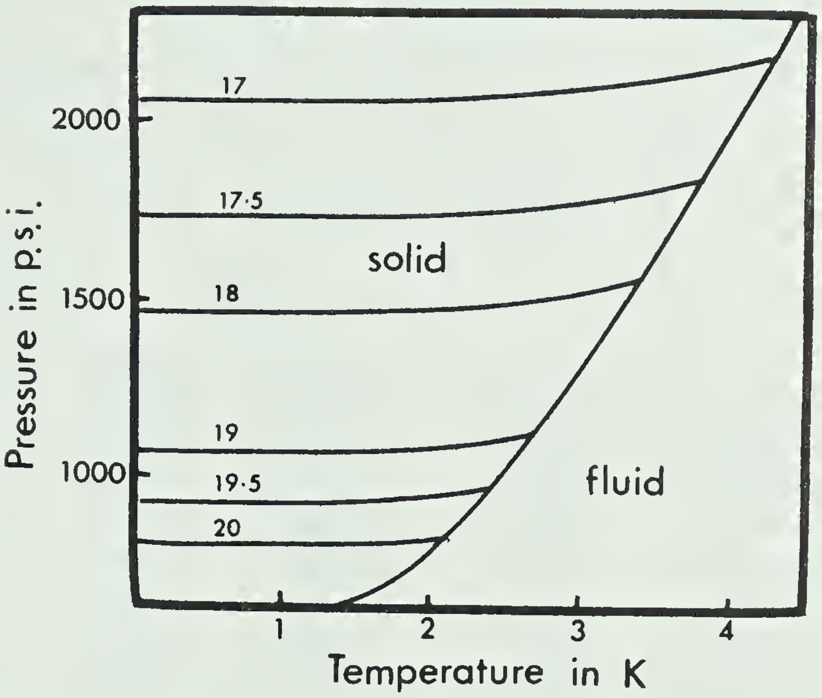

To estimate the pressure in the cell therefore at ~9K it is necessary to refer to isochores in fluid helium. The data shown in table 12 corresponds to such isochores which have been taken from Hill and Lousnasmaa (1959). A solid formed at ~800 p.s.i. corresponds to a molar volume of 19.5 cm^3 and to obtain the pressure in the fluid at this molar volume, a linear extrapolation (extrapolated values appear in parentheses) has been performed on the above data which shows the pressure to be ~1900 p.s.i. i.e. an increase of ~1100 p.s.i.

Employing standard curve fitting techniques to the experimental data of figure 23, the expected resistance difference between the normal and superconducting characteristics which corresponds to this pressure change is ~.7 ohm and as can be seen in figure 26 this is exactly what was observed. Thus we can see that there is excellent agreement between the pressure determined by the tunnel junction and that

[illegible]

[illegible]

[illegible]

TABLE 12

Pressure Values (in p.s.i.) Along Isochores of Fluid Helium

Molar Vol (cm^3) / Temp (K)	21.55	20.78	20.06	19.5	19.39
3.0	616.1	801.9	1021.7		
3.25	635.8	821.0	1041.5	(1257.9)	1312.0
3.5	654.9	840.8	1062.8	(1279.8)	1334.0
3.75	674.7	861.4	1084.9	(1302.4)	1356.8
4.0	695.3	882.7	1107.6	(1326.4)	1381.1
4.25	716.6	905.5	1131.3	(1351.1)	1406.1
4.50	738.7	929.0	1155.4	(1376.5)	1431.8
4.75	761.5	953.3	1180.4	(1402.7)	1458.2
5.0	785.0	978.3	1206.1	(1429.6)	1485.4
5.25	809.2	1003.3	1232.6	(1457.2)	
5.5	834.2	1029.0	1259.8	(1485.6)	
6.0	884.9	1082.7	1315.7	(1542.6)	
6.5	938.6	1138.5	1373.7	(1601.9)	
7.0	993.7	1195.8	1433.3	(1662.6)	
7.5	1050.3	1254.6	1494.3	(1724.8)	
8.0	1107.6	1314.2	(1556.0)	(1787.7)	
9.0	1225.2	1436.9	(1680.9)	(1913.8)	

predicted by the thermodynamics of the pressure transmitter. Using the junction in this fashion it has been possible to test whether the constant pressure freezing process used did in fact produce hydrostatic pressure in the sample chamber.

Although the previous thermodynamical argument verifies in general that the pressure was indeed hydrostatic, a more quantitative estimate was obtained by producing two junctions on the same substrate a fixed distance apart and monitoring the pressure at these points. By so doing the pressure was found to vary by <1% over a distance of ~1.5 cm after constant pressure freezing.

With particular reference to this work, the inescapable conclusion is that the tunnel junction is not only an accurate method of determining the pressure in the solid and in the fluid but it does so identically at the point of interest.

6. Pressure Dependence of the Density of States

For a strong coupling superconductor, the electronic density of states at the Fermi surface is renormalised according to:-

$$N_F = N_B\ (1 + \lambda) \qquad 6\text{-}21$$

where λ is the coupling strength and $1 + \lambda = Z$, the renormalisation constant, and $Z = m^*/m$ where m^* and m are the effective mass and mass of the electrons respectively. N_B denotes the band structure density of states.

The pressure dependence of the density of states therefore is, using equation 6-21:-

$$\frac{d\ln N_F}{dp} = \frac{d\ln N_B}{dp} + \frac{d\ln Z}{dp} \qquad 6\text{-}22$$

The pressure dependence of λ for 36 at % In in Pb was determined in these experiments from which (using the relationship $(1/x)\frac{dx}{dp} = d\ln x/dp$ and the fact that $Z = 1 + \lambda$)

$$\frac{d\ln Z}{dp} = -4.32 \times 10^{-6}\ \text{bar}^{-1} \qquad 6\text{-}23$$

or since $-\frac{1}{V}\ \frac{dV}{dp} = -\frac{d\ln V}{dp} = K_T$ 6-24

$$\frac{d\ln Z}{d\ln V} = 2.11 \qquad 6\text{-}25$$

where K_T is the isothermal compressibility of bulk lead. The quantity $d\ln N_F/dp$ has been measured by several workers which are shown in Table 13. Also appearing in this table are the values for the pressure dependence of the band structure density of states

using equation 6-22 and the value of dlnZ/dp obtained from these experiments. It is expected that dlnZ/dp for the alloy does not differ considerably from that of pure lead to which the values of column 3 pertain.

TABLE 13

Pressure Dependence of the Density States (Per Unit Volume)

Author	Experimental Method	$\frac{d\ln N_F}{dp}$ (10^{-6} bar^{-1})	$\frac{d\ln N_B}{dp}$ (10^{-6} bar^{-1})
Andres (1961)	critical field	+.62 ± 3.08	4.94
White (1961)	thermal expansion	-1.44 ± 1.02	2.88
Andres (1964)	critical field	+.14 ± 3.08	4.46
Harris (1969)	critical field	+.41 ± 4.72	4.73
			0.68*

*free electron gas value.

There appears to be a great deal of scatter in the data for $d\ln N_F/dp$. The value of Garfinkel & Mapother is apparently not correct as has been established by private communication and is therefore not included in Table 13. The data obtained from critical field measurements has a number of limitations largely involved with the extrapolations of experimental data to zero temperature. These limitations have been alluded to by Carbotte (1971).

To the present time, no knowledge of the pressure dependence of the band structure density of states exists either theoretical

or experimental. In view of this, the usual procedure is to assume the free electron value of $d\ln N_B/dp = K_T/3$ with no real justification.

It can be seen from column four of Table 13 that experimental values for $d\ln N_B/dp$ differ considerably from those of the free electron case.

Information about the band structure density of states can be obtained from De Haas - van Alphen measurements and such data exists for lead due to Anderson & Gold (1965). The pressure dependence of the Fermi surface has been studied for lead by Anderson et al (1966) also using the De Haas - van Alphen effect. They have determined the pressure dependence of the Fermi surface in lead from which it is possible to obtain information on the pressure dependence of the band structure density of states although they did not do this. It is next proposed to calculate the pressure dependence of the band structure density of states assuming it to be a function of energy and pressure only, thus:-

$$N_B = N_B(\varepsilon,P) \qquad 6\text{-}26$$

and where all the N's used are per unit volume.

From 6-26 $$\left(\frac{d\ln N_B}{dp}\right)_{F.S.} = \left(\frac{\partial \ln N_B}{d\varepsilon}\right)_p \frac{d\varepsilon_F}{dp} + \left(\frac{\partial \ln N_B}{\partial p}\right)_\varepsilon \qquad 6\text{-}27$$

where ε_F is the Fermi energy.

The two factors in the first terms on the R.H.S. of equation 6-27 are known experimentally from the work of Anderson and Gold and Anderson et al. An attempt is now made to calculate the second term (which is = 0 for free electrons).

We must have that:-

$$\int_0^{\varepsilon_F} N_B d\varepsilon = \frac{N}{V} \qquad 6\text{-}28$$

(where N/V is the number of electrons per unit volume and we also know that the number of electrons, N, must be conserved upon decreasing V, i.e. increasing pressure). The experimental evidence of Anderson & Gold however shows that:-

$$\frac{d\varepsilon_F}{dp} < 0 \qquad 6\text{-}29$$

Thus the integral on the left hand side of equation 6-28 would decrease unless N_B changes with pressure to accommodate the situation. This requires N_B to increase with pressure. Let us assume that the density of states increases then according to:-

$$N_B(P) = \alpha\, N_B(0) \qquad 6\text{-}30$$

where α is to be determined and the numbers in parentheses indicate the pressure. Thus:-

$$\int_0^{\varepsilon_F(P)} \alpha N_B(0) d\varepsilon = \frac{N}{V(P)} \qquad 6\text{-}31$$

and
$$\int_0^{\varepsilon_F(0)} N_B(0) d\varepsilon = \frac{N}{V} \qquad 6\text{-}32$$

since $V(P) = V + \left(\frac{\partial V}{\partial p}\right) dp$ and $\frac{1}{V}\frac{\partial V}{\partial p} = -K_T$

we have that $V(P) = V[1-K_T dp]$

or by expanding $\frac{1}{V(P)} \simeq \frac{1}{V}[1 + K_T dp]$

equation 6-31 thus becomes:-

$$\int_0^{\varepsilon_F(P)} \alpha N_B(0)\,d\varepsilon = \frac{N}{V} + \frac{N}{V} K_T dp \tag{6-33}$$

Equation 6-32 may be written in the form:-

$$\int_0^{\varepsilon_F(0)} N_B(0)\,d\varepsilon = \int_0^{\varepsilon_F(P)} N_B(0)\,d\varepsilon + \int_{\varepsilon_F(P)}^{\varepsilon_F(0)} N_B(0)\,d\varepsilon \tag{6-34}$$

The last term in equation 6-34 is to a good approximation

$$\int_{\varepsilon_F(P)}^{\varepsilon_F(0)} N_B(0)\,d\varepsilon = N_F \frac{d\varepsilon_F}{dp}\, dp$$

where N_F is the average density of states at the Fermi surface.

Thus equation 6-34 becomes:-

$$\int_0^{\varepsilon_F(0)} N_B(0)\,d\varepsilon = \int_0^{\varepsilon_F(P)} N_B(0)\,d\varepsilon - N_F \frac{d\varepsilon_F}{dp}\, dp = \frac{N}{V} \tag{6-35}$$

Substituting this expression in equation 6-33 for N/V gives:-

$$\int_0^{\varepsilon_F(P)} \alpha N_B(0)\,d\varepsilon = \int_0^{\varepsilon_F(P)} N_B(0)\,d\varepsilon - N_F \frac{d\varepsilon_F}{dp}\, dp + \frac{N}{V} K_T dp$$

$$= \int_0^{\varepsilon_F(P)} N_B(0)\,d\varepsilon - N_F \frac{d\varepsilon_F}{dp}\, dp + K_T \left[dp \int_0^{\varepsilon_F(P)} N_B(0)\,d\varepsilon + 0^2 \right]$$

where we have used equation 6-35 for N/V. Neglecting the second order small quantity gives:-

$$[\alpha - 1 - K_T dp] \int_0^{\varepsilon_F(P)} N_B(0)\,d\varepsilon = -N_F \frac{d\varepsilon_F}{dp}\, dp \tag{6-36}$$

making the reasonable assumption that $\int_0^{\varepsilon_F(P)} N_B(0)\,d\varepsilon \simeq \frac{N}{V}$ in equation 6- 36 and re-arranging terms gives:-

$$\alpha = 1 + dp \left(K_T - \frac{N_F}{N/V} \frac{d\varepsilon_F}{dp} \right) \tag{6-37}$$

Now by differentiating equation 6-30 we get:-

$$\frac{d\ln N_B(P)}{dp} = \frac{d\alpha}{dp} \qquad 6\text{-}38$$

which using equation 6-37 gives:-

$$\frac{d\ln N_B(P)}{dp} = K_T - \frac{N_F}{N/V}\,\frac{d\varepsilon_F}{dp} \qquad 6\text{-}39$$

We have now evaluated a form for the second term in equation 6-27 so that the final expression obtained for the pressure dependence of the band structure density of states at the Fermi surface is:-

$$\left(\frac{d\ln N_B}{dp}\right)_{F.S.} = \left[\left(\frac{d\ln N_B}{d\varepsilon}\right)_p - \frac{N_F}{N/V}\right]\frac{d\varepsilon_F}{dp} + K_T$$

or

$$\left(\frac{d\ln N_B}{dp}\right)_{F.S.} = \left[\varepsilon_F\left(\frac{d\ln N_B}{d\varepsilon}\right)_p - \frac{\varepsilon_F N_F}{N/V}\right]\frac{d\ln\varepsilon_F}{dp} + K_T \qquad 6\text{-}40$$

The validity of this relationship can be tested for the case of the free electron gas. In this case the terms on the right hand side of equation 6-40 are:-

$$\varepsilon_F\left(\frac{d\ln N_B}{d\varepsilon}\right)_p = \tfrac{1}{2} \qquad 6\text{-}41$$

$$\frac{\varepsilon_F N_F}{N/V} = \frac{3}{2} \qquad 6\text{-}42$$

$$\frac{d\ln\varepsilon_F}{dp} = \frac{2}{3}K_T \qquad 6\text{-}43$$

and upon substitution yield:-

$$\left(\frac{d\ln N_B}{dp}\right)_{F.S.} = \frac{K_T}{3} = .68 \times 10^{-6}\ \text{bar}^{-1}$$

which is in complete agreement with the value of Table 13.

Turning now to the case of lead, the work of Anderson & Gold shows

the term given by equation 6-41 to be ~-2.5 times that for the free electron case. The second term (given by equation 6-42) is approximately the same as that for free electrons while the third term (equation 6-43) has been determined by Anderson et al and found to be $(d\ln\varepsilon_f/dp)_{F.S.} = -.44 \times 10^{-6}\ \text{bar}^{-1}$.

Using these values in equation 6-40 gives for pure lead:-

$$\left(\frac{d\ln N_B}{dp}\right)_{F.S.} = 3.26 \times 10^{-6}\ \text{bar}^{-1} \qquad 6\text{-}44$$

It can be seen from Table 13 that this value is in very good agreement with the experimental values found in column four.

Using the definition of the heat capacity coefficient γ given by:-

$$\gamma = \frac{2\pi^2}{3} N_B Z k_B^2 \quad \text{(per unit volume)}$$

it can be shown that

$$\frac{d\ln\gamma}{dp} = \frac{d\ln N_B}{dp} + \frac{d\ln Z}{dp} \quad \text{at the Fermi surface} \qquad 6\text{-}45$$

By comparing this with equation 6-22 we see that

$$\frac{d\ln N_F}{dp} = \frac{d\ln\gamma}{dp}$$

Hansen et al (for their 12% data) calculate a value of $\frac{d\ln\gamma}{dp}$ using equation 6-45 and using a value of $\frac{d\ln N_B}{d\ln V}$ for free electrons of $-\frac{1}{3}$.

They then erroneously compare their value of $\frac{d\ln\gamma}{dp} = 4.0 \pm 1 \times 10^{-6}\ \text{bar}^{-1}$ with that of White and claim good agreement. The comparison however is not valid since White assumes the volume dependence of the band

structure density of states to be + 2/3 for the free electron case thus indicating the explicit inclusion of the volume in his calculations as opposed to those of Hansen et al whose calculated value is per unit volume.

Their value should therefore be compared with the value appearing in Table 13 in which case the agreement is poor.

The inescapable conclusion is that the use of the free electron value for the band structure density of states is not really justified and that it should be replaced, for lead at least, by a value such as derived in equation 6-44 which supports the experimental observations.

CHAPTER VII

CONCLUSIONS

In view of the fact that conclusions on the various results obtained permeate the discussions of Chapter VI, only the salient features are repeated here.

The Pb_xIn_{1-x} system exhibits a similar trend to weaker coupling as a function of applied pressure as can be seen from several viewpoints. The observed reduction in the gap ratio for example illustrates this directly.

The phonon spectra and gap function obtained from the inversion process indicate a general increase to higher energies as well as a decrease in structure amplitude (although the effect is less pronounced than for the samples containing lesser concentrations of indium). This is in good agreement with the theoretical prediction of Trofimenkoff and Carbotte who, using a scaled model phonon spectrum similar to those that are actually observed, predict a value for $d\ln\Delta/d\ln T_c \simeq 2.0$ compared with the values of 1.38 ±.53 and 1.52 ±.58 for the $Pb_{88}In_{12}$ and $Pb_{64}In_{36}$ alloys respectively. The strength electron-phonon interaction parameter λ was itself observed to decrease indicative of the general trend to weaker coupling.

The Grüneisen parameters calculated are in very good agreement with those of other workers. It is noticeable that with increased indium concentration the Grüneisen γ associated with the localised mode decreased considerably. This is in good agreement with the

findings of Galkin et al and is possibly tied in with the findings of Sood which show the local mode of vibration to exhibit at least two peaks in the phonon spectrum and whose structure and location are concentration dependent.

A value for the pressure dependence of the band structure density of states at the Fermi surface has been derived, and was found to be:-

$$\frac{d\ln N_B}{dp} = 3.26 \times 10^{-6}\ \text{bar}^{-1} \quad \text{for lead}$$

This value is suggested as a replacement for the free electron value of 0.68×10^{-6} bar^{-1} in future theoretical considerations of lead and lead like systems.

Throughout the experiments performed the tunnel junctions have themselves provided the most reliable method of pressure determination both in the solid and in the fluid. Their use in the solid helium bath provided direct evidence that this technique of pressure application does indeed result in hydrostatic conditions.

BIBLIOGRAPHY

Adler J.G. and Jackson J.E. (1966), Rev. Sci. Instr. 37, 1049.

Adler J.G., Jackson J.E. and Chandrasekhar B.S. (1966), Phys. Rev. Letters 16, 53.

Adler J.G., Jackson J.E. and Will T.A. (1967), Phys. Letters 24A, 407.

Allen P.B. and Silberglitt R. (1974), Phys. Rev. B9, 4733.

Anderson A.C. (1968), Rev. Sci. Instr. 39, 605.

Anderson J.R. and Gold A.V. (1965), Phys. Rev. 139, A1459.

Anderson J.R., O'Sullivan W.J. and Schirber J.E. (1967), Phys. Rev. 153, 721.

Andres K. (1961), Cryogenics 2, 93.

Andres K. (1964), Phys. Kondens Materie 2, 294.

Bardeen J., Cooper L.N. and Schrieffer J.R. (1957), Phys. Rev. 108, 1175.

Bermon S. (1964), University of Illinois Technical Report No. 1, Grant No. NSF-GP 1100 (unpublished).

Bogoliubov N.N. (1958), Nuovo Cimento 7, 794.

Bogoliubov N.N., Tolmachev V.V. and Shirkov D.V. (1959), A New Method in the Theory of Superconductivity (Consultants Bureau, Inc., New York).

Bridgman P.W. (1954), Daedalus (Boston) 83, 149.

Carbotte J.P. (1971), Phys. Rev. B4, 82.

Carbotte J.P. and Dynes R.C. (1968), Phys. Rev. 172, 476.

Carbotte J.P. and Vashishta P. (1971), Can. J. Phys. 49, 1493.

Cooper L.N. (1956), Phys. Rev. 104, 1189.

Dugdale J.A. and Dulbert J.A. (1957), Can J. Phys. 35, 720.

Dugdale J.S. and Simon F.E. (1953), Proc. Roy Soc. 218A, 291.

Edwards D.O. and Pandorf R.C. (1965), Phys. Rev. 140, A816.

Eliashberg G.M. (1960), Soviet Physics JETP 11, 696.

Eliashberg G.M. (1962), Soviet Physics JETP 16, 780.

Farrell D.E., Chandrasekhar B.S. and Culbert H.V. (1969), Phys. Rev. 177, 694.

Franck J.P. and Keeler W.J. (1967), Phys. Rev. 163, 373.

Franck J.P. and Keeler W.J. (1968), Phys. Rev. Letters 20, 379.

Frohlich H. (1950), Phys. Rev. 79, 845; (1950) Proc. Phys. Soc. A63, 778.

Galkin A.A., Svistunov V.M., Chernjak O.I. and Belogolovskii M.A. (1973), Solid State Communications 13, 1095.

Garfinkel M. and Mapother D.E. (1961), Phys. Rev. 122, 459.

Geilikman B.T. and Kresin V. (1965), Fiz. Tverd. Jela 7, 3294 (English Translation Soviet Physics. Solid State 7, 2659, 1966).

Giaver I., Hart H.R. Jr. and Megerle K. (1962), Phys. Rev. 126 941.

Goree W.S., McDowell B. and Scott T.A. (1965), Rev. Sci. Instr. 35, 99.

Gorter C.J. and Casimir H.B.G. (1934), Phys. Z. 35, 963; Z Techn. Phys. 15, 539.

Gray D.E. (Ed.) (1972), American Inst. of Phys. Handbook (McGraw Hill).

Hansen H.H., Pompi R.L. and Wu T.M. (1973), Phys. Rev. B8, 1042.

Harris E.P. (1970), Private Communication to Dr. J.P. Franck.

Hill R.W. and Lounasmaa

Keeler W.J. (1968), Thesis (unpublished).

Lazarev B.G., Sudovtsev A.I. and Smirnov A.P. (1957), J. Exptl. Theoret. Phys. 33, 1059 (English Translation Soviet Physics. JETP 6, 816, 1958).

London H. and London F. (1935), Proc. Roy. Soc. (London) A149, 71; (1934) Physica 2, 341.

McMillan W.L. (1968), Phys. Rev. 167, 331.

McMillan W.L. and Rowell J.M. (1965), Phys. Rev. Letters 14, 108.

McMillan W.L. and Rowell J.M. (1969), in Superconductivity, edited by R.D. Parks, 1, 602.

Meaden G.J. (1965), Electrical Resistivity of Metals (New York, Plenum Press).

Migdal A.B. (1958), Soviet Phys. JETP 7, 996.

Muhlschlegel B. (1959), Z. Physik 155, 313.

Nambu Y. (1960), Phys. Rev. 117, 648.

Nesmayanov A.N. (1963), Vapour Pressure of Chemical Elements (Elsevier).

Onnes H.K. (1911), Commun. Phy. Lab. Univ. Leiden No. 119B.

Rogers J.S. (1970), Rev. Sci. Instr. 41, 1184.

Rosenberg H.M. (1963), Low Temperature Solid State Physics (O.U.P.).

Rowell J.M., Anderson P.W. and Thomas D.E. (1963), Phys. Rev. Letters 10, 334.

Rowell J.M. and Kopf L. (1965), Phys. Rev. 137, A907.

Rowell J.M., McMillan W.L. and Anderson P.W. (1965), Phys. Rev. 14, 633.

Scalapino D.J. and Anderson P.W. (1963), Phys. Rev. 133, A921.

Scalapino D.J., Schrieffer J.R. and Wilkins J.W. (1966), Phys. Rev. 148, 263.

Schrieffer J.R., Scalapino D.J. and Wilkins J.W. (1963), Phys. Rev. Letters 10, 336.

Simon F.E. (1937), Trans. Faraday Soc. 33, 65.

Sood B.R. (1972), Phys. Rev. 6, 136.

Spain I.L. and Segall S. (1971), Cryogenics 11, 26.

Swihart J.C. (1962), I.B.M. Journal of Res. & Devel.

Thouless D.J. (1960), Phys. Rev. 117, 1256.

Toxen A.M. (1961), Phys. Rev. 123, 442.

Trofimenkoff P.N. and Carbotte J.P. (1969), Solid State Communications 7, 661.

Trofimenkoff P.N. and Carbotte J.P. (1970), Phys. Rev. B1, 1136.

Wada Y. (1964), Rev. Mod. Phys. 36, 253.

Waldorf D.L. and Alers G.A. (1962), J. Applied Phys. 33, 3266.

White G.K. (1962), Phil. Mag. 7, 271.

Wu J.M. (1967), Phys. Rev. Letters 19, 508.

B30108